SOLAR QUIET CURRENT AND CONDUCTIVITY-DEPTH PROFILES OF THE EARTH MANTLE FROM QUIET-TIME GEOMAGNETIC FIELD RECORDS IN ASIA SUB-REGION

MUSTAPHA ABBAS

FACULTY OF SCIENCE
UNIVERSITY OF MALAYA
KUALA LUMPUR

2018

SOLAR QUIET CURRENT AND CONDUCTIVITY-DEPTH PROFILES OF THE EARTH MANTLE FROM QUIET-TIME GEOMAGNETIC FIELD RECORDS IN ASIA SUB-REGION

MUSTAPHA ABBAS

THESIS SUBMITTED IN FULFILMENT OF THE REQUIREMENTS FOR THE DEGREE OF DOCTOR OF PHILOSOPHY

DEPARTMENT OF PHYSICS
FACULTY OF SCIENCE
UNIVERSITY OF MALAYA
KUALA LUMPUR

2018

UNIVERSITY OF MALAYA

ORIGINAL LITERARY WORK DECLARATION

Name of Candidate: **MUSTAPHA ABBAS**

Name of Degree: **DOCTOR OF PHILOSOPHY**

Title of Project Paper/Research Report/Dissertation/Thesis ("this Work"): **SOLAR QUIET CURRENT AND CONDUCTIVITY-DEPTH PROFILES OF THE EARTH MANTLE FROM QUIET-TIME GEOMAGNETIC FIELD RECORDS IN ASIA SUB-REGION**

Field of Study: **ASTRONOMY AND GEOPHYSICS**

I do solemnly and sincerely declare that:

(1) I am the sole author/writer of this Work;
(2) This Work is original;
(3) Any use of any work in which copyright exists was done by way of fair dealing and for permitted purposes and any excerpt or extract from, or reference to or reproduction of any copyright work has been disclosed expressly and sufficiently and the title of the Work and its authorship have been acknowledged in this Work;
(4) I do not have any actual knowledge nor do I ought reasonably to know that the making of this work constitutes an infringement of any copyright work;
(5) I hereby assign all and every rights in the copyright to this Work to the University of Malaya ("UM"), who henceforth shall be owner of the copyright in this Work and that any reproduction or use in any form or by any means whatsoever is prohibited without the written consent of UM having been first had and obtained;
(6) I am fully aware that if in the course of making this Work I have infringed any copyright whether intentionally or otherwise, I may be subject to legal action or any other action as may be determined by UM.

Candidate's Signature Date:

Subscribed and solemnly declared before,

Witness's Signature Date:

Name:

Designation:

SOLAR QUIET CURRENT AND CONDUCTIVITY-DEPTH PROFILES OF THE EARTH MANTLE FROM QUIET-TIME GEOMAGNETIC FIELD RECORDS IN ASIA SUB-REGION

ABSTRACT

This study investigate the month-by-month behavior of the external and internal ionospheric current system, their quiet fields and the conductivity-depth profile of Asia sub-region using selected geomagnetic field records from dip minimum to moderate solar activity years. The separation of the external and internal field contributions to the Sq variations was successfully carried out using spherical harmonic analysis (SHA). A transfer function was then employed to determine the conductivity profile to a depth of about 800 km from the paired external and internal coefficients of the SHA. The results reveal that the daytime external, internal and sum of the quiet fields for the horizontal and vertical components equatorward and poleward of the Sq focus exhibit daytime positive and negative amplitudes with the former increasing (decreasing) with increasing solar activity (latitudes) while the latter increases with increasing latitudes but show no linear relationship with increasing solar activity. Throughout the years, the external quiet field magnitudes are about twice larger than their corresponding internal and both exhibit slight phase variations that are believed to arise from electromagnetic induction effect. The external and internal equivalent currents contours are characterized by a single daytime vortex near mid-latitudes that linearly increased from the strong summertime amplitudes reaching ~-10.5 $\times 10^4$A during the dip minimum solar activity year 2008 to about 11.7 $\times 10^4$ and 15.5 $\times 10^4$A during low and moderate solar activity years 2017 and 2012 and the internal Sq current vortices are only about 0.8, 0.56 and 0.50 times as large in 2008, 2017 and 2012. The internal equivalent current vortices in winter months disappeared more frequently than the external and the disappearance of both external and internal current vortices decreases with increasing solar activity. The internal currents foci mostly

appeared slightly poleward than the external foci. At low latitudes there seems to be intrusion of stronger summertime current vortex of the opposite hemisphere into the winter hemisphere appearing most frequently during the pre-noon hours in the southern hemisphere and in the afternoon hours in the northern hemisphere. A regression line fitted to the estimated conductivity values show a downward increase in electrical conductivity with depths beneath this region. At depths range ~130 and 300 km, the profile showed an evidence of increase in conductivity followed by a sharp steep increase in conductivity profile at depth of about 310, 350 and 410 km in 2008, 2012 and 2017. Generally the increase in conductivity profile appeared more rapid during the moderate solar activity year 2012 and slower in 2017 and 2008. The profiles have not shown any significant variations in their depth of penetration despite major differences in their annual sunspot numbers, but the higher and rapid increase in conductivity profile in 2012 could be the effect of difference in solar activity. The profiles thus indicates that there may likely be major lateral heterogeneity in the electrical conductivity of the Earth's upper mantle.

Keywords: Ionosphere, Sq current, Mantle electrical conductivity

ARUS MATAHARI TENANG DAN PROFIL KEBERALIRAN-KEDALAMAN MANTEL BUMI DARIPADA REKOD KETIKA WAKTU MEDAN GEOMAGNETIK TENANG UNTUK KAWASAN SUB-RANTAU ASIA

ABSTRAK

Penyelidikan ini melihat perubahan bulanan dalam sistem arus ionosfera dalam dan luar, medan tenang mereka serta profil beberaliran-kedalaman kawasan sub-rantau Asia menggunakan rekod medan geomagnetik terpilih dari tahun paling minima kepada tahun yang mempunyai aktiviti matahari yang sederhana. Pemisahan sumbangan arus dalam dan luar kepada perubahan arus "Solar Quiet" (Sq) telah berjaya dilakukan dengan menggunakan kaedah "Spherical Harmonic Analysis" (SHA). Satu fungsi pemindahan kemudian digunakan bagi mangenalpasti profil keberaliran sehingga kedalaman lebih kurang 800km berdasarkan pasangan pekali luar dan dalam SHA. Hasil kajian menunjukkan medan tenang luar, dalam dan keseluruhan pada waktu siang untuk komponen mendatar dan menegak untuk arah khatulistiwa dan kutub dari fokus Sq mempunyai nilai amplitud positif dan negatif siang, dengan nilai positif meningkat ketika aktiviti matahari meningkat. Nilai negatif pula menurun pada masa yang sama. Nilai negatif meningkat dengan peningkatan latitud dan tidak menunjukkan hubungan linear dengan aktiviti matahari. Nilai luaran adalah dua kali ganda nilai dalaman, dan kedua-duanya menunjukkan sedikit perubahan fasa yang dipercayai berpunca daripada kesan induksi elektromagnetik. Kontur arus bersamaan dalam dan luar mempunyai satu pusaran berdekatan latitud tengah yang meningkat daripada amplitud musim panas iaitu ~-10.5 x10^4 A pada titik aktiviti minima tahun 2008 sehingga 11.7 × 10^4 (2017; tahun aktiviti rendah) dan 15.5 × 10^4A (2012; tahun aktiviti sederhana). Vorteks untuk arus Sq dalaman hanya 0.8, 0.56 dan 0.50 kali lebih besar untuk 2008, 2017 dan 2012. Vorteks arus besamaan dalaman kerap hilang pada musim sejuk daripada arus luaran, dan kejadian hilangnya kedua-dua vorteks berkurangan dengan peningkatan aktiviti matahari. Foci

arus dalaman kelihatan lebih terarah ke kutub berbanding luaran. Di latitud rendah, vorteks arus musim panas yang lebih kuat kelihatan menceroboh vorteks musim sejuk di hemisfera bertentangan, terutama pada waktu pagi di hemisfera selatan dan patang di hemisfera utara. Satu garisan regresi pada anggaran nilai keberaliran menunjukkan peningkatan keberaliran elektrik mengikut kedalaman di kawasan ini. Pada kedalaman 130 km hingga 300 km, terdapat peningkatan keberaliran, diikuti dengan peningkatan yang ketara pada kedalaman 310km, 350 km dan 450 km pada 2008. 2012 dan 2017. Secara umun, peningkatan keberaliran adalah lebih cepat pada 2012 (tahun aktiviti sederhana) dan lebih perlahan pada 2008 dan 2017. Profil-profil tidak menunjukkan sebarang perubahan ketara bagi kedalaman tembusan meskipun terdapat perbezaan jumlah titik matahari, tetapi peningkatan cepat profil keberaliran pada 2012 mungkin disebabkan perbezaan dalam aktiviti matahari. Oleh itu, profil-profil tersebut menunjukkan kemungkinan besar terdapat kepelbagaian dalam keberaliran elektrik manyel atas Bumi.

Kata kunci: Ionosfera, Arus Sq, Keberaliran elektrik mantel

ACKNOWLEDGEMENTS

First and foremost, thanks to almighty God for given me the strength and opportunity to complete this thesis writing after all the challenges and difficulties. I am deeply grateful to my supervisors Assoc. Prof. Dr. Zamri Zainal Abidin and Assoc. Prof. Dr. Huzaimy Mohammad Jusoh for their guidance and constructive comments on my dissertation. My thanks goes to the head of the department of Physics and the entire staffs of physics departments for their encouragements. I wish to specially thank Ching-Yee Kiew and Dr. Daniel Okor whose vast PYTHON and MATLAB knowledge was extensively utilized to obtain the result presented in this work. You are indeed a blessings to my life. I wish to specially thank Prof. Dr. Taha Rabe of National Research Institute of Astronomy and Geophysics, Egypt for a useful discussions and proof reading the entire thesis and making valuable contributions. Indeed your unique physical insight has greatly help in solving the most difficult aspect of this research. I benefitted greatly from the discussion with Assoc. Prof. Dr. Yoshikawa Akimasa during one of the international conference. My sincere gratitude goes to Prof. Dr. Obiora Daniel of University of Nigeria Nsukka (UNN) for his valuable contributions to this research work. I am deeply grateful to all the friends who have in one way or the other contributed to the success of this work, especially my student colleagues in the Radio Cosmology Lab (UM) especially Ching Yee Kiew, Israa Abdulqasim, Danial Ahmed, Farah. Also my colleagues in Electromagnetic Research Group (UiTM) so numerous to mention, i really appreciate you all. Last but not least, I would like to thank my entire family especially my wife Umuhabetu Mustapha and my wonderful children Sama'ila Mustapha, and Ibrahim Mustapha for their unconditional love, ever supporting and patience all the years that I have been away from them. My special thanks goes to the INTERMAGNET and MAGDAS group for providing high standard quality data used in this research work.

UT: 5:00 Hrs (MYS: 01:00 LT Hrs).

TABLE OF CONTENTS

LIST OF FIGURES

LIST OF TABLES

LIST OF SYMBOLS AND ABBREVIATIONS

INTERMAGNET	:	International Real-Time Magnetic Observatory Network
LOWESS	:	Locally Weighted Scatterplot Smoothing
MAGDAS	:	Magnetic Data Acquisition System
$MSqH_{ext}$	:	Monthly solar quiet for horizontal external field
$MSqD_{ext}$	:	Monthly solar quiet for eastward external field
$MSqZ_{ext}$	:	Monthly solar quiet for vertical external field
$MSqH_{int}$	:	Monthly solar quiet for horizontal internal field
$MSqD_{int}$	:	Monthly solar quiet for eastward internal field
$MSqZ_{int}$	:	Monthly solar quiet for vertical internal field

LIST OF APPENDICES

CHAPTER 1: INTRODUCTION

1.1 The Quiet Sun

The sun is a big star in the Milky way group. It is almost spherically symmetric mixtures of ionized gases (the plasma), self-gravitating and radiating with diameter of about 7×10^5 km. By volume, the sun is constituted of hydrogen of about 81.7 %, followed by helium of about 18.17 % while carbon, nitrogen, oxygen and other metals form about 0.07 % (Campbell, 2003). The sun has been an enormous energy source; release it in the form of electromagnetic radiations and also mass ejection. The ejection may be in the form of explosive in the case of flares, or in a progressive and relatively quiet pattern as the case of solar wind. The sun release its energy in the form of neutrinos, the end product of nuclear reactions in the solar core. The nuclear fusion is primarily responsible for generating solar energy, establishing high energy photons which take millions of years to travel through the sun to arrive at the solar surface, where they are radiated as visible light. In the sun's interior, the four protons (^{1}H) fused to form helium (^{4}He) and approximately 4×10^{-12} J of energy is produce for each helium atom (Campbell, 2003). The sun rotates in a non-uniform way faster inside and slower on the outer surface. The Tail end of the sun is most often regarded as the magnetopause, a collision place between the solar wind and the interstellar medium, several millions of kilometers away. The sun follow the solar cycle of approximately 11 years and this is marked by the increase and decrease of sunspot numbers-a temporally darker region on the solar surface (Campbell, 2003). As solar activity increases these darker regions (sunspots) increases-implication that few sunspots occur during low solar activity with larger occurrence at maximum solar activity. During these processes the magnetic field lines of the sun changes in response to the solar cycle.

1.1.1 Active Sun, Sunspot, Solar Cycle, Coronal Holes

Even though the sun has just been described as a quiet system, there are still some active places that sometimes occur on the surface of the sun. Active changes that sometimes occur on the solar surface are easy to identify when measurements are made at selected light wavelengths of stronger emissions.

The solar electromagnetic radiations from short-wavelength, high energy X-rays emitted through the visible spectra to the long wavelengths of the infrared illuminate the Earth and its atmosphere (Campbell, 2003). Generally, when the wavelength of a disturbance is shorted in the spectrum, there will be greater solar emission response to the variable solar activity. The ionization in the upper atmosphere respond to the variable changes of energetic solar emission after about 500 secs, (8.3 mins) for the light from the sun to reach the Earth surface (Campbell, 2003).

The particular part on the solar surface where these changes takes place are commonly known as active regions. Photographs of the solar surface sometimes show dark spots. These dark regions on the solar surface are called sunspots. They are composed mainly of dark central core known as the umbra surrounded by a slightly lighter surface known as the penumbra. In the umbra, the magnetic field is oriented perpendicular to the surface while at the penumbra the magnetic field are mostly parallel to the surface (Solanki & Rüedi, 2003).

Measurement obtained from the infrared intensity, temperature as well as magnetic field inside the sunspots shows that the sunspots magnetic field strength decreases with time irrespective of the solar cycle and are slightly cooler (4,600 K) than the solar surface due to their reduced temperature (Livingston & Penn, 2009). Sunspot activity is usually monitored using sunspot number R, which takes into account the entire numbers of the sunspots that occur in the photosphere. A unit of R is approximately equal to an area of

about 6 x 10^{-8} of the visible solar surface hemisphere. Averagely, the maximum sunspot numbers is near 108 and its minimum is about 5. The variations in the minimum and maximum sunspots activity influence the daily variability of the solar quiet (Sq). The sunspots also vary with solar cycle and the 11-year sunspot cycle is actually a 22-year cycle in the solar magnetic field and also shows similar hemispheric magnetic polarity on alternate 11-years (Livingston & Penn, 2009). At any given sunspot cycle, the larger pairs of sunspots in the northern hemisphere exhibit the same polarity while in southern hemisphere they show opposite polarity. The north-south differences on the occurrence of sunspots has been extensively studied and the result shows that the appearance differ between hemispheres-an indication that one hemisphere may experience more active region than the other (e.g., Carbonell et al., 1993; Zharkov & Zharkova, 2006). The sunspots frequently appear in groups or pairs and follow solar cycle trend with frequent and violent occurrences during solar maximum. Livingston & Penn (2009) reported that the occurrence of sunspot decreases during solar minimum years-implication that the solar energy input to the Earth decreases.

Coronal holes are linked to solar activity processes such that they are composed of low-density plasma on the solar surface with magnetic fields that opens freely into interplanetary space. During minimum solar activity, coronal holes cover the northern and southern polar caps of the sun, and exist at all latitudes during the active period of the sun. These holes are mostly considered to be responsible for the continuous outflow of solar wind and series of solar terrestrial magnetic disturbances (Okeke, 1995).

1.2 Geomagnetic Field Elements

Geomagnetic field of the Earth obviously varies with time and location on the globe. This variation may be classified into short and long term. The short term has its origin

attributed to sources above the Earth surface while the long term variation originates from sources beneath the Earth surface. The geomagnetic field of the Earth been a vector field is often described using various magnetic elements. The geomagnetic elements are mostly taken to be major components that are parallel to the geographic north and east directions and also the vertically downward as shown in Figure 1.1. The geographic northward (X), eastward (Y) and vertical (Z) pointing downward are sometimes referred to as XYZ-components. These geomagnetic field elements are mostly use by non-magnetic survey ship at the sea and spacecraft carrying on-board installed magnetometers. Another way to describe the Earth magnetic field is by the use of horizontal (H), the declination (D) and the vertical or downward (Z) components which are commonly referred to as HDZ-components. In the ancient times, the direction of the sailing ship was simply based on the measurement of declination (D) – is the angle formed between the true magnetic north and the freely suspended compass needle (see Figure 1.1). Therefore, the ancient observation used the HDZ system of vector representation of the magnetic field of the Earth (Campbell, 2003). The magnitude or intensity F of the field is measured using the unit of magnetic field, namely the Tesla (T).

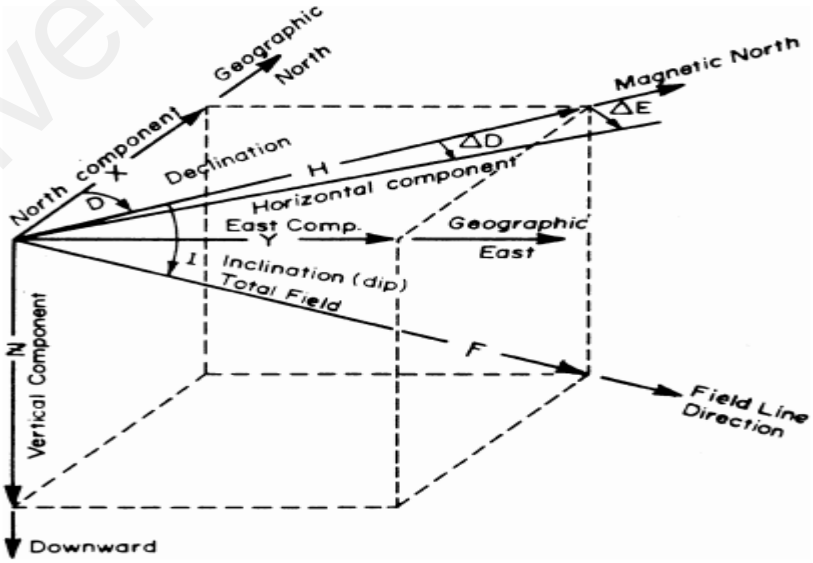

Figure 1.1: Geomagnetic field elements for a northern hemisphere adopted from Campbell, (2003).

However, because the Tesla (T) is such a strong field, the magnetic field of the Earth is too weak with highest intensity of about 6 x 10^{-5} T at the magnetic poles. Hence, the practical unit of geomagnetic field for any geophysical exploration is given in gamma (γ). 1-gamma is approximately equal to 10^{-9} T or preferably nanotesla (nT) (Campbell, 2003).

The main equations relating the geomagnetic field elements are given by:

$$X = HcosD \tag{1.1}$$

$$Y = HsinD \tag{1.2}$$

The total field strength F is given by:

$$F = \sqrt{X^2 + Y^2 + Z^2} \quad \sqrt{H^2 + Z^2} \tag{1.3}$$

The angle of inclination is the between the total field and the horizontal plane. It is sometimes called the dip angle, expressed as;

$$tanI = \frac{Z}{H} \text{ Or } I = t\text{an}^{-1}\left(\frac{Z}{H}\right) \tag{1.4}$$

Presently the XYZ systems are the most preferred coordinates for reporting magnetic field observations. The angular relationship between the XYZ and HDZ is given in Figure 1.1 mathematically it is expressed as;

$$H = \sqrt{X^2 + Y^2} \tag{1.5}$$

$$H = t\text{an}^{-1}\frac{Y}{X} \tag{1.6}$$

The declination (D) is in degrees (D°) which can be expressed in magnetic eastward field strength D (nT) using the following relation:

$$D(nT) = Htan(D^{\circ}) \tag{1.7}$$

1.3 Geomagnetic Field Variations

The geomagnetic field of the Earth surface extends from the Earth's interior (core) to the outer surface (Earth crust) up to the upper atmosphere and interact with the solar wind. The geomagnetic field changes in time and never constant at any particular place on the Earth surface. In other words, the field changes with time from one place to another. The changes in the Earth magnetic field may be in terms of its declination or inclination and the intensity of the field may also vary from few nanotesla (nT) to thousands of nT. Sometimes the changes in the field may be periodic or random depending on the level of magnetic activity. There are two basic variations of the field - the spatial (space) and the temporal (time) as shown in Figure 1.2. The temporal variation of the geomagnetic field consists of the secular and the transient variations as clearly shown in Figure 1.2.

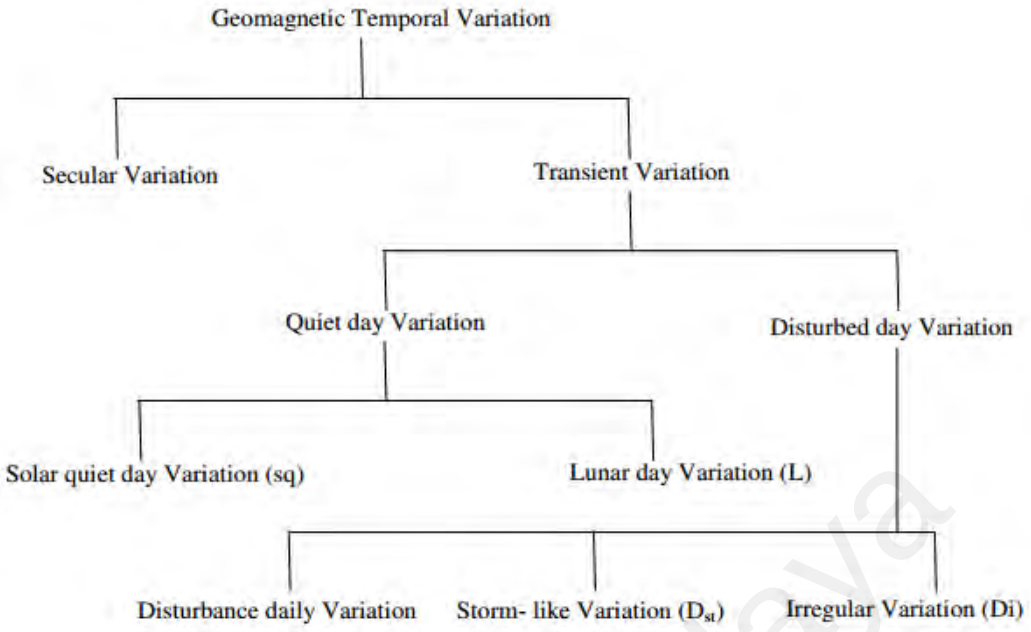

Figure 1.2: Organogram of geomagnetic temporal variation adopted from Okeke, (1995).

1.3.1 Secular Variations

Geomagnetic secular variation refers to changes in the magnetic field of the Earth on time scales of approximately a year or more. These variations depict various changes in the Earth's interior and the most rapid changes are mostly associated with changes in the magnetosphere or ionosphere (Lanza and Meloni, 2006). The intensity and inclination of the Earth main field vary with time and these changes may be small but with significant impact on geomagnetic field ranging over several years. Both the secular variation and the Earth's main field originate from the same sources within the Earth's interior. Hence, secular variations of geomagnetic field provide essential knowledge on the dynamics of the conductive fluid in the Earth's core and the origin of the geomagnetic field itself (Lanza & Meloni, 2006).

1.3.2 Transient Variations

The transient variations of geomagnetic field are sometimes called the short term variations which are observed during quiet and disturbed period and have their sources

attributed to electric currents from the Earth's interior, ionosphere and magnetosphere. They are classified into two: quiet day variation (regular variation) and disturbance day variations (irregular variations). The daily regular variation of the Earth's magnetic field sometimes referred to S_R is observed on basic quiet days and the irregular variations are observed on days during magnetic disturbances (Amory-Mazaudier, 2009).

1.3.2.1 Quiet Day Variations

The daily geomagnetic field variations have been discovered by Graham in 1722 when he first noticed the motion of a freely suspended compass needle to a particular direction. Ever since this innovative discovery, various elaborate research workers have conducted various studies to examined and ascertain the features and origin of the geomagnetic field. On the basis of this (Stewart, 1882) put forward a theory, that the variations are caused by electric currents induced by the dynamo action in the conducting region of ionized gas carried by wind of global scale across the geomagnetic lines of forces. Few years' later (Appleton & Barnett, 1925) found that the electric currents responsible for the daily variations flow horizontally at an altitude of about 100 km in the conducting E-region of the ionosphere. During minimum solar terrestrial disturbances, the electric currents generate the quiet daily variations. The diurnal variations which are sometimes refer to as solar daily variations are the most prominent of the regular variations. Its features on each magnetic component and their dependence on season and solar cycle suggest that they are modulated by solar ultra-violet radiations. Since astronomical factors regulate atmospheric dynamo processes, regular variations depend on certain parameters which include, time of the year, solar activity and geomagnetic latitude. These regular variations are observed on days with no stronger magnetic disturbances in the magnetosphere generated by other sources.

(a) **Solar Quiet Day variations**

In the absence of solar-terrestrial magnetic disturbances the magnetic field that span from approximately 60 °S to 60 °N show smooth regular occurrence patterns that are mainly composed of the 24-, 12-, 8-, and 6-hours spectral components. These variations are mostly referred to as solar quiet (Sq) variations (Campbell, 2003; Chapman & Bartels, 1940). Campbell (2003) defined the solar quiet variations as a field that changes slowly with local time in the absence of solar magnetic disturbances. The solar quiet variations are consequences of electric current that are flowing in the dynamo region at an altitude between 90 and 150 km in the E-region of the ionosphere. In this region, there are sufficient ionized plasma caused by photo-ionization due to solar radiation of the upper atmosphere and the presence of wind transport the conducting plasma across the Earth's main field resulting to fluctuating current that is responsible for the observed solar quiet (Sq) variation at the ground surface. The solar quiet (Sq) variations are obtain by subtracting the lunar and magnetospheric effects from the solar variations. Chapman & Bartels (1940) explained explicitly that Sq variation at mid-low latitude is obtained by simply taking the average of five quiet days of any month.

(b) **Lunar Day Variations (L)**

The lunar daily variation represented by the symbol (L) relied on the lunar time. They are regular variations that changes in phase and amplitudes with each day of the lunar month taken from one new moon to the next. The magnitude of the lunar variations are just few nanotesla (nT) that are hardly observed on magnetograms and occur because of gravitation of the moon caused by atmospheric tides (Campbell, 2003). They are observed at all latitudes exception of equatorial region where it coincides with the magnetic equator (Vestine, 1960). Unlike the Sq variation which exhibit diurnal variation, the lunar (L) variation is predominantly semi-diurnal variation much like the ocean tides.

1.3.2.2 Disturbance Day Variations

Disturbance variations are caused as a result of interaction of the magnetic field of the solar wind and the Earth's magnetosphere (Gunnarsdóttir, 2012). The interaction result in the transfer of energy and plasma thereby generating currents in the magnetosphere and ionosphere. This process generate geomagnetically induced current (GIC) that sometimes cause severe damage to electrical and spacecerafts.

1.4 Internal Magnetic Field (IMF)

The Earth's natural magnetic characteristics can be due to its dynamical internal physiochemical processes. The wide speculations that the Earth geomagnetic field is generated by a relative bar magnetic situated somewhere within the Earth is just mere figurative, and does not hold, though the shape of the field is somehow identical to a magnetic dipole with its north pole placed in the southern hemisphere. The Earth behaves as a uniformly magnetized sphere with lines of forces near the poles and much close together such that it provides relatively stronger field at this location (Basavaiah, 2012). This field decreased to about half of its intensity near the magnetic equator. The position of the magnetic poles is not fixed but rather changes with time and is known as polar wandering. The knowledge of how and where the Earth's magnetic field (EMF) is produced required in-depth understanding into the Earth's interior. Recent studies suggested that the liquid outer core to a large extent acts as self-existing dynamo accounting for the Earth's magnetic field (EMF) owing to its enhanced electrical conductive materials and internal movement.

1.5 The Ionosphere

The ionosphere is that portion of the Earth upper atmosphere with sufficient amount of ions and electrons of thermal energy capable to influence radio propagation over a long distance places on the Earth. It extends from about 80 – 1000 km altitude comprising of the uppermost part of mesosphere and overlaps the thermosphere and exosphere (see Fig. 1.3). The ionosphere owns its existence to ultraviolet radiation from the sun. The ultraviolet (UV) rays and X-rays emanating from the sun caused heavy ionization in this region. The amount of ionization in the ionosphere depends primarily on the sun and its level of activity (Campbell, 2003). The ionosphere is composed of a number of layers that are identified by the letters D, E and F.

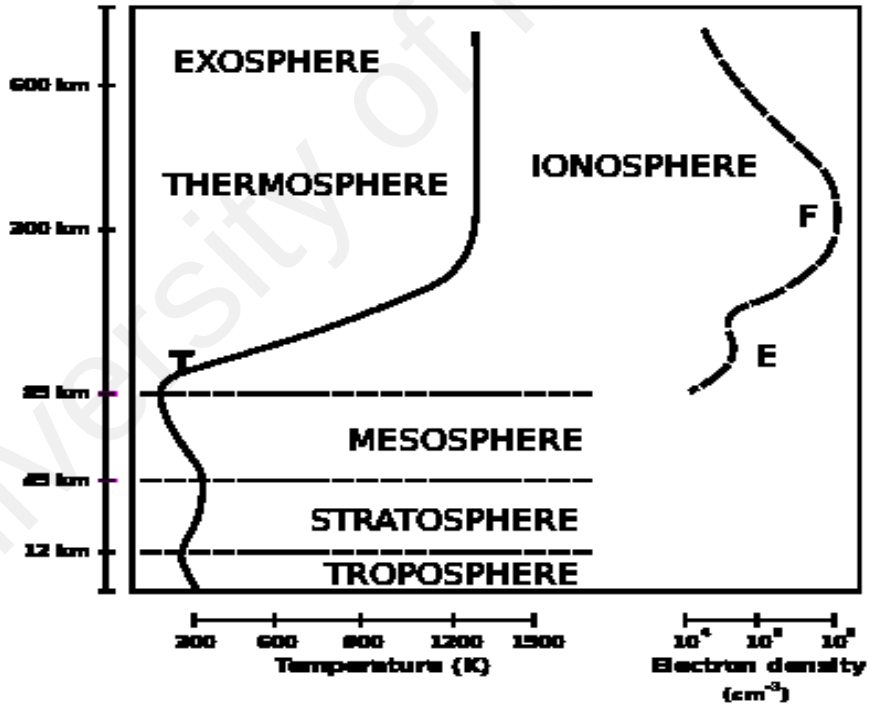

Figure 1.3: Schematic structure of the ionosphere adopted from Campbell, (2003).

1.5.1 The D Region

The D-region is the innermost ionospheric region that extends from about 50 to 100 km, with a daytime maximum electron density (Ne) of about 10^3cm at a height of about

85 km (Mitra, 1968). It is evident that different sources of ionization generate the D region electron density distribution. These sources include; solar radiation at upper levels and galactic cosmic rays from lower levels. In addition, during high solar activity, hard X-rays are generated which also ionized N_2 and O_2. At nigh-time, free electrons in this region disappear because of the electron recombination with oxygen ions to form electrically neutral oxygen molecules. This implies that the recombination rates are very much high in this region. This region has been reported to be responsible for majority of the absorption experienced by high frequency (HF) signals that completely exploit the sky wave mode.

1.5.2 The E Region

The E-region is mostly referred to as the Kennelly-Heaviside layer. It is the middle portion of the ionosphere located at a height of about 90 to 150 km above the Earth's surface (see Figure 1.3). Usually, at oblique incidence, this region reflect radio waves with frequencies lower than about 10 MHZ and may contribute a bit to absorption on greater frequencies. In this region, ionization is caused by soft X-ray and ultraviolet (UV) radiation from the sun, ionizing molecular oxygen (O_2). Ionization in the E-region considerably decrease at night-time leaving below a smaller portion and this weakens the electrical conductivity of the region during the night-time hours.

1.5.3 The F Region

The F-region, also known as the Appleton-Barnett region extends from the height ~160 to approximately 700 km above the Earth surface (see Figure 1.3). This region has the greatest concentration of free electrons suggesting that signals penetrating this region may likely escape into outer space. The ionization in this region persist during the night-time but with little changes in the ion distribution, during the daytime, the layer split into

two; the smaller layer known as F_1 and above this layer is the more highly ionized dominant layer known as the F_2.

1.6 Ionospheric Dynamo

A dynamo is generally refers to anything that generates power. The ionospheric dynamo generated current system is a unique process by which plasma (a conductor) is transported across the Earth's main field similar to the way in which current is generated in the wire connected to a hydroelectric plant dynamo across the magnetic field of a big permanent magnet (Campbell, 2003). The major difference with the hydroelectric plant dynamo is that its conductor are ionospheric plasma whose conductivity varies with time of the day, day of the year, seasons of the year and also magnitude of the solar activity (Rastogi, 1989). The ionospheric dynamo has a tensor conductivity-implication that the ease with which the electric current flow through the medium depends on the direction of the transport of the conductive plasma with respect to the Earth's main field. The driving mechanism for both thermotidal motions and winds of global scale differ with the global geographic locations.

1.7 Ionospheric Current System

The ionospheric current is generally referred to currents flowing in the conducting layer of the Earth's atmosphere (ionosphere). The ionospheric currents act as external sources of magnetic field observed at the ground surface (e.g., Takeda and Iyemori, 2003). The electric current in the ionosphere is simply a differential processes (motion) of opposite charged particles. There are basically three main forces that generate the differential motion of the ions and electrons commonly found in the ionosphere: collision, gravitational, magnetic and electric fields. The ionospheric currents consists of two basic components viz, Pedersen and Hall currents which flow at right angle to each other and

are fed by currents flowing into the ionosphere via the magnetic field lines. A magnetometer or rocket carrying onboard installed magnetometers detect these ionospheric currents with ground based magnetometers more sensitive to the Hall currents. Some of the common ionospheric currents includes: solar quiet (Sq) current system, disturbance polar 1 and 2 current systems, and Lunar current.

1.7.1 Solar Quiet (Sq) Current System

On days designated as 'quiet' for the solar-terrestrial environment of fields and particles, the current generated through the dynamo process in the E-region of the ionosphere is most often referred to as solar quiet current or simply Sq current. It exhibit peak amplitudes at height between 90 and 170 km due to greater Pedersen and Hall conductivities at these height range (Pedatella et al., 2011). In the southern hemisphere it flows in a clockwise direction and counter-clockwise in the northern hemisphere (Yamazaki et al., 2009). The structure and strength of the Sq current is controlled by the tidal wind and ionospheric conductivity of the dynamo region. The sensitivity of the Sq current to changes in solar activity caused it to be stronger in local summer and weaker in winter which is consistent with the level of ionization. The Sq current is primarily responsible for the geomagnetic daily variations at the ground surface (Schuster, 1889).

1.7.2 Lunar (L) Current

The lunar (L) currents are weaker than Sq current driven by (2, 2) tidal mode in the upper atmosphere. The L current exhibit similar shape with the Sq current but has four vortices. During the daytime, L current is strongly enhanced and fluctuate around zero at night-time. The lunar current generate geomagnetic lunar variation that is smaller than the solar quiet variation (Yamazaki et al., 2011). The L current effect is stronger near the

dip magnetic equator due to presence of cowling conductivity which significantly enhanced the current.

1.7.3 Disturbance polar-1 (DP_1) current system

The DP_1 is often described an equivalent current system that is primarily composed of electric current cell located on the night side (Amory-Mazaudier, 2009). At the upper atmosphere, the solar wind plasma interacts with the polar geomagnetic field to produce magnetospheric electric convection field of global scale that is directed from dawn to dusk. Charge separation occurs at the magnetopause and this region is connected to the ionospheric dynamo region through the geomagnetic field lines with footpoint within the auroral region. The DP_1 currents from the auroral region are connected to the mid-low latitude region through the field-aligned currents (FACs). This implies that DP_1 represent variations that have their origin attributed to the auroral electrojet and polar substorms (Amory-Mazaudier, 2009; Nishida, 1968).

1.7.4 Disturbance Polar-2 (DP_2) Current System

The DP_2 are mostly described as the magnetic effect of current systems at high latitudes that are associated with the coupling of magnetosphere and ionosphere (Amory-Mazaudier et al., 2017). DP_2 arise due to penetration of magnetospheric electric field (MEF) into low-latitude region and this cause total orientation of the plasma resulting to migration of field-aligned currents (FACs) into and out of the ionosphere. They exist during the quiet and disturbed periods but are more enhanced during the disturbed period, (Chapman & Bartels, 1940). The fluctuation of DP_2 were observed to coincide with the southward and northward turning of the interplanetary magnetic field (IMF) (Nishida, 1968).

1.7.5 Small-Scale Ionospheric Current System

In the ionosphere, current vortices are commonly found and range in small scale sizes which are either in motion or static. They are resultant effect of localized fluctuating currents into the ionosphere from geospace. Current flowing into the ionosphere through the magnetic field lines is closed by the Pedersen current inside the ionospheric plane that diverge at the point of entrance of the FAC. Assuming the ionosphere is not heterogeneous, there exist also a divergent electric field which drives a horizontal Hall current at right angle to it and the magnetic field in the ionosphere. Source of the FAC, the Pedersen and Hall currents exhibit different characteristics with the former pointing radially outward and the latter flows in circle around the point source. Because the Pedersen current diverges, its strength decreases relative to the square of its radius from the point source. Similar scenario applies to the Hall current and electric field.

1.8 E-region Conductivity

The daytime E-region electrical conductivity is of utmost importance during the ionospheric dynamo process. The density of air decreases with increasing height in the atmosphere and this allows the electrons to be relatively collision free at height above the base (80 km) in the E-region (Rastogi, 1989). Contrary to this, the positive ions are constantly subjected to frequent collisions with the neutral atmosphere from the base at approximately 80 km to the top of the E-region at about 130 km height. The consequence of this is that current of the electrons would not be neutralized by an opposite current of positive ions in the intervening region (Rastogi, 1989).

The most important collision frequency v in the E-region is between the electrons and non-ionized air particles (neutrals). If the electric field, *E* in the medium is directed along the magnetic field lines, then the electric conductivity for a current with similar orientation is given by:

$$\sigma_0 = \frac{ne^2}{mv} \tag{1.8}$$

Where *n* is the electron concentration, v is the collision frequency, *e* is the charge, σ_0 is the longitudinal conductivity which also represent the actual electrical conductivity. In a situation in which the electric field is perpendicular to the Earth's main field **B,** two separate electrical conductivities have to be considered: the Pedersen conductivity (σ_1) which represent current in the direction parallel to the electric field (Rastogi, 1989). This conductivity in the E-region dynamo is expressed as;

$$\sigma_1 = \sigma_0 \left(\frac{v^2}{w^2+v^2}\right) \approx \sigma_0 \left(\frac{v}{w}\right)^2 \tag{1.9}$$

The second is the Hall conductivity (σ_2 which represents current that is perpendicular to the electric field). This is given as;

$$\sigma_2 = \sigma_0 \left(\frac{vw}{w^2+v^2}\right) \approx \sigma_0 \left(\frac{v}{w}\right) \tag{1.10}$$

Where *w* is the gyrofrequency. Equations 1.8-1.10, shows that when **B** and **E** are parallel, we use Equation 1.8 to estimate the σ_0 and when perpendicular, two conditions are involve: (a) the current (i.e. particle velocity) is parallel to electric field **E**, we use Equation 1.8 for σ_1, (b) when the current (particle velocity) is perpendicular to **E** we apply

Equation 1.10 for σ_2. Usually, the directions of **E** and **B** will definitely form an angle; therefore its parallel and perpendicular components will make all the three electrical conductivities to come to play simultaneously. Figure 1.4 illustrates the respective magnitudes of the electrical conductivities measured in Siemens/meter against the height for a typical summer noontime at mid-latitude location. In the Figure, it is apparently seen that the Hall conductivity dominates the Pedersen conductivity at the dynamo region (80-130 km) where electrons are the carries of currents.

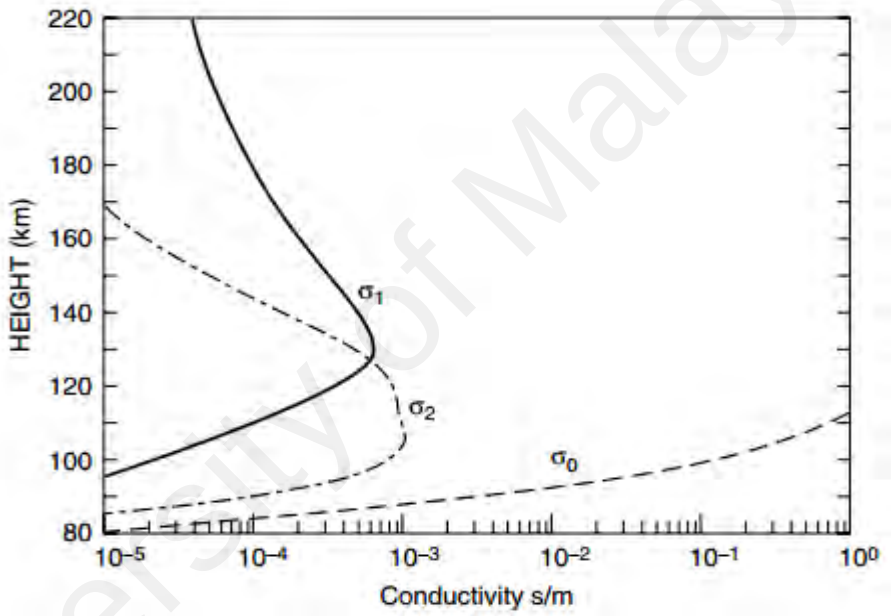

Figure 1.4: Schematic representation of parallel (σ_0, Pedersen conductivity (σ_1, and Hall (σ_2 conductivities in summer at midlatitude location adopted from Campbell, (2003).

The current mostly flow favorably in a direction that is perpendicular to the orthogonal electric and magnetic fields (Campbell, 2003). During the night-time hours, the dynamo currents in the lower part of the F-region play significant role, since the electron production and recombination rate have depleted the ionization in the D and E region with a gradual decay in ionization of the F-region due to low level of the density of ions for recombination.

1.9 Equatorial Electrojet

The equatorial region shows unique features because in this region, the Earth's magnetic field lines are almost horizontal and the region is most exposed to the sun's ionizing radiation. Most of the electromagnetic radiations from the sun directed towards the Earth atmospheric surface preferentially arrives the equatorial region (Matsushita, 1967). The enhanced ionization generated due to strong thermal heating in this region provide the unique condition for an enhanced dynamo-generated atmospheric current system that is responsible for the sharp amplification of the solar quiet daily variations, lunar quiet daily variations, and solar flare occurrences in this region (Rastogi, 1992). It is now obvious that the abnormal enhancement of these daily variations in the sunlight hours at the equatorial region is actually caused by overhead eastward current. At the dip equatorial electrojet region where the magnetic and electric field are orthogonal, the resulting upward E X B drift of the electrons generate substantial negative charges at the upper part and positive charges at the lower part of the ionospheric E-region. The electric field caused the electrons to drift westward (eastward) during the daytime (night-time) hours. This westward drift of the electrons cause strong eastward current flow within a narrow latitudinal belt flanking the dip equator principally during the daytime hours named as "equatorial electrojet current" (Chapman, 1951). The intensity of the equatorial electrojet (EEJ) current depend upon several ionospheric parameters such as the strength of the geomagnetic field, electron density, ionospheric conductivity, ambient temperature, eastward electric field (Patil et al., 1990). Studies on the electrical structure of the equatorial electrojet revealed that is highly sensitive to changes even as far as magnetosphere and interplanetary space (Rastogi, 1989). Setia et al. (1980) demonstrated the importance of the equatorial electrojet in the distribution of ionization at low latitudes. Rastogi et al. (1971) concluded that the extension of equatorial eastward field after the

sunset hours create necessary condition for the occurrence of equatorial F-region irregularities.

1.10 Earth Structure and its Major Layers

The Earth has a shape of an oblate spheroid due to the fact that it is slightly flattened at the poles and bulging at the equator (see Figure 1.5). It is structured into three (3) basic layers that differ both in physical and chemical compositions. These layers are: crust, mantle and core.

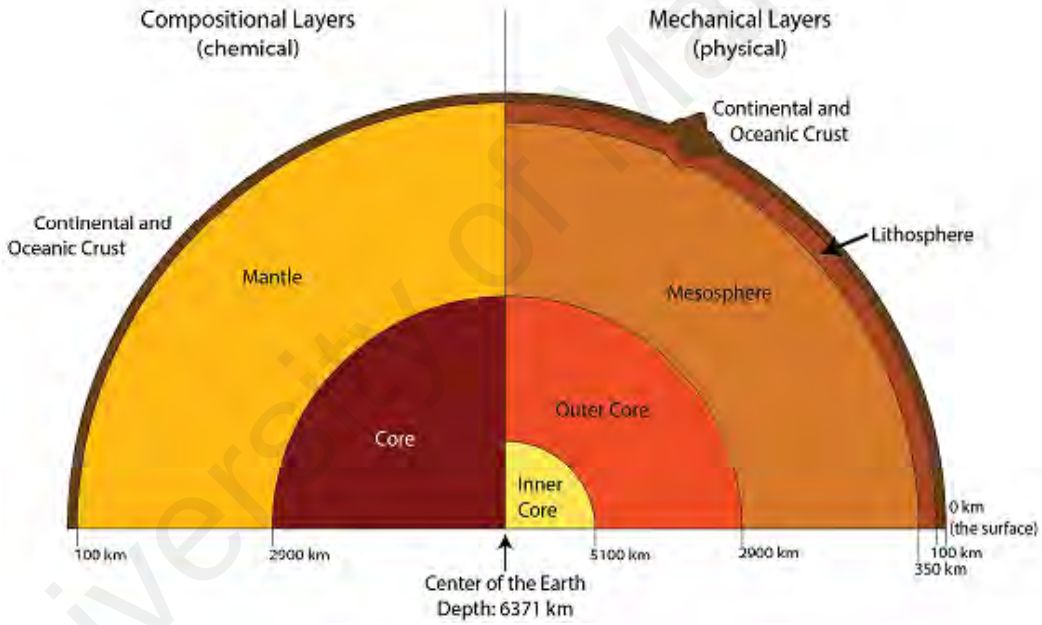

Figure 1.5: Stratification of the Earth's structure source: Meghani, (2016).

1.10.1 The Earth Crust (Lithosphere)

The crust is the solid outer surface of the Earth formed as a result of differentiation and absorption of primeval rock materials from the mantle rock through the dissociation of the melt from the unmelted present mantle rocks (Basavaiah, 2012). The dissociation occurred through a gradual uplift of lighter magma that later formed the solid part of the crust. The crust is composed of aluminium metal most often described as a thin surface

layer with thickness ranging between about 8 and 16 km beneath the oceans and 60-80 km under the mountains. It consist of three layers: sediments, metamorphic and igneous rocks. In any region, one of these layers is lacking. The basalt layer is indispensable and indicate earlier origin while the granite may be of later origin (Subbotin et al., 1965). It has been widely observed that certain regions of the Earth's crust are characterized by low velocity zones. Similar low velocity zone has been detected in the Eastern part of Indian (Kaila et al., 1987). The crustal seismic low velocity zone is regional and not global (Marquis & Hyndman, 1992).

The Earth crust is the most inhomogeneous geosphere and electric currents flow in region with significant lateral conductivity differences such as along the seacoast, in large sedimentary basins and in deep continental rift valleys (Shankland & Ander, 1983). Studies revealed that some regions of the crust exhibit high electrical conductivity that extends into the mantle (e.g., Garland, 1975; Stanley et al., 1977; Ander, 1980). The enhanced electrical conductivity of the crust has been attributed to the presence of water (e.g., Olhoeft, 1981). Graphite in metasedimentary rocks has been found to contribute to the enhanced crustal electrical conductivity (e.g., Alabi et al., 1975; Garland, 1975; Sternberg & Clay, 1977). The crust may be classified into two basic forms differing in composition, thickness and altitude of interfaces: the continental and oceanic crust.

1.10.1.1 Earth Continental crust

The continental crust is the oldest and about 50 km thick. It is made up of igneous rocks that are composed of silicon and aluminium. The average density of the continental crust is about 2.7 g/cm^3 less than the ultramafic materials that makes up the mantle.

1.10.1.2 Earth Oceanic Crust

The oceanic crust is the upper most part of the oceanic portion of a tectonic plate. It is mainly composed of mafic rocks or sima, rich in iron and magnesium. It is about 10 km thick and much denser, having mean density of about 2.9 g/cm^3.

1.10.2 The Mantle of the Earth

The mantle is that region of the Earth's interior between the base of the crust and core, subdivided into two major parts, namely, the upper and lower mantle. It is made up of mostly Fe, Si and Mg in that order (Basavaiah, 2012). The upper mantle extends from the base of the crust to a depth of about 650 km. The most abundant mineral of the upper mantle is the olivine-rich in magnesium and iron content. At depth range between 350 and 750 km in the upper mantle is the transition zone with sharp increase in seismic velocity and electrical conductivity (Campbell et al., 1998). The lower mantle begins at a depth of about 650 km and stretches to a depth of about 2900 km in the core-mantle. The lower mantle is composed mostly of perovskite-rich materials.

1.10.2.1 The Asthenosphere

The asthenosphere is that viscous, ductile and mechanically weak region just beneath the lithosphere in the depth range between 100 and 150 km within the upper mantle. The asthenosphere is almost a solid region, although some of its region such as below the mid-ocean ridges appears as molten (Poirier, 2000). The thickness of the asthenosphere ultimately depends on the temperature of a region.

1.10.3 The Earth's Core

The core is that part of the Earth which is equal to the diameter of the whole Earth and one third (1/3) of its entire mass. It is divided into: inner (solid) and outer (liquid) part.

The characteristic, nature and material content that build up the core are of utmost importance in understanding the dynamics of the internally generated field. Most of the Earth's main field (EMF) is internally generated specifically within the liquid outer core (Basavaiah, 2012). The most common element in the core is iron, which has a density of about 7860 kg/m^3 on the Earth's surface. Due to enormous temperature and pressure conditions of the core, the density increased to a range of about 900 to 12 000 kg/m^3. Besides iron, there are traces of nickel and other impurities in material forms in the core. A discontinuity was earlier proposed within the core at a depth of about 1280 km from the center of the Earth and this clearly distinguishes the inner from the outer core. The inner core is solid in nature with temperature of about 5778 K equal to that of the sun's surface, while the outer core is liquid with temperature much less than that of the inner core (Basavaiah, 2012).

1.10.3.1 The Electrical Conductivity of the Earth Interior

The electrical conductivity of the Earth is a parameter that strongly depends on the physical, chemical and thermal conditions of the Earth's interior. These parameters in the Earth's interior are depth dependent and makes the Earth's interior a region of horizontally stratified layer. Investigation of electrical conductivity of the Earth's interior helps in the characterization of the chemical composition and physical state of the Earth's interior at various depths. It also identifies zones of the crust and upper mantle where tectonic movements and regional metamorphism lead to distinct part of conductivity (Chandrasekhar, 2011). Utada et al. (2003) concluded in their work that the electrical conductivity of the Earth's interior is highly heterogeneous more especially at crustal and upper mantle depths. The crustal plates are in constant motion which is an indication that outer rigid layer known as the lithosphere drift over a weak layer (asthenosphere). The asthenospheric region of the mantle corresponds to region of low velocity and presumably

a zone of partial melting (Campbell, 1987). The mantle is mostly considered to be an embodiment of silicate materials with high magnesium-rich olivine content to a depth of about 400 km-a depth level in which the phase transition of olivine to spinel is anticipated. These silicate materials are insulators at surface temperature but semi-conducting at mantle temperatures. The semi-conduction property is due to the presence of impurities and the existence of free ions and electrons in their crystals lattice (Campbell, 1987).

Generally, a sharp increase in velocity, Mohorovicic discontinuity bounds the crust and the upper mantle. In the mantle at depth between about 100 and 200 km is a zone with seismic low velocity after which a sharp increase in velocity is encountered and continued in steps near the depth of 400 and 670 km. These depths bound the transition zone in the mantle identified with anomalously high electrical conductivity. Research shows that the electrical conductivity in the transition zone and also in the lower mantle are controlled by phase changes in the mineral composition, temperatures as well as chemical composition. However, there are some certain mantle materials that affect the electrical conductivity of the mantle. For example, Laboratory studies revealed that for a certain composition and phase of the mantle materials, the electrical conductivity increases exponentially with increasing temperature (Tozer, 1970). Generally, the temperature of the Earth's interior increases with depth, in similar manner the electrical conductivity also increases with depth (Campbell, 1987). The enhanced temperature and pressure in the mantle depth causes a read-adjustment of the mineral composition and this manifest as phase transition steps in the seismic velocity as earlier identified on seismic records (Anderson, 1967) and the consequence of such effect modify the electrical conductivity as evidently observed beneath Malaysian region (Abidin et al., 2018b).

1.11 Problem Statement

The Earth's magnetic field is undoubtedly a superposition of signals of various sources most of which comes from currents generated in the Earth's core and only a fraction comes from other sources (Yamazaki & Maute, 2017). Among other sources are the currents flowing in the ionosphere and within the Earth's interior (Campbell et al., 1998). During quiet days these currents are generally referred to as solar quiet or simply Sq currents and are responsible for the regular geomagnetic field variations at the ground surface (e.g., Pedatella et al., 2011). The Sq current has been extensively studied from single and few geomagnetic observatories but its external and internal currents with their fields have not been given much adequate attention possibly due their smaller amplitudes. Some of the early works on the external and internal currents with their associated fields includes the works of (Campbell & Schiffmacher, 1985; 1988; Campbell et al., 1998). Knowing that the ionospheric conductivity is relatively a complex function of both latitude and longitude (Kamide et al., 1981), the extent of variations of both external and internal field with latitudes, day of the year, seasons and solar activity remain a challenge to the ionospheric community hence the need for this study. Several works have been carried out on the application of Sq. Among such works includes determination of baseline for geomagnetic indices (Mayaud 1980; Love & Gannon, 2009) for monitoring solar radiation activity (Svalgaard & Cliver 2007; Svalgaard, 2016) and only few works have been actually carried out on the application of Sq current on electrical conductivity of the deep Earth probably due to large data set and complex mathematical procedure that are required. The most recent ones are the works of (Obiora et al., 2016) in the African sector during low solar activity and the knowledge on the conductivity of the mantle from dip minimum to moderate solar activity is obscured. On this regard this work determine for the first time whether the intensity of Sq current system during dip minimum, low and

moderate solar activity has any significant effect on the electrical conductivity of the deep Earth.

1.12 Research Objectives

This study incorporate the striking features of the upper atmosphere and that of the Earth interior:

i) To determine the monthly latitudinal variability pattern of the external, internal and sum (total) of the quiet field variations from the dip minimum to moderate solar activity.

ii) To determine the behavioral pattern of the Sq current system (both external and internal) during different solar activity years.

iii) To determine for the first time the conductivity-depth profile of the Earth mantle from the dip minimum to moderate solar activity.

1.13 Structure of the Thesis

- Chapter 1 provides a general overview on the concept of ionosphere, various current systems, stratification of the Earth's interior, challenges facing the ionospheric community and the objective of this study.
- Chapter 2 generally review some of the past works on Sq current from other regions of the world and its application in determining electrical conductivity of the Earth's interior. This section also review the relations between the electrical conductivity of the Earth interior estimated from Sq current system with seismic discontinuity and velocity of the mantle.
- Chapter 3 focuses on data selection and data analysis procedures to achieve the set objective of this work.

- Chapter 4 present the results and discussion on some of the phenomena associated with the external and internal currents and their associated fields and conductivity-depth profile of Asia sub-region from dip minimum to moderate solar activity.
- Chapter 5 provide detail discussion of the features, responses of the Sq current system with their fields to the latitudinal variability and increasing solar activity. It also gives a detail discussion of the mantle conductivity with increasing solar activity. The possible reasons for the observed features in chapter 4 are also discussed.
- Chapter 6 draws a conclusion on the major findings in this study and future work.

CHAPTER 2: LITERATURE REVIEW

2.1 Review on Solar Quiet (Sq) Current System

Everyday currents are generated through a dynamo process in the E-region of the ionosphere. The basic theory is that wind of global scale and solar thermal heating origin transport conductive particles across the main field of the Earth, hence generating an electromotive force (EMF), establishing electric fields and currents (Chapman & Bartels, 1940; Pedatella et al., 2011; Richmond, 1979; Richmond et al., 1976). The apparent manifestation of the electric current is the existence of geomagnetic daily field variations at the ground surface earlier identified by (Schuster, 1889; 1907). The current generated through the dynamo process exhibit peak amplitudes between 90 and 180 km owing to the considerable Pedersen and Hall conductivities at these height range (Pedatella et al., 2011). During days when solar magnetic disturbances are minimal, the current generated through the dynamo process is called solar quiet or simply 'Sq current' and the field associated with it is called solar quiet or Sq field. The field exhibit smooth and regular variations between magnetic latitudes ~60 °S to 60 °N, indication that the Sq current system are dominant within this latitude range beyond which are affected by auroral activities (Vichare et al., 2017). The Sq current system flows in a systematic pattern in northern and southern hemispheres. At the northern hemisphere it flow counter-clockwise direction and flowing clockwise in the southern hemisphere. The center of these current vortex is most often times referred to as the Sq current focus. The common characteristics of the Sq current system is its conspicuous seasonal and solar cycle variations. Differences in ionospheric conductance and wind systems caused the Sq current to be hemispherically asymmetric with greater (weaker) intensity of currents in summer (winter) in consonance with the level of ionization (Pedatella et al., 2011). The current intensity in the summer has been attributed to be approximately three times larger than the winter hemisphere (Yamazaki & Maute, 2017). Most at times the summertime Sq

current vortex has been observed to penetrate into the winter hemisphere (Campbell et al., 1993). Such intrusion into the winter hemisphere is only possible through the field-aligned currents (FACs), (Fukushima, 1979); meridional currents (Mazaudier & Venkateswaran, 1985) or the antisymmetric tides earlier described by (Stening et al., 1989).

The entire strength and structure of the Sq current is mainly controlled by ionospheric and tidal winds of the dynamo region. Studies have shown that significant day-to-day variability exists in the Sq current system even among similarly quiet days (e.g., Stening et al., 2005). Many research workers have observed conspicuous day-to-day variability both in intensity and structure of the Sq current system (Mayaud, 1965; Stening, 2008; Suzuki, 1978, 1979; Takeda, 1984; Takeda & Araki, 1984). Various mechanisms have been employed to explain the obvious day-to-day variations of the Sq current system. For instance (Miyahara & Ooishi, 1997) by means of numerical simulation study, investigated the effect of neutral winds on the ionospheric dynamo and found that waves propagating from below contributes substantially to the daily variations of the dynamo generated current during most of the quiet days. Kirchhoff & Carpenter (1976) and Rastogi, (1993) observed that changes in the daily variations of Sq current at low latitude is due to combined effect of both ionospheric conductivity and wind system. In addition to the (1, 2) tidal mode known as the major contributor to the Sq current, other tidal modes such as the (2, 2), (2, 3) and (2, 4) influence the Sq current to some extent causing fluctuations in the intensity and structure of the current system (Brown & Williams, 1969; Malin, 1973; Matsushita, 1967; Winch, 1981). Observations have shown that the intensity of the Sq current is about twice as large during maximum solar activity than the minimum (Takeda, 1999; 2002b). The variations in the magnitude of Sq current between maximum and minimum solar activity is established as a result of the linear relationship existing between

ionospheric conductivity and solar flux. This variation has been attributed to changes in ionospheric conductivity (Takeda, 2002b). Rastogi (1993) reported that the variations of Sq current is mainly due to corresponding changes in the ionospheric E-region ionization density during the epoch.

Campbell (1989) and Matsushita (1967) observed that the shape and strength of the Sq current system exhibit longitudinal variability. The main field of the Earth, **B,** which varies with longitude modulates **U X B** field and ionospheric conductivity resulting in longitudinal variation of the dynamo generated currents (Le Sager & Huang, 2002). Stening (1971) reported that the longitudinal variations in the intensity of the Sq current arise from the longitudinal variations of the Earth's main magnetic field. In addition to longitudinal variation, the focus of the Sq current system show latitudinal variations. Stening et al. (2005) used array of data from Australian, Japanese and Pacific regions and observed meridional movement of the Sq current focus from one quiet day to another. Matsushita (1960) and Shiraki (1972) studied seasonal variations of focus latitude in North America and West pacific region. Their results show that the focus latitude in summer are higher than in winter. Matsushita and Maeda (1965) examined the Sq current vortices using the global IGY geomagnetic data stations distributed around the globe which they grouped into three zones: zone 1 (Europe-Africa), zone 2 (Asia-Australia) and zone 3 (North-South America). They observed higher latitudinal position of the external current center in summer than in winter hemisphere in the southern hemisphere for all the zones with similar appearance only at zone 3 in northern hemisphere. In contrast to these observations (Patil et al., 1985) examined the focus position in India-Russian region and found that the latitudinal position of the focus is higher in winter than in summer and equinoxes. Stening & Winch (2013) applied spherical harmonic analysis technique and found that the northern focus shifts towards lower latitudes in September and moves

closer to the equator in December. Vichare et al. (2017) recently observed the latitudinal variations of the Sq current focus along Indo-USSR region and observed that the focus is slightly poleward in winter than in summer and drops to less than 20° near September. Takeda (1990) reported that the difference in the latitude of the Sq current focus between the summer and winter hemisphere may be due to difference in the winds between both hemispheres. The Sq current vortices in winter are reported to occur at earlier and later local time in summer and winter hemisphere (e.g., Takeda, 2002b; Yamazaki et al., 2011). Such movement of the Sq current vortex could be due to the magnetic effect of field-aligned currents that is flowing from the vortex center in winter to the summer hemisphere (Fukushima, 1979; Takeda, 1982; Abidin et al., 2018a).

2.2 Review of the Electrical Conductivity of the Earth's Interior Due to Solar Quiet (Sq) Current System

Ionospheric current define mainly as the current flowing in the conductive layer of the upper atmosphere (Ionosphere) generated when global prevailing wind system of solar thermal heating origin transport conductive particles across the main field of the Earth. Early observations revealed that the Sq current flow into the conductive Earth structures and the extent to which it penetrate depends upon the effective wavelength of the source current and the conductive properties of the Earth's interior (Chapman, 1919). Over a century ago that Gauss applied the spherical harmonic analysis (SHA) technique to the global data on the Earth surface. He reported in his general theory of terrestrial magnetism that most of the Earth's main field originates from internal sources. Years later (Schuster, 1889) applied the spherical harmonic analysis (SHA) to the Earth magnetic field and presented for the first time an information on the electrical conductivity of the deep Earth. He uniquely separated the observed Sq fields into their internal and external origin and showed that larger part of the Sq field comes from external origin with the assumption

that the other smaller part originate from electric current induced into the conducting Earth structure by the source field. With the help of Lamb's theory, he further clarify that both field co-exist on the Earth surface and assumed the induced part correspond to the fluctuating current in a uniformly sphere of radius *r* that is much less than that of the Earth.

On the basis of this (Chapman, 1919) performed the first quantitative estimate of the electrical conductivity of the Earth's interior using the separated external and internal field. He found that the field associated to internal origin arise from currents induced into the conducting Earth by the source field of radius qR_e and having conductivity $k=3.6 \times 10^{-3}$ e.m.u. However (Chapman & Whitehead, 1923) investigated the possible effect of the oceans and other conductive strata on the Earth conductivity and found no any substantial influence of oceans on the Earth conductivity due to the fact that the ocean are interrupted by land masses as such the intensity of the current induced in them is greatly reduced. Chapman & Price (1930) used fields during the disturbance storm time (Dst) and showed that the current induced into the conducting Earth's interior during this period penetrate deeper than those of quiet periods. They concluded that the conductivity of the Earth increases with increasing depth but the precise increase was not known due to limitation of their model. Later (Lahiri & Price, 1939) constructed a model that successfully account for the actual amount of fields induced during quiet and disturbance storm time (Dst) but could not also account for the precise increase in conductivity with depth. One feature common to these models is that they indicate that a fairly high electrical conductivity bound the sub-surface area and beyond a certain depth limit, the conductivity of the Earth rapidly increases with depth and steepen at depth range between 400 and 800 km, as earlier discussed by (Price, 1970).

Based on this (Rikitake, 1950; Rikitake, 1966) deduced the conductivity-depth profile for several types of variations including Sq and Dst variations. He observed that for each variation, the conductivity rises from about 10^{-12} e.m.u at 400 km depth to 10^{-11} e.m.u at 1200 km depth. Rikitake's result certainly support the general conclusion from previous models that somewhere beneath the base of the upper mantle, the conductivity increases most rapidly with depth till at about 800 km. He interpreted this rapid increase to phase changes in the mantle materials such as olivine-spinel transformation which is mostly associated to sudden increase in conductivity. Research workers have also used secular variations to estimate the conductivity of the mantle beneath the crustal surface. For instance, from secular studies (Runcorn, 1955) obtained conductivity values between 10^{-9} and 10^{-8} e.m.u at lower half of the mantle.

McDonald (1957) further elaborates on the penetration of the secular variation field into the lower mantle with an assumption of variable conductivity of the Lahiri-Price form and obtained the conductivity distribution for the lower mantle. Schmucker (1970, 1987) provided set of equations for describing the deep Earth conductivity with a transfer function that utilizes the separated external and internal spherical coefficients for a given location. This transfer function to a large extent provided the required depth equal to the substitute conductors that would produce the needed electromagnetic response of the conducting Earth's interior to the field from external source.

Campbell & Anderssen (1983) used array of geomagnetic field records for the solar quiet year 1965 to estimate the electrical conductivity profile beneath the North American sector. They employed spherical harmonic analysis (SHA) technique and Schmucker's modified transfer function for substitute conductor was then applied to the separated external and internal harmonic coefficients to deduce the electrical conductivity profile

beneath this region. Their work yielded conductivity values in the depth range between 140 and 540 km that may be represented by $\sigma = 0.0067e^{0.007d}$ where d denote the depth in kilometers. They observed small perturbations in the conductivity which indicates some layering at 140-220, 220-400, and 400-600 km depth that match the absolute characteristics of the Earth's density in these depth intervals. Campbell & Schiffmacher (1986) examined the electrical conductivity properties of the upper mantle beneath North America, Europe, Central and East Asian sectors utilizing the 24-, 12-, 8-, and 6-hrs spectral component of the quiet field variations for each sector. They applied Schmucker's equivalent substitute conductor technique and obtained conductivity values to a maximum depth of about 600 km. These authors observed differences in the conductivity structure of the Earth interior with higher values in the North America at depth above 275 km while in the East Asian sector they observed higher values below 300 km depth.

From array of magnetic observatories distributed over southern Australia (Campbell & Schiffmacher, 1987) applied the generalized form of Schmucker's transfer function on the separated external and internal Sq current and obtained the conductivity profile between 250 and 550 km depth. They observed a steady composition slightly above 250 km and a change in the mineral composition near 325 to 375 km resulting into break in conductivity values at this depth range after which a steady composition was observed to a depth of about 540 km. In the southern Australian region (Campbell et al., 1998) observed similar break in conductivity values but deeper into the Earth's interior at depth range between 470 and 800 km. The southern conductivity profile agrees closely with the southeast Australian conductivity to a depth of about 250 km as earlier estimated by (Lilley et al., 1981a, 1981b; Woods & Lilley, 1979). Campbell & Schiffmacher (1988) applied SHA to the quiet field records of 1965 over seven subcontinents and their results

showed high conductive region at depth range between 100 and 200 km in Europe, Central Asia and South American sectors while Africa and East Asia had no evidence of increased conductivity at shallow depths. At this depth range (Jones, 1983) earlier observed high conductivity beneath the Fennoscandian region. The monumental work of (Campbell & Schiffmacher, 1988) over the seven subcontinental regions of the Earth shows apparent increase in conductivity profile at depth range between 150 and 350 km in Europe. Similar increase was also reported beneath the Himalayan, southern Australian and West African region (Arora et al., 1995; Campbell et al., 1998; Obiora et al., 2015). These authors reported that such increase does not match any specific discontinuity but it does correspond to the highest depth at which the roots of old continent in the mantle are detectable in seismic records.

Campbell & Schiffmacher (1988) observed rapid increase in electrical conductivity at depth below 400 km in the African and Central Asian region while South American region showed the least conductivity values. Similar increase was observed beneath Himalayan and North Central region of Nigeria (Arora et al., 1995; Obiora et al., 2015). Such increase is similar to the global models that indicate increase in electrical conductivity at depth interval of 400 to 800 km and depict phase transition of mantle materials from olivine to spinel structures as earlier discussed by previous research workers (e.g., Adam, 1980; Arora et al., 1995; Campbell et al., 1998; Omura, 1991; Schultz & Larsen, 1990). Results from array of geomagnetic observatories in India by (Chandrasekhar, 2011) showed that the electrical conductivity profile of the upper mantle beneath the region is bounded by inhomogeneous layers to a depth of about 400 km in consistent with the earlier global conductivity models of the upper mantle (Kelbert et al., 2009; Kuvshinov & Olsen, 2006). The profile showed a well resolved high conductivity at depth range between 125 and 150 km beneath Indian region similar to what was

observed beneath Central Europe and Central Asia (Campbell & Schiffmacher, 1988) hence suggest lithosphere-asthenosphere boundary.

The sharp increase in electrical conductivity at depth ranges between 350 and 500 km beneath Central Asia and Africa was earlier estimated (Campbell & Schiffmacher, 1988). Similar profile was also observed in North Central region of Nigeria (Obiora et al., 2015). Campbell & Schiffmacher (1988) reported that the apparent phase transition steps in seismic records occur at depth level where enhanced temperatures and pressure cause readjustment of the mineral composition. Such transition and modification should of course reflect on any realistic conductivity depth profile as evident at depth range between 400 and 800 km. Campbell & Schiffmacher (1986) worked on the upper mantle sub-continental electrical conductivity for North America, Europe and Asia, they had evidence for discontinuities near 255-300 km and at 450-600 km. These depths are near phase change earlier identified on seismic records by (Dziewonski & Anderson, 1981).

2.3 Electrical Conductivity Profiles Estimated from Sq Current System and Their Relations to Seismic Discontinuity and Velocity Within the Mantle

Arora et al. (1995) used magnetic records distributed in Himalayan region to estimate the electrical conductivity profile. The SHA process used spherical polynomials up to degree n=23 and order m=6. Schmucker's transfer function was then applied and yielded about 152 conductivity values at depth range between 50 and 470 km. They observed a gradual increase of the conductivity profile from the sub-crustal surface to a peak of about 0.06 S/m near 125 km depth followed by a minimum of about 0.04 S/m near 210 km depth with second peak of about 0.07 S/m near 275 km. Mechie et al. (1993) used peaceful nuclear explosion to model the mantle velocity beneath northern Eurasia. Based on the propagation of Pn-waves, those authors identified two basic layers separated by about 30-

40 km thick transition zone. The upper zone through which the Pn-waves with velocity of 8.1-8.3 km/sec propagate extends down to a depth of about 100-140 km. The second layer which starts at about 130-140 km depth and extend to about 200-250 km depth overlie a region of low velocity (8.3-8.5 km/sec). This low velocity zone extend to a depth of about 300 km. The transition zone with depth range of about 100-140 km has a low velocity of 8.1-8.3 km/sec and the second low velocity zone is at depth of about 200-300 km all of which match well with the high electrical conductivity zones observed in the Himalayan region (Arora et al., 1995). Another velocity depth model established by (Beghould et al., 1993) beneath Tibetan plateau indicate low velocity zone that is centered at 275 km depth which is in excellent agreement with high electrical conductivity profile reported beneath the Himalayan region (Arora et al., 1995). Earlier surface depression studies by (Mitchel, 1987) showed layer of low velocity for the S-waves at a depth range of 100 and 110 km beneath the Himalayan region which coincides with the asthenosphere identified with the high electrical conductivity. This agrees with the high electrical conductivity at depth of about 125 km beneath the Himalayan region (Arora et al., 1995).

In a similar study (Graves & Helmberger, 1988) used old pacific (PAC) obtained from waveform modeling of long-period multi-bounce SH-waves and found a low velocity zone in the depth range of about 75-225 km. At these depth ranges, an evidence of discontinuity in electrical conductivity profile was observed beneath North Central region of Nigeria (Daniel & Francisca, 2013; Obiora et al., 2015). Anderson (1979) and Douglas (1986) earlier suggested that the discontinuity at a depth of about 220 km represents the boundary in which phase transition of garnet iherzolite to eclogite occur. This suggestion was further clarified by (Leven et al., 1981; Revenaugh & Jordan, 1991). These authors reported that the transformation would not cause any significant discontinuity if likely iron content in the eclogite is put into consideration. Vidale & Benz (1992) proposed that

the discontinuity at depth of ~220 km represent the base of a partially molten layer and this seems not to hold in the continental shield where little or no partial melting is expected (Karato, 1992).

Campbell & Schiffmacher (1988) earlier reported that the systematic phase transition observed in seismic velocity occur at depth levels in the mantle where enhanced temperature and pressure cause the mantle mineral composition to readjust. Such readjustments modify any realistic electrical conductivity-depth profile. Campbell & Schiffmacher (1986) used spherical harmonic coefficients of Sq field over North America, Europe and Asia to determine the equivalent electrical conductivity profile beneath these three continental regions and the result shows a gradual increase of conductivity with increasing depth from about 30-650 km with some evidence for discontinuities near 225-300 km and also near 450-600 km. Lilley et al. (1981a, 1981b) estimated electrical conductivity profile beneath Southeast and Central Australian region. Their Central Australian profile indicates changes near 100 and 200 km and also near 450 and 600 km. Obiora et al. (2015) recently estimated the electrical conductivity profile beneath the North Central region of Nigeria. The SHA procedure extended for polynomial coefficient of degree n=12 and order m=4 and the analysis yielded conductivity values at a depth range between about 50-1100 km. The conductivity profile showed an evidence of discontinuity at depth range between 214-420 km and 420-640 km. Also similar discontinuities were observed at depth of 350-390 km and 610-680 km beneath the Malaysian region (Abidin et al., 2018). These observations are similar to earlier report by (Campbell et al., 1998) that showed major mantle discontinuities occur in the transition zone at depth between 350 and 750 km. These depths range correspond to region with abrupt rise in seismic velocity as earlier identified in the Preliminary Earth Model (PREM) by (Dziewonski & Anderson, 1981; Kennett & Engdahl, 1991). These locations

are near phase transition depths of the mantle mineral composition earlier identified on seismic records by (Dziewonski & Anderson, 1981).

The mantle electrical conductivity profile estimated using the separated Sq current system in West African sub-region by (Daniel & Francisca, 2013) gave evidences of discontinuity in the electrical conductivity profile near these depths (71-165 km). They correlated their electrical conductivity profile with the velocity-depth profile earlier determined from seismic records averaged over the entire Earth by (Dziewonski & Anderson, 1981). They observed a general correspondence with less steep increase in conductivity at depth range between 71 and 165 km with anomalously high seismic velocity. The electrical conductivity profile beneath North Central region of Nigeria by (Obiora et al., 2015) shows a sharp rise in electrical conductivity at the depth range between 100 and 230 km. Also, similar high electrical conductivity was observed at depth range between 125 and 150 km beneath Indian region (Arora et al., 1995). Campbell & Schiffmacher (1988) used quiet geomagnetic field records of 1965 to estimate the conductivity profile beneath seven sub-continental regions that includes Central Europe and Central Asia. Their profile indicates high conductivity values at depth above 300 km in Central Europe and Asia. These depths correspond to zone or region of global seismic low velocity as identified on seismic record (Dziewonski & Anderson, 1981; Kennett & Engdahl, 1991).

Campbell et al. (1998) used Australia-Wide Array of Geomagnetic Stations (AWAGS) to estimate the electrical conductivity profile beneath this region. They observed high electrical conductivity profile at depth range of about 150 and 350 km. similar high electrical conductivity profile was also reported in the West African sub-regions (Daniel & Francisca, 2013; Obiora et al., 2015; Obiora et al., 2014). Such increase

in electrical conductivity through the upper mantle down to its base at 350 km match the highest depth at which the roots of old continents in the mantle are detectable in seismic records (Campbell et al., 1998). From similar study (Campbell & Schiffmacher, 1987) used array of geomagnetic field records distributed over southern part of Australia to determine the conductivity profile beneath this region. They applied Schmucker's transfer function for substitute conductor to the separated external and internal spherical harmonic analysis coefficients and deduced the electrical conductivity in the depth range 200 to 600 km. They observed a clear break in conductivity values at depth range between 325 and 375 km. Earlier (Goncz & Cleary, 1976) used Raleigh wave seismic velocity beneath Australian region and reported constant velocity at this depth range, (200-400 km).

2.4 General Overview on the Electrical Conductivity and Mineral Composition of the Earth Structure

The Earth's interior consists of the crust, mantle and core that differ in their physical and chemical compositions and are also subjected to different temperature and pressure. Studies revealed that some regions of the crust exhibit high electrical conductivity that extends down to the mantle (e.g., Adam, 1980; Garland, 1975; Jiracek et al., 1979; Stanley et al., 1977). Magnetotelluric study beneath the south East Pacific rise shows an enhanced electrical conductivity profile that is strongly anisotropic near mid-ocean ridge (Evans et al., 2005). Various mechanisms have been suggested to be responsible for the anomalous electrical conductivity of the crust. For example (Drury & Hyndman, 1979; Hyndman & Hyndman, 1968; Olhoeft, 1981) attributed the anomalous crustal conductivity to presence of water with high ionic content. Alabi et al. (1975) and Stesky & Brace (1973) attributed their responses to magnetic oxides and graphite. Studies have also shown that lateral variations of electrical conductivity are quite large at shallow depths and become smaller as the depth increases. Seismic velocities also exhibit similar lateral variations at the same

depth range which may be due to differences in petrology, temperature or crystal orientation as earlier identified on seismic records (Nataf et al., 1984).

The asthenosphere is regarded as a weak layer located just beneath the lithosphere at a depth range between about 100 and 220 km and dominated by geophysical anomalies such as strong attenuation of seismic waves (Yoshino & Katsura, 2013). Seismologically, this region has been identified with low velocity and distinct high electrical conductivity (e.g., Baba et al., 2010; Evans et al., 2005; Lizarralde et al., 1995). Yoshino et al. (2006) reported that the oceanic asthenosphere is highly conductive and anisotropic in some locations. They attributed the anisotropic nature of the electrical conductivity to olivine hydration.

Various suggestions have been put forward to explain the high electrical conductivity of the asthenosphere. For example, a petrological study has earlier shown that melts are thermodynamically stable in the asthenosphere due to traced volatile components such as H_2O and CO_2. These traced elements are also responsible for the enhanced electrical conductivity of the asthenosphere (Shankland & Ander, 1983). Evidences have emerged that partial melt exist in the global seismic low velocity zone (asthenosphere) and this enhances the electrical conductivity of the zone as widely reported by research workers (e.g., Shankland et al., 1981). Laboratory experiment (Hirth & Kohlstedt, 1996; Karato & Jung, 1998) confirmed its existence and also attributed the enhanced electrical conductivity to partial melt and olivine hydration.

Olivine is known as the most abundant and major constituent of the mantle rocks, unstable at high temperature and pressure, indication that the mineral composition of the mantle changes with increasing depth (Katsura & Ito, 1989; Xu et al., 1998). Laboratory

and geophysical observations extensively discussed that olivine undergo phase changes to much denser structure under high pressure that is equivalent to about 390-450 km depth and also at about 750 km depth (Fowler, 1990). Ito & Katsura (1989) and Xu et al. (1998) extensively discussed that the phase transition of olivine (α – phase) into wadsleyite correspond to a discontinuity at depth of ~410 km. Similarly, the transition from wadsleyite to ringwoodite (γ – Phase) correspond to discontinuity at depth of 520 km which is not globally observed (Deuss & Woodhouse, 2001).

The dissociation of the Ringwoodite to yield (Mg,Fe) Si O_3 perovskite and magnesiowustite within the mantle is much consistent with the discontinuity at depth of 660 km (Ito & Takahashi, 1989; Xu et al., 1998). Ito & Katsura (1989) reported that the α-phase transformation of olivine to β- and γ- phases is primarily responsible for the much reported discontinuous changes in the Earth's mantle electrical conductivity. The discontinuities at depth of 410 and 660 km uniquely bound the transition zone generally identified with high electrical conductivity (Utada et al., 2003). Ohtani & Sakai (2008) and Wood (1995) reported that the presence of hydrous wadsleyite and hydrous ringwoodite in the transition zone cause the mantle to be a water solubility zone. These minerals which are major constituents of the mantle transition zone are able to store water of more than 2 w% suggesting that the transition zone is the most abundant water reservoir on Earth (Ohtani & Sakai, 2008).

Karato (1990) used geophysical observations and reported that the presence of water even in small quantity can strongly influence the electrical conductivity of the mantle. Laboratory experiment (Nishihara et al., 2003) is consistent with the geophysical observation that the enhancement of the electrical conductivity in the transition zone is mainly controlled by the presence of water. Civet et al. (2015) used the swarm satellite

field measurements to study the electrical conductivity of the mantle and found that it depends on the internal structure through the pressure, temperature, oxygen fugacity and composition. They further clarify that the Earth mantle composition may not necessarily be its mineral content but also the chemistry of the phase such as the ionic content and minor phases like partial melt and water.

Schock et al. (1989) and Yoshino & Katsura (2009) reported that the increase in electrical conductivity with increasing temperature demonstrate the enhancement of the activation enthalpy indication of increase in ionic conduction mechanism in the olivine at high temperature condition. Results beneath the north-eastern China (Ichiki et al., 2001) showed high electrical conductivity in the transition zone caused by water released from a stagnant slab. Xu et al. (1998) found that the increase in conductivity at a depth of 410 km discontinuity which correspond to the olivine-wadsleyite phase transition is of order 2 while that of wadsleyite to ringwoodite transition at depth of about 520 km is minor with anticipation that the conductivity at 660 km discontinuity to be very small. Yoshino & Katsura (2013) reported that the mantle beneath Philippine Sea and Central China possessed a descending slab stagnates at the transition zone with incredibly high electrical conductivity than those of Europe or Canada. The discrepancies in electrical conductivity of the transition may be due to variation in water content, temperature and other conductive materials (Abidin et al., 2018b). Magnetic studies have equally shown lateral heterogeneities exist in electrical conductivity of the mantle transition zone (e.g., Booker et al., 2004; Ichiki et al., 2001; Kelbert et al., 2009). Olivine and wadsleyite that are considered the chief mantle constituents exhibit significant differences in their electrical conductivity due to variations in the amount of water content in them (Yoshino & Katsura, 2013).

Shankland & Waff (1977) earlier reported that the solidus of mantle materials also triggers partial fusion deep down into the Earth thereby increasing electrical conductivity of the Earth's mantle. Zharov (1983) theoretically predicted a conductive layer at depth range between about 700 and 900 km. This conductive layer was later detected using magnetic data from Magnetovariation soundings (Roberts, 1984; Schultz & Larsen, 1987; Semenov, 1989). Rotanova et al. (1993) used MAGSAT satellite data to confirm the existence and global features of this conductive layer. Lateral variations of this conductive layer on global scale have been reported by various research workers (e.g., Schultz & Pritchard, 1999; Semenov & Jozwiak, 1999).

The 1-D electrical conductivity profile of the Earth's mantle derived using swarm satellite magnetic field data showed an increase in conductivity from ~0.001 S/m at a depth of 400 km to about 10^{o} S/m at 900 km depth. This increase in electrical conductivity may be associated to the mineralogical phase transformation of the upper mantle into their lower mantle phases as earlier identified by (Xu et al., 2000). Schultz et al. (1993) reported that this smooth monotonic increase in conductivity is much consistent with most models that showed abrupt jumps in upper to mid-mantle conductivity. The result of the amplitude and phase characteristics of the 27, 13 and 9-day geomagnetic field variations distributed over Europe shows that the electrical conductivity beneath northern Europe increases at depth of about 1000 km (Pecova et al., 1980). In a similar study (Roberts, 1986) concluded that conductivity zones may vary in depth from about 600 km in north-western Europe to about 800 km in the southern part. 1-D electrical conductivity beneath mid-mantle in Europe-Asia region shows a slow increase in conductivity from ~1.0 S/m at 1000 km depth to about 10 S/m at 1900 km, after which the conductivity increases much faster in the depth range of 1900-2100 km as estimated by (Semov & Jozwiak, 1998).

Results from modern geoelectric sounding shows high electrical conductivity at the base of the mantle located below the depth of 2100 km. The electrical conductivity of the lower mantle has been determined using electromagnetic induction and internal source method (McDonald, 1957; Kolomyceva, 1972); Shankland & Ander, 1983). Results revealed that the conductivity of the lower mantle varies by more than 3 order of magnitudes at a depth range of 1000 to 2900 km. Based on the results of the C-response for a period of 6 and 300 hrs (Olsen, 1998) shows that there is a general increase of the R$\{C\}$ which may likely indicate lower conductivity in the north.

CHAPTER 3: METHODOLGY

3.1 Application of Spherical Harmonic Analysis (SHA)

Spherical harmonic analysis (SHA) is a special technique of modelling certain quantity that varies with position located on the surface of a sphere. The technique is used to describe geomagnetic field around the globe such that its harmonics are employed to model the three basic orthogonal components (H, D and Z) of the magnetic field. It uses harmonic functions that satisfy Laplace's boundary equation in a spherical coordinates (Brett, 1988; Yamazaki & Maute, 2017). The harmonic function (a model) is obtained data distributed globally in a way that the difference between the model and observations is negligibly small. The concept of spherical harmonic analysis is analogous to Fourier series for variations in time but the SHA uses a 2-D model (i.e. a function of latitude and local time) (Yamazaki & Maute, 2017). The mathematical procedure for the SHA was first introduced into geomagnetism by (Gauss, 1841). Schuster (1889, 1907) used it for the first time to model the solar quiet (Sq) field. The analysis technique allows estimating equivalent current system responsible for the Sq field at the Earth surface. The outstanding feature of the SHA is that it uniquely separate Sq fields into their external and internal parts according to their origin and this led the early scientists to conclude that the larger part of Sq field variations at the ground surface originates from sources external to the Earth's surface (Schuster, 1889; 1907).

To describe the Sq field using spherical harmonic analysis (SHA) several methods are used but the most basic ones are the 'instantaneous method' and 'slice method'. The instantaneous method is employed specifically to estimate the Sq field and the equivalent current system at a specific moment in time using magnetic field records distributed across the sphere (Malin & Gupta, 1977; Suzuki, 1978; Takeda, 1999, 2002a, 2002b; Takeda & Araki, 1984). This method makes use of wide range of simultaneous

measurements that are globally distributed. It is particularly useful when measurements are available over a spherical surface of the Earth (Yamazaki & Maute, 2017). The slice technique is apply when magnetic stations are distributed along the north-south region (hemisphere) with an assumption that the 24 hours of the Sq field variation represent 360° of longitudinal variation in accordance to (Cambell & Schiffmacher, 1988; Campbell & Schiffmacher, 1985; Kawasaki et al., 1989; Matsushita & Xu, 1982; Yamazaki et al., 2010; Yamazaki et al., 2011). Campbell (1990) compared results from the instantaneous method and slice method and found a good agreement exist between the two methods. The latter method (slice method) is employed in this study. In SHA, the mathematical concept originates from Maxwell's steady-state equations for the magnetic field **B**, given as;

$$\nabla . \boldsymbol{B} = 0 \tag{3.1}$$

$$\nabla \times \boldsymbol{B} = \mu_{\circ} J \tag{3.2}$$

where $\mu_{\circ}$ is the magnetic permeability of free space and J represents the current density. When the sources of magnetic field are assumed to be absent in the region under consideration, then

$$\nabla \times \boldsymbol{B} = 0 \tag{3.3}$$

The field B can be expressed using the magnetic potential *V*, as;

$$B = -\nabla V \tag{3.4}$$

Equations 3.1 and 3.4 yield;

$$\nabla^2 V = 0 \tag{3.5}$$

Equation 3.5 is called the Laplace's equation which in spherical coordinates with its source at the Earth's center can be expressed as;

$$\frac{\partial}{\partial r}\left(r^2 \frac{\partial V}{\partial r}\right) + \frac{1}{sin\theta}\frac{\partial}{\partial \theta}\left(sin\theta \frac{\partial V}{\partial \theta}\right) + \frac{1}{sin^2\theta}\frac{\partial^2 V}{\partial \phi^2} = 0 \tag{3.6}$$

In which r, θ and ϕ represent the radial distance, colatitude and longitude. The magnetic potential is associated with the orthogonal components of the magnetic field as given in the relation below;

$$X = \frac{1}{r}\frac{\partial V}{\partial \theta}, \qquad Y = \frac{-1}{rsin\theta}\frac{\partial V}{\partial \phi}, \qquad Z = \frac{\partial V}{\partial r} \tag{3.7}$$

Equation 3.6 has a general solution that is compose of two essential parts as given in the equation below;

$$V = (r, \theta, \phi) = C + V_{ext}\ (r, \theta, \phi) + V_{int}\ (r, \theta, \phi) \tag{3.8}$$

where C, θ, r and ϕ represent constant of integration, geomagnetic colatitude, Earth's radius and local time of the station.

3.2 Data Selection

In the data selection, the first criteria adopted to ensure good and quality data are used was to select days in which the geomagnetic disturbance index Kp values are not greater than 3 as earlier suggested (e.g., Campbell et al., 1998). These values are obtained as published from the world data center Catalogue for the year 2008, 2012 and 2017 at

(Sakyo-ku, 2017). These years are chosen based on their annual sunspot numbers (R_z) that are minimum 2.9 in 2008, moderate 57.6 in 2012 and low 21.7 in 2017. These years allowed the determination of Sq current and upper mantle conductivity from the deep minimum to moderate solar activity. To avoid severe magnetic activities, days with $Kp \leq 3$ were carefully selected and this yielded a total of 27, 18 and 21 days for the years 2008, 2012 and 2017 respectively. These days have least solar-terrestrial magnetic disturbances, thus represent the Sq fields generated by fluctuating currents in the E-region of the ionosphere. Two sets of data are used in this study: the Magnetic Data Acquisition System (MAGDAS) and International Real-time Magnetic Observatory Network (INTERMAGNET) data. The two data sets had their sample records available in minute average values and the original recordings of the fields across all the stations are in Universal time (UT). The intermagnet data are recorded as orthogonal north, east and vertically downward field components as X, Y and Z and the X and Y are transformed to their respective northward (H) and eastward (D) coordinate system using the relation given in 1.4 to 1.6. In an earlier study (Price and Wilkins, 1963) observed that the effect of true Sq field are limited to 60 °N and beyond which are affected by magnetic disturbances. The disturbances in the current pattern at higher latitudes was also observed by (Fairfield, 1963). Hasegawa (1960) found that the daily variations of Sq field at higher latitudes derived from the international quiet days of the polar year show similar pattern with solar disturbed (SD) variations indication of possible disturbances. Hence, to avoid possible influence of extraneous features that may likely masked the true features of the Sq current, the study follow the earlier criteria adopted (Matsushita and Maeda, 1965). These authors used magnetic stations whose dip latitudes are well below ±70° on either side of the hemisphere to deduce the feature of the Sq current. It is believed that the latitudes below ±70° geomagnetic latitudes provides to a large extent true features of the Sq current system. Due to lack of simultaneous measurements of both hemispheres in

each year considered in the study, only the southern hemisphere field record were engaged during the dip minimum solar activity year 2008, and northern hemisphere during low and moderate solar activity years 2017 and 2012. Tables 3.1 and 3.2 shows the list of MAGDAS and INTERMAGNET stations and their coordinate systems used in the study. The INTERMAGNET data records are available for all the stations exception of Zhaoqing (GZH) and Changchum (CNH) in 2017.

Table 3.1: List of MAGDAS data stations and their coordinates system used in the study.

		Geographic		**Geomagnetic**
Name	**Code**	**Lat (°N)**	**Lon (°E)**	**Lat (°N)**
Langkawi	LKW	6.30	99.78	-3.30
Perak	PER	3.72	111.53	-5.92
Manado	MND	1.44	124.84	-7.80
Kupang	KPG	-10.20	123.40	-19.58
Cooktown	CKT	-15.48	145.25	-24.62
Rockhamp	ROC	-23.19	150.31	-32.40
Crib Point	MLB	-38.36	145.18	-49.46
Macquarie Island	MCQ	-54.50	158.96	-64.54

Table 3.2: List of INTERMAGNET data stations and their coordinates system used in the study.

		Geographic		Geomagnetic
Name	Code	Lat (°N)	Lon (°E)	Lat (°N)
Dalat	DLT	11.94	108.48	2.60
Phu thuy	PHU	21.03	105.97	10.78
Zhaoqing	GZH	22.00	112.45	12.74
Kanoya	KNY	31.42	130.88	20.50
Kakioka	KAK	36.63	140.19	27.37
Beijing Ming Tom	BMT	40.30	116.20	30.04
Changchum	CNH	44.08	124.86	31.00
Memenbetsu	MMB	43.91	144.15	35.35
Irkutsk	IRT	52.27	104.45	41.84
Parantuka	PET	52.97	158.25	46.10
Magadan	MGD	60.05	144.19	53.49

3.3 Method of Data Analysis

The analysis procedure presented in this work consist of two essential parts. The first part deals with selection of data that will yield the best Sq field of each geomagnetic observatory used in the analysis. The second part concerned the formation of analytical representation of these Sq fields (as a function of geomagnetic latitude and local time of the magnetic observatory) with harmonic Fourier and Legendre components on each longitude sector, hence provide the external and internal field component used for the identification of both external and internal currents and estimation of electrical conductivity of the deep Earth. Figure 3.1 provides the basic steps followed to obtain the desired objectives of this study. The appendix provides a brief overview on the data processing routine. The appendix provides a brief overview on the data processing routine.

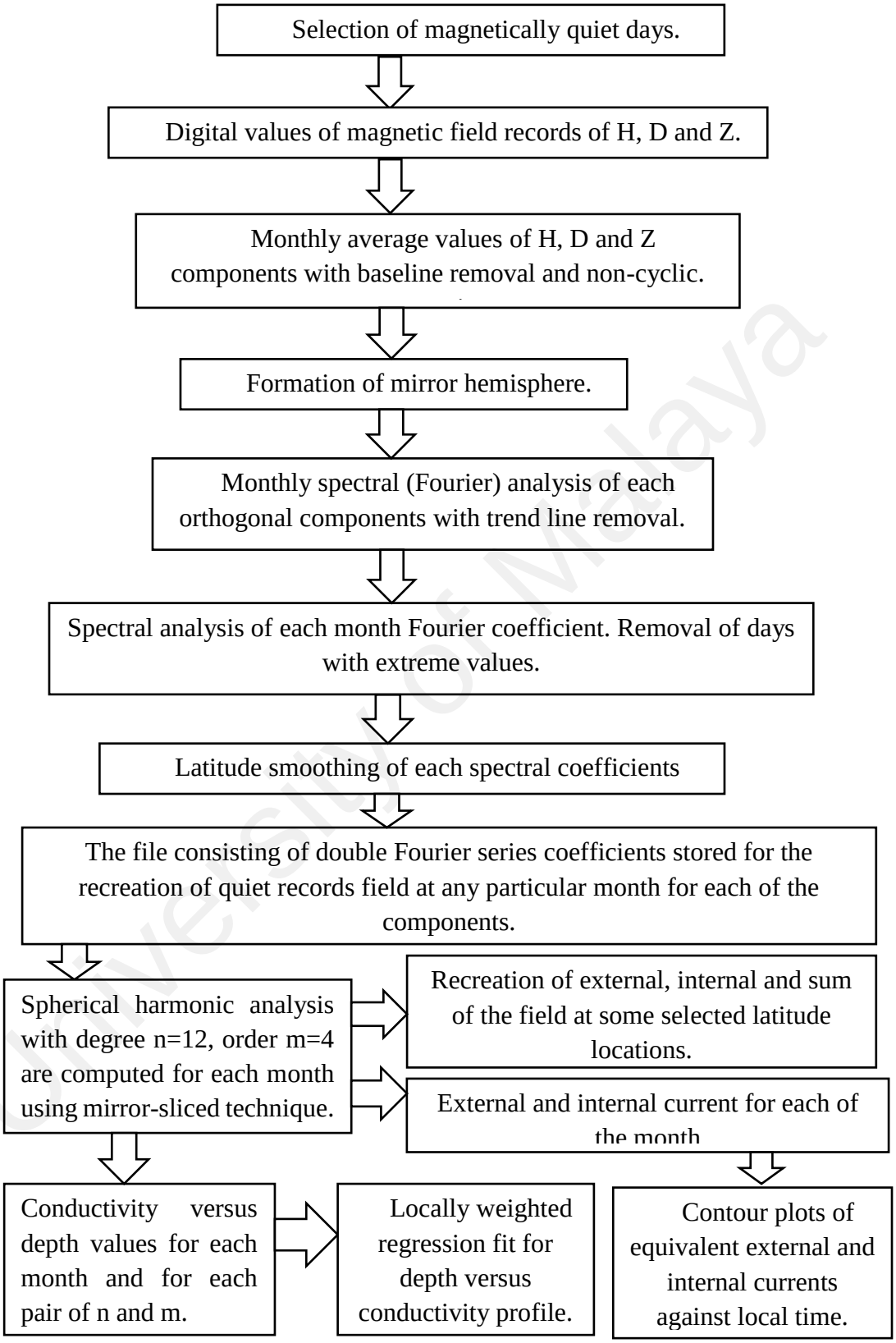

Figure 3.1: Flow diagram for spherical harmonic analysis of Sq daily field variations and upper mantle conductivity.

3.3.1 The Solar Quiet Field Representation

As depicted in Figure 3.1, the selected data sets (with Kp $\leq$ 3) used in this study consists of 1-minute averages which were binned to hourly values by taking average of every sixtieth minute values and this process reduced the data to 24 hourly values of each selected quiet day in the study. This procedure is carried out on each orthogonal components (H, D and Z). The little differences in longitude at the stations were adjusted by carefully rearranging the Sq field variations in local time (LT). In taking the baseline, the average of night-time values are used for a simple reason that during these periods the source of currents in the ionosphere has practically disappeared (e.g., Price & Wilkins, 1963; Malin & Gupta, 1977). The baseline values of each of the three orthogonal field component were obtained from its 2 hourly flanking the mid-night values as earlier suggested by research workers (e.g., Price & Wilkins, 1963). The relations is expressed below;

$$\left.\begin{aligned} H_\circ &= \frac{H_{01} + H_2 + H_{23} + H_{24}}{4} \\ D_\circ &= \frac{D_{01} + D_{02} + D_{23} + D_{24}}{4} \\ Z_\circ &= \frac{Z_{01} + Z_{02} + Z_{23} + Z_{24}}{4} \end{aligned}\right\} \tag{3.9}$$

where H_{01}, H_{02}, H_{23} and H_{24} represents the hourly values of H at 01:00, 02.00, 23:00 and 24:00 LT hours. Similarly for D_{01}, D_{02}, D_{23} and D_{24} and also Z_{01}, Z_{02}, Z_{23} and Z_{24}. The hourly departure of H, D and Z that are approximately equal to the hourly solar quiet (Sq) field for each component are obtained by subtracting the baseline ($H_\circ$, $D_\circ$ and $Z_\circ$) values

for a particular day from each of the hourly values of that same particular day. This is expressed in the relation below;

$$\left.\begin{aligned}\Delta H &= H_t - H_\circ \\ \Delta D &= D_t - D_\circ \\ \Delta Z &= Z_t - Z_\circ\end{aligned}\right\} \qquad (3.10)$$

where t is the time in hours and ranged from 01:00 to 24:00 LT while H_t, D_t and Z_t are the hourly local time of the H, D and Z component for each particular hour of the day. ΔH, ΔD and ΔZ are the solar quiet variations for any particular hour. The ΔH, ΔD and ΔZ were further corrected for non-cyclic variations such that the differences in values of each of the orthogonal component at the 24th LT and the 1st hour of the same day are eliminated as earlier described by (Matsushita & Maeda, 1965; Matsushita & Campbell, 1967). This was achieved by making little linear adjustment on the daily hourly values of each of the components ΔH, ΔD and ΔZ in such a way that the hourly values of ΔH, ΔD and ΔZ at 01:00 LT, 02:00 LT,……24:00 LT are merely regarded as X_1, X_2, ……X_{24}. This is expressed using the relation;

$$X_k = \frac{X_1 + X_{24}}{24} \qquad (3.11)$$

The hourly adjusted values may be expressed as;

$$X_1 + 0\Delta_k, X_2 + 2\Delta_k \ldots X_{24} + 23\Delta_k \qquad (3.12)$$

This may also be represented as;

$$\left.\begin{aligned} \Delta H_t &= X_t + (t-1)\Delta_t \\ \Delta D_t &= Y_t + (t-1)\Delta_t \\ \Delta Z_t &= Z + (t-1)\Delta_t \end{aligned}\right\} \tag{3.13}$$

Hence the corrected non-cyclic hourly departure yields the best representation of the Sq field for each month through the years. These Sq fields manifest direct effect of the ionospheric source currents and current induced into the conducting Earth structure that changes slowly but smoothly with latitude (Campbell et al., 1998). As the Earth rotates around the sun, the magnetic observatory in each latitude was assumed to be riding with the Earth under a fixed subsolar ionospheric current system. These magnetic observatories sampled the behavior of the field source current and the current induced to flow in the conducting Earth beneath the observatory (Campbell et al., 1998). The variations of Sq field at any of the latitude in 24 hours represented the measured field through 360° of a sphere. Campbell et al. (1998) called this technique "cloning" a sphere from a longitudinal "slice" sample. The mathematical notation of this technique shows spherical symmetric conducting properties of the Earth of which only the primary slice longitude is evaluated. Hence, the 24-, 12-, 8-, and 6-hours spectral components of the day-to-day variations of Sq field corresponds to $\left(\frac{360}{m}\right)^{\circ}$ components of longitudinal field change which has an order represented by m.

Next, a hemispheric mirror modelling technique was applied. This model utilizes the field values of the hemisphere that is of primary interest in the study to create a secondary hemisphere in the opposite hemisphere. This was achieved by simply assuming that the variations of H-field in the secondary hemisphere was similar to the primary hemisphere but its D and Z components are caused to be oppositely directed by simply changing the

appropriate sign of the two (D and Z) components. This was also achieved by simply multiplying the components (D and Z) by minus one (-1) so as to conform to the reversed source-current vortex as extensively discussed (e.g., Campbell and Schiffmacher, 1985; Campbell et al., 1988; Campbell 1990; Campbell et al., 1998; Campbell, 2003). At this stage a hemisphere has been successfully created with oppositely directed Sq current vortex to the primary one. It appears oppositely directed to the primary one because the thermotidal and prevailing wind motions are forcing the ionospheric charges in a direction opposite to the main magnetic field of the Earth (Campbell & Schiffmacher, 1988). In the mirror hemisphere, the variations of the Sq field formed for the three orthogonal components from the primary one are shifted by six months to represent the seasonal differences such that the summer hemisphere of the primary stations correspond to the winter hemisphere of the secondary hemisphere. In a similar way, for each month the harmonic coefficients for an analysis sphere was created with field values at all 2.5° latitude increments. At this stage, a complete sphere has been successfully created consisting of the primary and secondary hemisphere and the outcome of the analysis is strictly apportioned to the primary region of interest.

3.3.2 Spherical Harmonic Analysis of Sq

The next step in the analysis procedure is to represent for each region the field across all the latitudes for any particular time of the year by a family of Fourier cosine and sine harmonic coefficients. Earlier (Campbell, 2003; Campbell & Schiffmacher, 1985) estimated the spectral contributions to the Sq field and found that only the 24-, 12-, 8- and 6-hr harmonics components are of larger size to contribute significantly to the Fourier analysis. The higher magnitudes at these hours are due to the effect of Earth's rotation and not on the characteristics of the signal at any given day. These spectral components (24-, 12-, 8-, and 6-hr) of the quiet daily field variations are regarded to correspond to the

$\left(\frac{360}{m}\right)^{\circ}$ component of longitudinal field changes. On the basis of this, the detrended Sq field records from Equation 3.13 are used to determine for each station the 24-, 12-, 8-, and 6-hr month-by-month Fourier sine and cosine coefficients. The annual and semi-annual Fourier components of 12 (months) daily coefficients in each year were also determined at each 2.5° geomagnetic latitude increments from the geomagnetic equator to northward and southward poles as earlier suggested by (Cambell & Schiffmacher, 1988; Campbell & Schiffmacher, 1985; 1987). In this study, the southward and northward poles are below ±70° geomagnetic latitudes. In each year, the Fourier coefficients obtained are stored in a separate file and these values represent the year's Sq field variations for each component. For any geomagnetic component W (H, D and Z), the Sq field could be constructed from;

$$\Delta W = \sum_{m=1}^{4}\{C_m\, cos(15mt) + S_m\, sin(15mt)\} \tag{3.14}$$

where ΔW represent the changes for the H, D or Z field component from the daily mean value of the surface field records. The t is the local time (LT) in hours at the stations, while C_m and S_m are the cosine and sine amplitude coefficients as given in the equation below;

$$C_m = A_m^0 + \sum_{Q=1}^{2}\left\{A_m^{AQ} cos(30MQ) + B_m^{AQ} sin(30MQ)\right\} \tag{3.15}$$

$$B_m = B_m^0 + \sum_{Q=1}^{2}\left\{A_m^{BQ} cos(30MQ) + B_m^{BQ} sin(30MQ)\right\} \tag{3.16}$$

where m is the order from 1-4 for the 24-, 12-, 8-, and 6-hours spectral components. Q is 1 for annual and 2 for semi-annual, while M represent the decimal month (represented as 0.00 for January 1 and 12.00 for December 31). The As and Bs are the Fourier amplitude coefficients and the mainline letters are the annual and semi-annual

coefficients. Any linear trend on the recorded Sq field variation that will introduce some errors in the sinusoidal amplitude coefficients were completely removed before the Fourier analysis was performed. The file containing each of the 40 Fourier coefficients representing each of the three orthogonal field directions were carefully arranged according to geomagnetic latitudes of the stations and were smoothed and detrended. In spherical harmonic representation of Sq field, three different coordinate systems are usually used: the geographic, geomagnetic and dip latitudes. Each of these coordinates has its own peculiar advantage. However, the geographic and geomagnetic coordinates have the advantage of representing each spectral component wavelength of the Sq field by the spatial distance over the entire globe, this feature is particularly important especially when the outcome of the SHA analysis are to be used to estimate the electrical conductivity of the Earth's interior (Campbell & Anderssen, 1983). The global observations of Sq fields are more symmetric with respect to geomagnetic axis than the geographic and this cause the SHA coefficients series for the Sq to converge more easily and rapidly with geomagnetic expansion. Therefore, the analysis in this study will proceed with the geomagnetic coordinate system.

In SHA the field components are obtained from magnetic potential function having two converging infinite series of terms (Campbell, 1998; Campbell & Schiffmacher, 1985). The magnetic potential of the quiet field obtained from the daily mean values are from currents of external and internal sources. These magnetic potentials are expressed as;

$$V_n^m = C + a\sum_{n=1}^{\infty}\sum_{m=0}^{n}\left\{\left(a_n^{me}\left(\frac{r}{a}\right)^n + a_n^{mi}\left(\frac{a}{r}\right)^{n+1}\right)cos(m\phi) + \left(b_n^{me}\left(\frac{r}{a}\right)^n + b_n^{mi}\left(\frac{a}{r}\right)^{n+1}\right)sin(m\phi)\right\}\mathrm{P_n^m}(\theta) \quad (3.17)$$

Where *C*, θ, *a*, *r* and ϕ represent integration constant, geomagnetic colatitude, geocentric distance, Earth's radius and local time of the station. From Equation 3.17 the first series with r^n, as n which is the term number is increasing, the r^n becomes larger and larger indication approaching the source current responsible for the external field in the increasing direction of r. On the other hand, the second series with $\left(\frac{1}{r}\right)^n$ terms appear larger and larger as r becomes smaller and smaller indicating that it is approaching the current responsible for the internal field in the decreasing r direction. The a_n^{me}, b_n^{me} and a_n^{mi}, b_n^{mi}correspond to the Gauss coeficient with *e* and *i* indicating external and internal field sources. In the course of the analysis, it was observed that terms after a certain values of *n* make no significant contribution to the magnetic potential, hence the spherical harmonic analysis was carried out on the magnetic potential function *V* for order *m*=1 to *m*=4 and degree *n*=m to *n*=12. Any further increase in the number of degree does not make any significant contribution on the magnetic potential. From Equation 3.17, the longitudinal dependence of both magnetic field potential are given by Fourier series, while its latitudinal dependence is represented by a series of Schmidt quasi-normalized associated Legendre functions P_n^m. This function are estimated using the following recursive formula as provided in (Campbell, 2003).

$$R_n^m = \sqrt{n^2 - m^2} \tag{3.18}$$

$$P_0^0 = 1;\ P_1^0 = (cos);\ P_1^1 = (sin\theta) \tag{3.19}$$

$$P_m^m = \sqrt{\frac{2m-1}{2m}} sin(\theta) P_{m-1}^{m-1} \text{ for } m > 1, n = m \tag{3.20}$$

$$P_n^m = \frac{(2n-1)\, cos\,\theta\ P_{n-1}^m - R_{n-1}^m P_{n-2}^m}{R_n^m} \text{ for } n > m \tag{3.21}$$

$$\frac{dP_n^m}{d\theta} = \frac{n\, cos\,\theta P_n^m\,(cos\theta) - R_n^m P_{n-1}^m}{sin\,\theta} \text{ (except for } \theta = 0 \text{ or } 180°) \tag{3.22}$$

Equation 3.22 is undefined at the poles (for $\theta = 0$ or 180°).

To determine the spherical harmonic Gauss coefficients, the following values are first obtained;

$$a_n^m = \frac{2n+1}{4n(n+1)}\left(\sum_0^{180} X_c^m \frac{dP_n^m}{d\theta} sin\,\theta + Y_s^m\, mP_n^m\right)\Delta\theta \tag{3.23}$$

$$b_n^m = \frac{2n+1}{4n(n+1)}\left(\sum_0^{180} X_s^m \frac{dP_n^m}{d\theta} sin\,\theta + Y_c^m\, mP_n^m\right)\Delta\theta \tag{3.24}$$

$$C_n^m = \frac{1}{4}(2n+1)\sum_0^{180} Z_c^m P_n^m\, sin\,\theta\,\Delta\theta \tag{3.25}$$

$$d_n^m = \frac{1}{4}(2n+1)\sum_0^{180} Z_s^m P_n^m\, sin\,\theta\,\Delta\theta \tag{3.26}$$

where X_c^m and X_s^m represent the cosine and sine coefficients of the Fourier component of the northward (ΔH) field change at colatitude (θ). The $\Delta\theta$ in these equations is the step increment which is equivalent to 2.5^0 ($\Delta\theta = 2.5^\circ$) used in the analysis. The θ is the geomagnetic colatitude.

The spherical harmonic Gauss coefficient for the external and internal part is then computed using the equations below;

For the external part;

$$\left.\begin{aligned} a_n^{me} &= \frac{[(n+1)a_n^m + C_n^m]}{2n+1} \\ b_n^{me} &= \frac{[(n+1)b_n^m + d_n^m]}{2n+1} \end{aligned}\right\} \tag{3.27}$$

The internal part is given as;

$$\left.\begin{aligned} a_n^{mi} &= \frac{[na_n^m - C_n^m]}{2n+1} \\ b_n^{mi} &= \frac{[nb_n^m - d_n^m]}{2n+1} \end{aligned}\right\} \tag{3.28}$$

The potential function was separated into external and internal source contributions. With reference to Gauss coefficients, the external fields in the orthogonal directions (with X pointing towards geomagnetic northward, Y eastward and Z vertically downward) are reconstructed from the external spherical harmonic analysis as series of Fourier cosine and sine of the terms;

$$X_c^m(\theta) = \sum_{n=m}^{12} a_n^{me} \frac{dP_n^m}{d\theta} \tag{3.29}$$

$$X_s^m(\theta) = \sum_{n=m}^{12} b_n^{me} \frac{dP_n^m}{d\theta} \tag{3.30}$$

$$Y_c^m(\theta) = -\frac{m}{\sin\theta} \sum_{n=m}^{12} b_n^{me} \frac{dP_n^m}{d\theta} \tag{3.31}$$

$$Y_s^m(\theta) = -\frac{m}{\sin\theta} \sum_{n=m}^{12} a_n^{me} \frac{dP_n^m}{d\theta} \tag{3.32}$$

$$Z_c^m(\theta) = \sum_{n=m}^{12} n a_n^{me} P_n^m \tag{3.33}$$

$$Z_s^m(\theta) = \sum_{n=m}^{12} n b_n^{me} P_n^m \tag{3.34}$$

where X_c^m, Y_c^m and Z_c^m represents the cosine coefficients of the external orthogonal field components and X_s^m, Y_s^m and Z_s^m represent the Sine coefficients. For the internal horizontal component X, eastward Y and vertical Z, their fields are reconstructed from the SHA coefficients as series of Fourier cosine and sine terms that are expressed as;

$$X_c^m(\theta) = \sum_{n=m}^{12} a_n^{mi} \frac{dP_n^m}{d\theta} \tag{3.35}$$

$$X_s^m(\theta) = \sum_{n=m}^{12} b_n^{mi} \frac{dP_n^m}{d\theta} \tag{3.36}$$

$$Y_c^m(\theta) = -\frac{m}{\sin\theta}\sum_{n=m}^{12} b_n^{mi}\frac{dP_n^m}{d\theta} \tag{3.37}$$

$$Y_s^m(\theta) = -\frac{m}{\sin\theta}\sum_{n=m}^{12} a_n^{mi}\frac{dP_n^m}{d\theta} \tag{3.38}$$

$$Z_c^m = \sum_{n=m}^{12} n a_n^{me} P_n^m \tag{3.39}$$

$$Z_s^m = \sum_{n=m}^{12} n b_n^{me} P_n^m \tag{3.40}$$

For the vertical component, the equation below are used:

$$Z_c^m(\theta) = -\sum_{n=m}^{12}(n+1) a_n^{mi} P_n^m \tag{3.41}$$

$$Z_s^m(\theta) = -\sum_{n=m}^{12}(n+1) b_n^{mi} P_n^m \tag{3.42}$$

The sphere in which the spherical harmonic analysis was done was spherically created to accommodate the boundary conditions of the Gauss method. At any particular geomagnetic latitude (90 - θ), any or all of the three orthogonal external or internal field components are obtained from the external and internal SHA coefficients using the following relations;

$$\left.\begin{aligned} X(\theta,\phi) &= \sum_{m=1}^{4}[X_c^m(\theta)\cos(m\phi) + X_s^m(\theta)\sin(m\phi)] \\ Y(\theta,\phi) &= \sum_{m=1}^{4}[Y_c^m(\theta)\cos(m\phi) + Y_s^m(\theta)\sin(m\phi)] \\ Z(\theta,\phi) &= \sum_{m=1}^{4}[Z_c^m(\theta)\cos(m\phi) + Z_s^m(\theta)\sin(m\phi)] \end{aligned}\right\} \tag{3.43}$$

The equivalent current function $J(\phi)$ in Amperes (A) for any hour of the day $\phi/15$ is expressed as;

$$J(\phi) = \sum_{m=1}^{4}\sum_{n=m}^{12}\{U_n^m\cos(m\phi) + V_n^m\sin(m\phi)\}P_n^m \tag{3.44}$$

The external current system is given by;

$$U_n^m = -K\left[\frac{2n+1}{n+1}\right] a_n^{me}\left(\frac{a}{R}\right)^n \tag{3.45}$$

$$V_n^m = -K\left[\frac{2n+1}{n+1}\right] b_n^{me}\left(\frac{a}{R}\right)^n \tag{3.46}$$

For the internal current system, it is expressed as;

$$U_n^m = K\left[\frac{2n+1}{n}\right] a_n^{mi}\left(\frac{R}{a}\right)^{n+1} \tag{3.47}$$

$$V_n^m = K\left[\frac{2n+1}{n}\right] b_n^{mi}\left(\frac{R}{a}\right)^{n+1} \tag{3.48}$$

where $K = \frac{5R}{2\pi}$ and R denote the Earth radius given in kilometers, a is the radius of the sphere of the equivalent current location. Throughout the study, a is assumed to be approximately equal to R so that the ratio $\frac{a}{R}$ and $\frac{R}{a}$ becomes 1 and the factor was omitted.

3.3.3 Conductivity of the Earth's Upper Mantle

For electrical conductivity-depth modelling of the Earth using quiet field, the field must originate from source currents that are completely of external origin to the Earth and currents induced into the conductive Earth structure. The source current must also be type with a regular occurring pattern and changes slowly but smoothly from one quiet day to the other. It is imperative that the solar quiet Sq current deduced from quiet magnetic field records at standard observatories meet these criteria for probing the Earth's electrical conductivity-depth structure from the crustal surface to the lower mantle as will soon be shown in this study.

3.3.3.1 Transfer Function Utilizing Spherical Harmonic Coefficients (SHC)

Schmucker (1970) provided set of equations for profiling the conductivity with a transfer function equivalent to a substitute conductor. This method required external and internal spherical harmonic coefficients obtain in a certain region as input parameters. Campbell & Anderssen (1983) observed that for deep-Earth conductivity determination from the paired of external and internal coefficients of the SHA, the special mathematical method associated with the SHA allows each of the Gauss spherical harmonic coefficients to be analyzed separately (independently) for an induction response, a process which required computation of complex ratio of the internal to the external component (S_n^m) of the quiet geomagnetic surface field and represented in terms of phase and amplitude. This method also establishes a complex number transfer function, $C_n^m = Z - iP$ for generating electrical conductivity profile utilizing the spherical harmonic coefficients as input parameters.

The generalized form of Schmucker's transfer function C_n^m is expressed as;

$$C_n^m = Z - iP \tag{3.49}$$

The Schmucker's transfer function for a substitute conductor given in Equation 3.49 has two complex parts: real *(Z)* and the imaginary (-*P*) parts. Campbell and Anderssen (1983) expressed the real *(Z)* and the imaginary (-*P*) parts in terms of external and internal SHA coefficients given as;

$$Z = \frac{R}{n(n+1)}\left\{\frac{A_n^m[na_n^{me}-(n+1)a_n^{mi}]+B_n^m[nb_n^{me}-(n+1)b_n^{mi}]}{(A_n^m)^2+(B_n^m)^2}\right\} \tag{3.50}$$

$$\mathrm{P} = \frac{\mathrm{R}}{\mathrm{n(n+1)}}\left\{\frac{A_n^m[nb_n^{me}-(n+1)b_n^{mi}]-B_n^m[na_n^{me}-(\mathrm{n}+1)a_n^{mi}]}{(A_n^m)^2+(B_n^m)^2}\right\} \tag{3.51}$$

the R is the Earth radius expressed in kilometers (km); hence the magnitudes of Z and P are expressed in kilometers. The coefficients A_n^m and B_n^m are obtained using the spherical harmonic coefficients for the external and internal field as given below;

$$\left.\begin{aligned} A_n^m &= a_n^{me} + a_n^{mi} \\ B_n^m &= b_n^{me} + b_n^{mi} \end{aligned}\right\} \tag{3.52}$$

For every (*m*, *n*) set of spherical harmonic coefficients, the equivalent depth (in km) to the uniform substitute layer was estimated using the relation;

$$d_n^m = Z - P \text{ (km)} \tag{3.53}$$

and has a uniform substitute –layer conductivity (*S/m*) given by;

$$\sigma_n^m = \frac{5.4 \times 10^4}{m(\pi P)^2} \quad (\text{Sm}^{-1}) \tag{3.54}$$

The ratio of the internal to the external components of the quiet field variation S_n^m is given as;

$$\mathrm{S_n^m} = \mathrm{u} + \mathrm{iv} \tag{3.55}$$

where

$$u = \left[\frac{(a_n^{me})(a_n^{mi}) + (b_n^{me})(b_n^{mi})}{[(a_n^{me})]^2 + [(b_n^{me})]^2}\right] \tag{3.56}$$

$$v = \left[\frac{(b_n^{me})(a_n^{mi}) - (a_n^{me})(b_n^{mi})}{[(a_n^{me})]^2 + [(b_n^{me})]^2}\right] \tag{3.57}$$

The validity of Equations 3.53 and 3.54 is bounded by three basic conditions. The first of these conditions is given by;

$$0° = \arg(C_n^m) \geq -45°; \tag{3.58}$$

The second condition is that

$$80° \geq \arg(S_n^m) \geq 10.5°; \tag{3.59}$$

For the SHA amplitudes given by Equation 3.52 not to be too small, since decrease in amplitudes of the coefficients lead to relative error in the SHA coefficients, the third condition is set at;

$$[(A_n^m)^2 + (B_n^m)^2]^{0.5} \geq G_m \tag{3.60}$$

Equations 3.58 and 3.59 are basically introduced to cope with any likely outliers in the data and the SHA coefficients of very small amplitudes which will yield poor conductivity estimates, where G_m is a different constant value for each m data set. The values of G_m are determined by simply taking arbitrary values and are tested for all *m* and 0.5 was found to yield the best estimates. When G_m > 0.5, the conductivity-depth slightly decreases and enhances the removal of higher m components that are by nature of the source current of lower amplitudes. The conductivity-depth determination of this present study uses Schmucker's transfer function as earlier mentioned. This uses the external and internal SHA coefficients of a given site as input parameter. The SHA coefficients are basically obtained from the fittings of a potential function. In the conductivity determination using the Sq current sources, some certain features are usually observed.

Firstly, the polynomial terms with values of (n-m) >1 are not from the real quiet time ionospheric currents but arise primarily from currents flowing at the polar latitudes (Arora et al., 1995; Campbell & Schiffmacher, 1988). Such higher Legendre wavelengths are avoided. Secondly, the major contribution to the potential function that defines the Sq comes from fields that describe the region of the major Sq current vortex and are described by the polynomial terms $(n-m) = 1$ (Campbell, 1990). Such selection provided conductivity profiles that have lateral heterogeneity in latitude expected of a given site (Campbell & Schiffmacher, 1988). The movement of the Sq current focus through the years results to slight changes in the coefficients of the polynomials that constitute the potential function. The conductivity estimates from these coefficients during these processes reflect such changes. The conductivity values obtained on the restriction of n-m=1 were fitted to a unique profile using the locally weighted regression technique (Lowess), as earlier explained by (Cleveland, 1979) with a smoothing factor of 0.5.

CHAPTER 4: RESULTS OF THE ANALYSIS

Three years magnetic field records are engaged in this study as earlier mentioned. The solar activity in these years are extremely minimal in 2008, moderate in 2012 and low in 2017 respectively. During these periods the annual sunspot numbers are 3.9, 84.4 and 21.8 in 2008, 2012 and 2017 which makes it appropriate to study the Sq current and their associated fields from the dip minimum to moderate solar activity year. It is interesting to note that the dip minimum solar activity year 2008 correspond to the year of descending phase of the solar cycle 23 and year 2017 is a year of low solar activity which also correspond to the year of descending phase of solar cycle 24. Hence throughout the remainder of this text, the Sq current and their associated magnetic fields will be discussed in accordance to their ascending annual sunspot numbers i.e from dip minimum to moderate solar activity years, 2008, 2017 and 2012. The external and internal Gauss coefficients obtained in each month using spherical harmonic analysis technique allow us to reconstruct the monthly mean (MSq) field for each of the orthogonal components (H, D and Z) at some selected latitude locations of the study. Figures 4.1 to 4.9 shows the latitudinal time series plots of the month-by-month external, internal and sum (external plus internal) of the quiet geomagnetic field variations reconstructed from spherical harmonic analysis (SHA) coefficients. The fields provide the nature of latitudinal variability of the phase and intensity of the external and internal induced current systems responsible for the observed quiet fields.

It is clearly evident from Figure 4.1 (panel H1) that the external horizontal (H) fields $MSqH_{ext}$ are characterized by night-time (17:00-07:00 LT) negative variations at the latitudes of LKW, MND and KPG on the southern hemisphere during the dip minimum solar activity year 2008 with similar appearance at DLT, PHU and fluctuate at KNY in

the northern hemisphere during low and moderate solar activity years 2017 and 2012, see Figures 4.2 (panel H2) and 4.3 (panel H3).

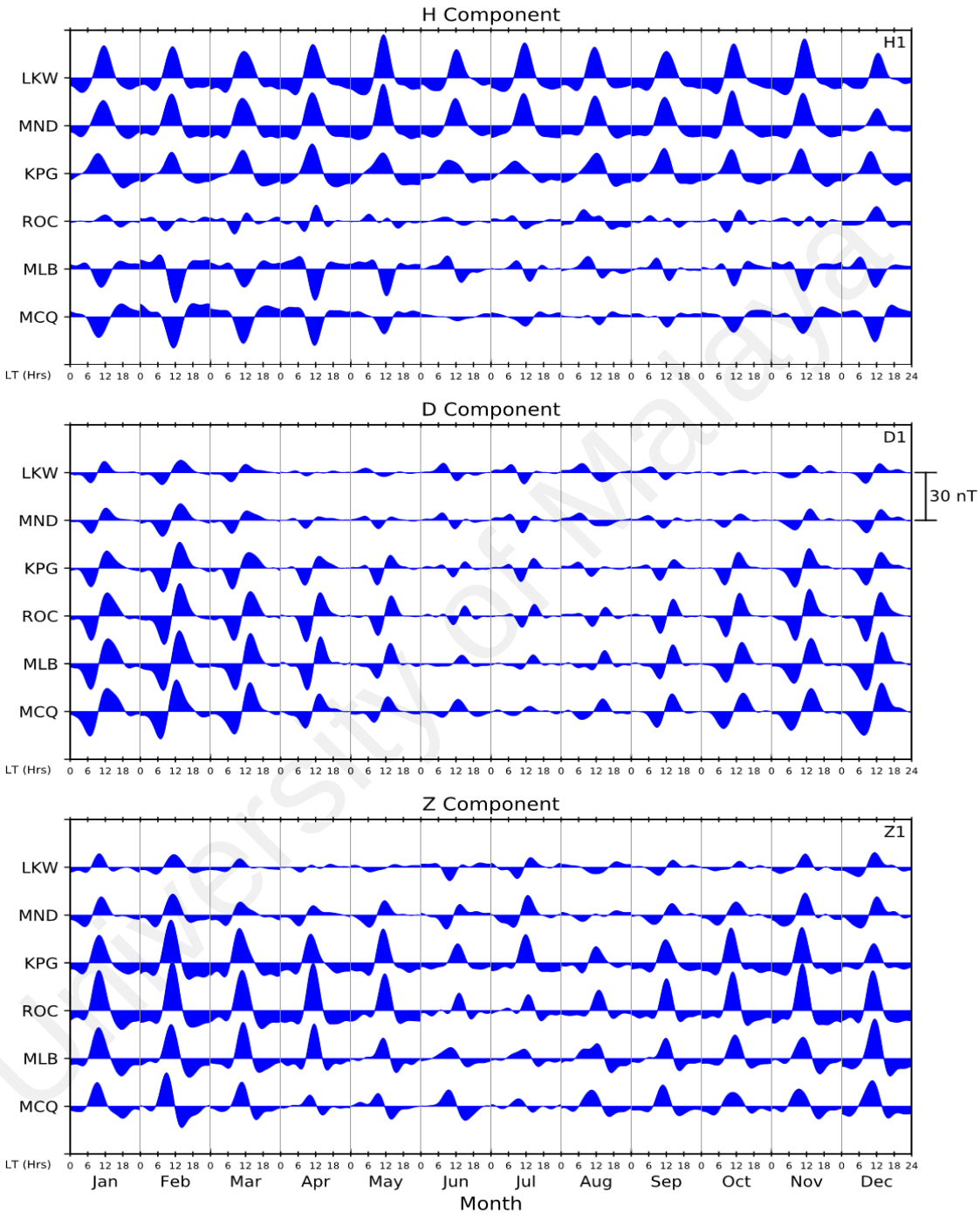

Figure 4.1: Month-by-month external field variations of the three orthogonal components (H, D, and Z) reconstructed from the external spherical harmonic coefficients at some selected magnetic observatories in 2008.

At night-time when negative $MSqH_{ext}$ amplitudes are observed at the latitudes of LKW to KPG, positive $MSqH_{ext}$ amplitudes are observed at the latitudes of MLB and MCQ, see Figure 4.1 (panel H1). Similar night-time positive $MSqH_{ext}$ amplitudes are seen at the latitudes of BMT up to MGD during low and moderate solar activity years 2017 and 2012 as depicted in Figures 4.2 (panel H2) and 4.3 (panel H3).

Apart from these night-time variations, the daytime diurnal variations of $MSqH_{ext}$ amplitudes appeared positively enhanced between 06:00 and 16:00 LT hrs at the latitude LKW and MND and decreases substantially with a phase shift at the latitude of ROC, then changeover to negative amplitudes at MLB and MCQ in the southern hemisphere during the dip minimum solar activity as shown in Figure 4.1 (panel H1). Similar features are observed in the northern hemisphere, the daytime $MSqH_{ext}$ amplitudes appeared positively enhanced between 06:00 and 16:00 LT hrs at DLT and PHU with a substantial decrease and phase shift at KNY, thereafter change to negative amplitudes during low and moderate solar activity as depicted in Figures 4.2 (panel H2) and 4.3 (panel H3). During these periods, the daytime maximum positive $MSqH_{ext}$ amplitude ~30 nT occurred at LKW in May 2008 as shown in Figure 4.1 (panel H1). As solar activity increases, $MSqH_{ext}$ amplitudes increased to about 40 and 60 nT each in March at DLT in 2017 and 2012 as depicted in Figures 4.2 (panel H2) and 4.3 (panel H3). These peak amplitudes are observed between 10:00 and 11:00 LT hours and thus indicate the effect of increasing solar activity. Above these latitudes, the daytime maximum negative $MSqH_{ext}$ amplitude reached ~-25, -15 and -20 nT in February at MCQ during the dip minimum solar activity and in June each at MGD during low and moderate solar activity. These peak amplitudes are mostly observed around (11:00-12:00 LT) hrs.

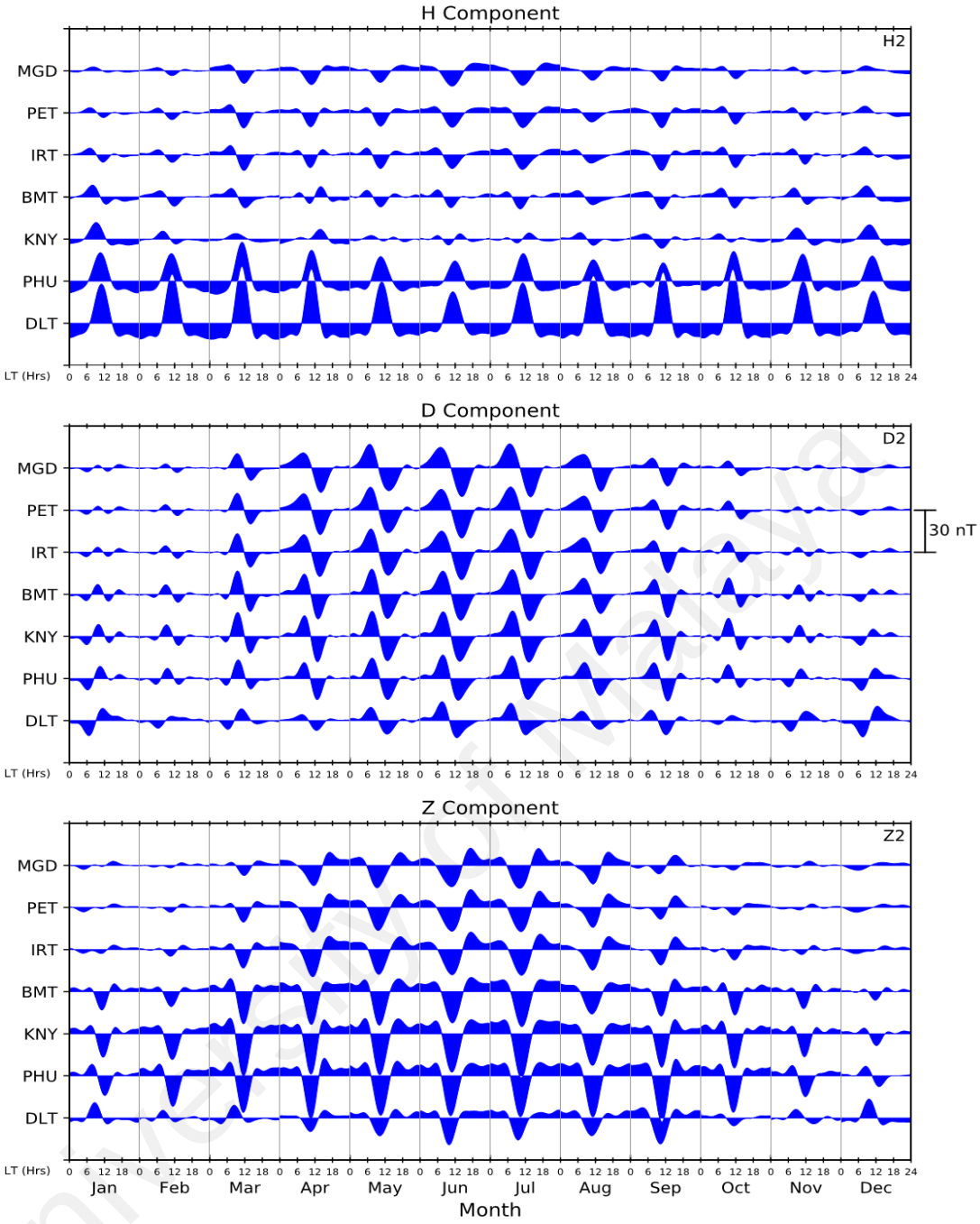

Figure 4.2: Month-by-month external field variations of the three orthogonal components (H, D, and Z) reconstructed from the external spherical harmonic coefficients at some selected magnetic observatories in 2017.

It is obvious from these magnitudes that the daytime positive $MSqH_{ext}$ amplitudes increases from dip minimum to moderate solar activity in response to increasing effect of solar activity while their negative variations have not really conform to any pattern thus suggest involvement of other physical processes.

Figures 4.1 to 4.3 (panels D1 to D3) shows the external field variations of the eastward D component $MSqD_{ext}$ during the dip minimum, low and moderate solar activity years 2008, 2017 and 2012. These fields as earlier discussed are reconstructed from the spherical harmonic coefficients. As can be observed from Figure 4.1 (panel D1), the $MSqD_{ext}$ amplitudes show regular occurring pattern with pre-noon negative amplitudes between 01:00 and 11:00 LT hrs and afternoon positive amplitudes between 12:00 and 18:00 LT hrs expected of stations southward of the magnetic dip equator (southern hemisphere). These variations are mostly observed during the summer and equinoctial months (September-March). During these periods, $MSqD_{ext}$ reached maximum pre-noon and afternoon amplitudes ∼-20 nT and 25 nT around 10:00 and 13:00 LT hrs at MLB in December and February 2008, see Figure 4.1 (panel D1). At the northern hemisphere, the positive and negative $MSqD_{ext}$ amplitudes during the pre-noon and afternoon sectors are features that persist across the latitudes mostly during the summer and equinoctial months (March-October) as shown in Figures 4.2 (panel D2) and 4.3 (panel D3). These variations are typical signature of northerly stations. During these periods, the maximum pre-noon amplitude that $MSqD_{ext}$ could reach was ∼20 and 25 nT around 08:00 LT in May each at KNY in 2017 and 2012. While their afternoon maximum reached ∼-25 and -30 nT around 13:00 LT hrs in June and May at MGD in 2017 and 2012 respectively, see Figures 4.2 (panel D2) and 4.3 (panel D3). In both hemispheres, pre-noon and afternoon $MSqD_{ext}$ amplitudes appeared stronger (weaker) in summer (winter) months and generally increases with increasing solar activity. Apart from these normal variations, negative

$MSqD_{ext}$ amplitudes are apparently seen between 05:00 and 07:00 LT hrs in March and October as depicted in Figures 4.2 (panel D2) and 4.3 (panel D3). Another small positive $MSqD_{ext}$ amplitudes appeared between 16:00 and 18:00 LT hrs in April, May and September during low solar activity as shown in Figure 4.2 (panel D2). These features are abnormal and suggest involvement of other physical processes.

During the winter months, the ionospheric currents shows a different behavior given rise to two forms of $MSqD_{ext}$ variations: those with "M shape" and "W shape" variations. In the southern hemisphere, the $MSqD_{ext}$ amplitudes with "W shape"variations are specifically observed at the latitudes of ROC and MCQ in June and July and those with an "M shape" amplitudes are seen at the latitudes of MND, KPG in June, July and September as depicted in Figure 4.1 (panel D1). Similar "M shape" amplitudes have been earlier observed in the Australian region by (Stening et al., 2005). The "W shape" that appeared in few months during the dip minimum solar activity year 2008 increases during low solar activity seen in winter months (January, February and November) across all the latitudes as demonstrated in Figure 4.2 (panel D2) exception of DLT. These variations became prevalent and conspicuous during moderate solar activity apparently seen across all the latitudes during the winter months (November-February) also exception of DLT on the magnetic equator, see Figure 4.3 (panel D3). The $MSqD_{ext}$ amplitudes at LKW and DLT closer to the magnetic equator appeared weak. Careful observation of $MSqD_{ext}$ variations at LKW during the winter months (May-August) revealed noticeable absence of prominent northward and southward flow of current expected during the pre-noon and afternoon hours in the southern hemisphere rather a southward and northward flow of current is seen generating negative and positive amplitudes around these periods. These variations are in sharp contrast to expectation of station located southward of the magnetic equator and thus suggest the presence of other currents.

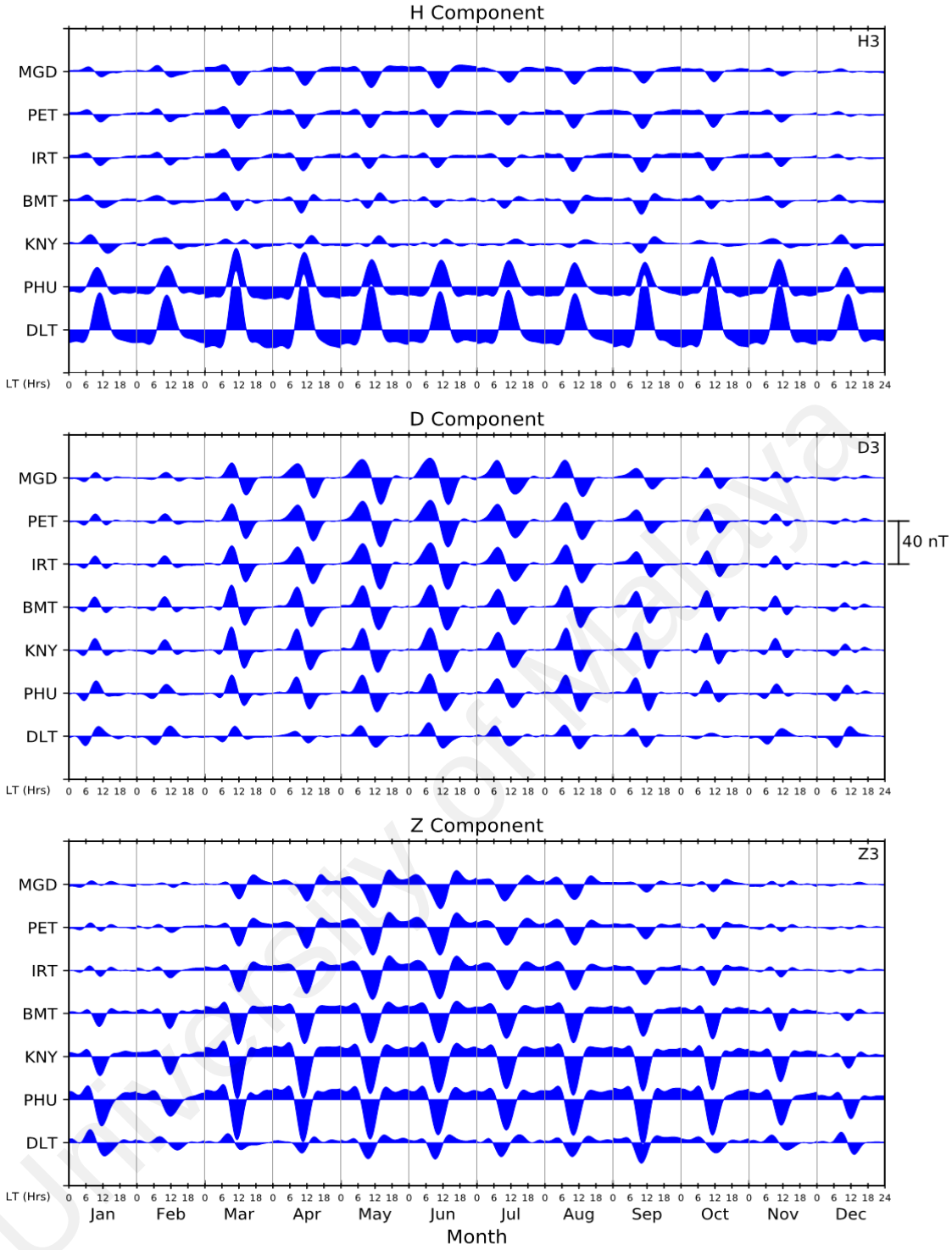

Figure 4.3: Month-by-month external field variations of the three orthogonal components (H, D, and Z) reconstructed from the external spherical harmonic coefficients at some selected magnetic observatories in 2012.

The behavior is no different in the northern hemisphere, the $MSqD_{ext}$ variations at DLT during the winter months (November-February) showed absence of southward and northward flow of current vortex expected during the pre-noon and afternoon hours rather a dominant northward and southward current flow is seen at these latitudes. This variation pattern is contrary to a northerly station and thus suggest presence of opposite current vortex.

Figures 4.1 to 4.3 (panels Z1 to Z3) shows the external quiet geomagnetic field variations of the downward Z component $MSqZ_{ext}$ reconstructed from SHA coefficients during the dip minimum to moderate solar activity years 2008, 2017 and 2012. It is obvious from Figure 4.1 (panel Z1) that $MSqZ_{ext}$ show night-time negative amplitudes between 17:00 and 07:00 LT in most cases and change to daytime positive amplitudes between 08:00 and 16:00 LT hrs. These variations which are observed across all the latitudes are consistent with the typical Z-component located southward of the magnetic dip equator as earlier established by (Chapman, 1919). Exception to these variations are LKW and MND. In these stations (LKW and MND), the $MSqZ_{ext}$ amplitudes are greatly reduced and fluctuate particularly in winter months (April-August). Apart from these variations, the peak amplitudes reached about 31 nT around 11:00 LT in February at the latitudes of ROC during dip minimum solar activity as given in Figure 4.1 (panel Z1). In the northern hemisphere, the $MSqZ_{ext}$ show night-time positive amplitudes that changed to daytime negative field variations. These variations pattern are typical of the Z-component northward of the magnetic dip equator in accordance to Chapman's theory. Exception to these variations is DLT with daytime positive $MSqZ_{ext}$ amplitudes during the winter months (November-March) see Figure 4.2 (panel Z2). During these periods, the highest amplitudes ~-33 and -42 nT occurred around 11:00 LT hrs at PHU each in September during low and moderate solar activity as illustrated in Figures 4.2 (panel Z2)

and 4.3 (panel Z3). The $MSqZ_{ext}$ amplitudes appeared weaker at DLT closer to the magnetic dip equator, stronger at mid-latitudes and decreases with increasing latitudes. The variations of $MSqZ_{ext}$ also increases with increasing solar activity.

Figures 4.4 to 4.6 (panels H4 to H6) shows the internal field variations of the horizontal component $MSqH_{int}$. The $MSqH_{int}$ amplitudes also exhibit night-time variations that changes erratically both in phase and magnitudes during the dip minimum solar activity year as depicted in Figure 4.4 (panel H4). As solar activity increases, the variation of $MSqH_{int}$ become relatively calm and assumed smooth regular occurring pattern during low and moderate solar activity years as illustrated in Figures 4.5 (panel H5) and 4.6 (panel H6). The $MSqH_{int}$ variations reflect most features associated with the $MSqH_{ext}$ with a similar night-time negative amplitudes at the latitudes of LKW, MND, KPG and ROC beyond which the amplitudes appeared positively enhanced mostly between 14:00 and 06:00 LT hrs as depicted in Figure 4.4 (panel H4). Similar night-time negative $MSqH_{int}$ variations are observed at the latitudes of DLT, PHU and KNY and became positively enhanced above these latitudes as shown in Figures 4.5 (panel H5) and 4.6 (panel H6). Besides these night-time variations, daytime positively $MSqH_{int}$ amplitudes are observed at the latitudes of LKW, MND and ROC, beyond which it changed to negative variations mostly between 07:00 and 15:00 LT hrs in the southern hemisphere as indicated in Figure 4.4 (panel H4). Similar daytime positive $MSqH_{int}$ amplitudes occurred at the latitudes of DLT up to KNY and changed to negative variations above these latitudes in the northern hemisphere as illustrated in Figures 4.5 (panel H5) and 4.6 (panel H6). The daytime maximum positive $MSqH_{int}$ amplitudes reached ~12 nT around 11:00 LT at MND in February during dip minimum solar activity as shown in Figure 4.4 (panel H4). This magnitude increased slightly to ~13 and 14 nT

in March and April each around 10:00 LT at DLT during low and moderate solar activity as illustrated in Figures 4.5 (panel H5) and 4.6 (panel H6).

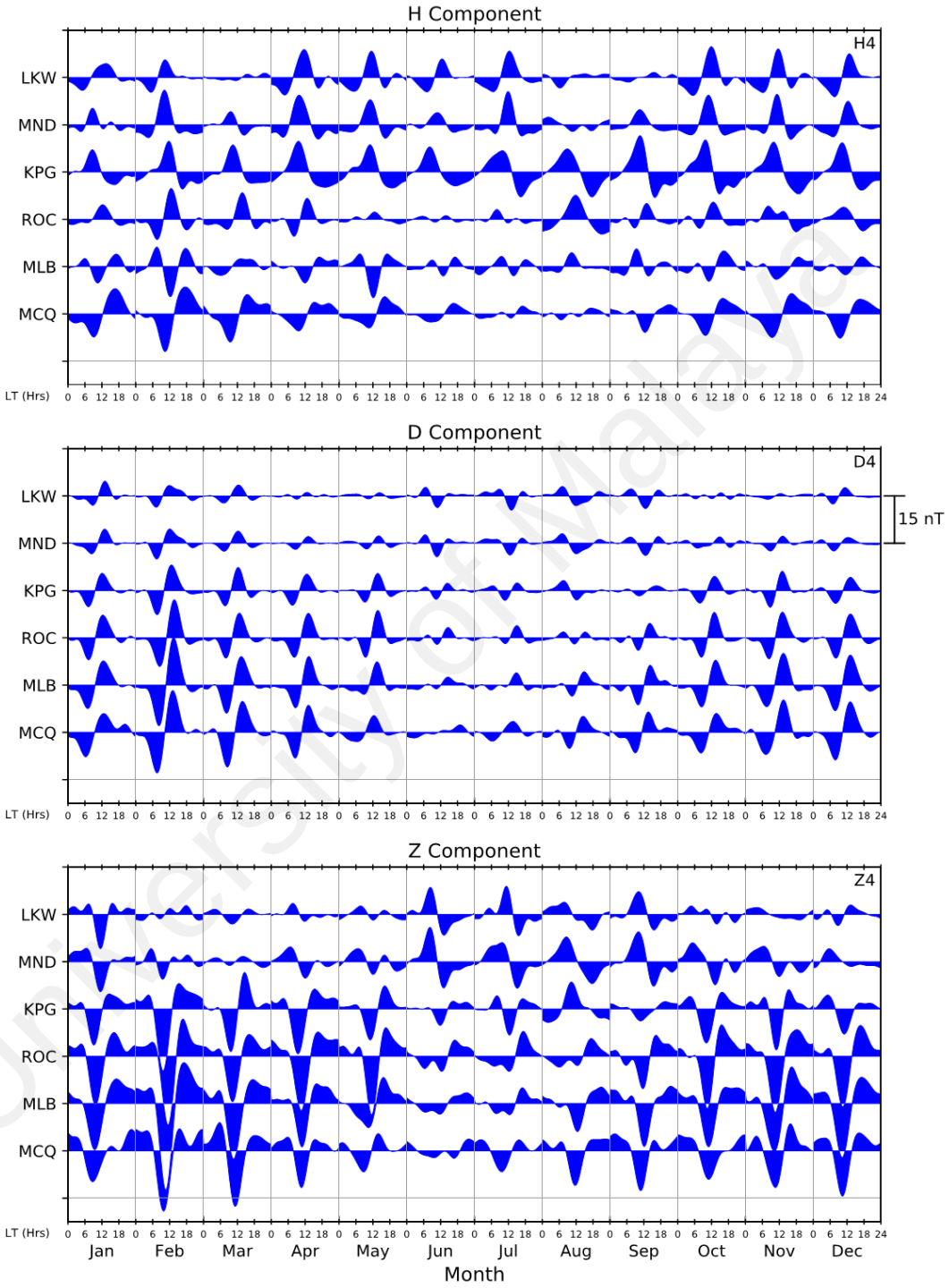

Figure 4.4: Month-by-month internal field variations of the three orthogonal components (H, D, and Z) reconstructed from the internal spherical harmonic coefficients at some selected magnetic observatories in 2008.

Their daytime negative $MSqH_{int}$ amplitudes reached ~-13 nT in February around 10:00 LT hrs at MCQ during the dip minimum solar activity as shown in Figure 4.4 (panel H4) and decreases to about ~-5 and -6 nT around 11:00 LT hrs in June each at MGD during low and moderate solar activity, see Figures 4.5 (panel H5) and 4.6 (panel H6). These magnitudes just like the external fields, the daytime positive $MSqH_{int}$ amplitudes show the effect of increasing solar activity and their negative amplitudes have not shown any linear relationship with increasing solar activity. Generally, two kinds of diurnal variations are generally apparent across the latitudes during the daytime; positive and negative variations. The daytime positively enhanced $MSqH_{ext}$ and $MSqH_{int}$ amplitudes decreases with increasing latitudes and their negative amplitudes appear weak at mid-latitudes and seem to increase with increasing latitudes.

The variations of $MSqD_{int}$ also reflect most features associated with the external fields with similar pre-noon and afternoon negative and positive amplitudes in the southern hemisphere during the summer and equinoctial months (September-April), see Figure 4.4 (panel H4). The pre-noon maximum $MSqD_{int}$ amplitude ~-14 nT and its afternoon peak amplitude ~17 nT appeared around 08:00 and 13:00 LT hrs in February at MLB during the dip minimum solar activity year 2008, see Figure 4.4 (panel D4). In the northern hemisphere, $MSqD_{int}$ exhibit positive and negative pre-noon and afternoon variations seen mostly during the summer and equinoctial months. The maximum pre-noon positive $MSqD_{int}$ amplitudes reached ~8 nT and 9 nT around 06:00 LT each at MGD in May 2017 and July 2012 as shown in Figures 4.5 (panel D5) and 4.6 (panel D6).

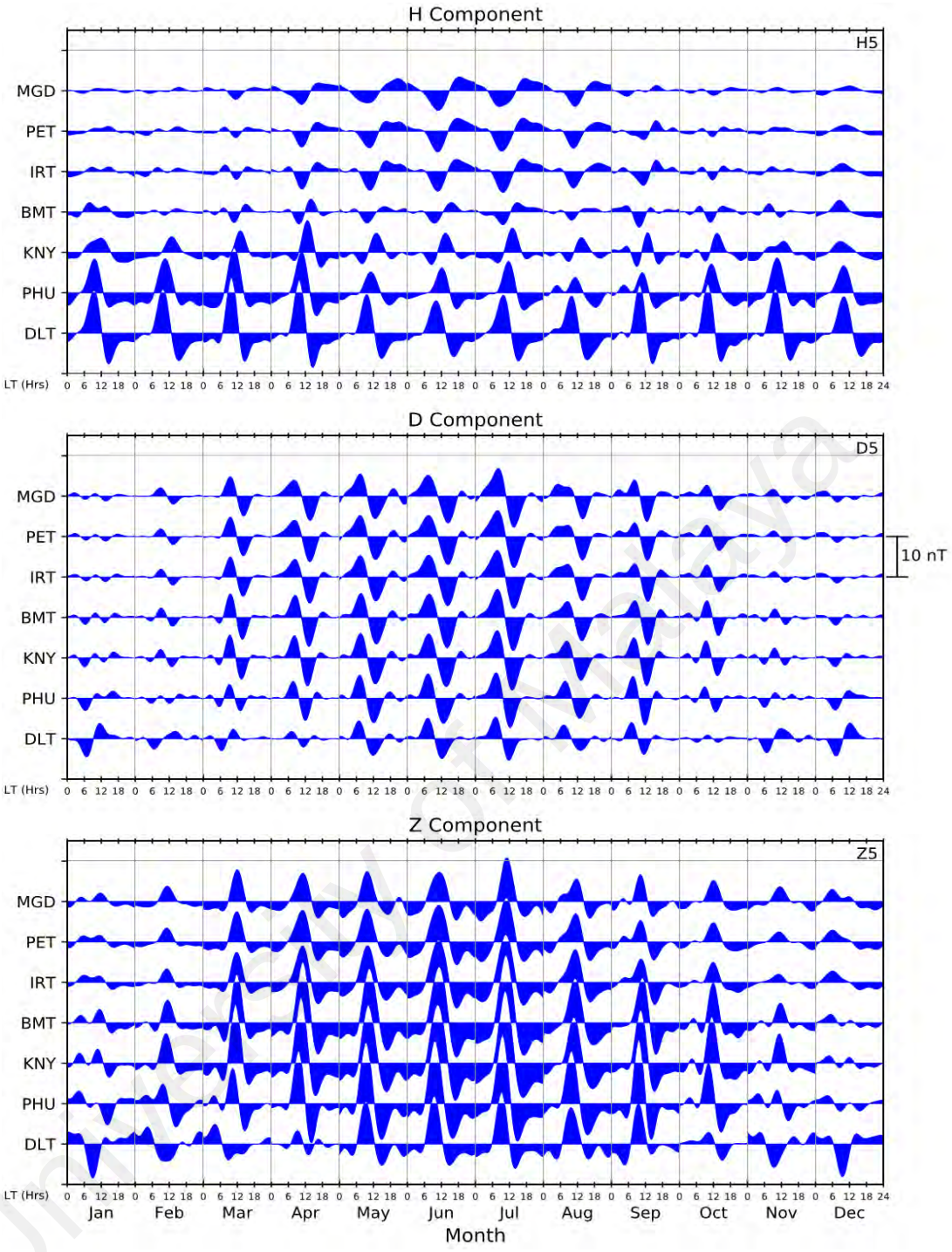

Figure 4.5: Month-by-month internal field variations of the three orthogonal components (H, D, and Z) reconstructed from the internal spherical harmonic coefficients at some selected magnetic observatories in 2017.

The maximum afternoon negative amplitude values ~-9 and -13 nT were observed around 12:00 LT each at MGD in May 2017 and July 2012. These $MSqD_{int}$ magnitudes in summer and equinoctial months indicates that the north-south component of the induced current is southward and northward during the pre-noon and afternoon hours as given in Figures 4.5 (panel D5) and 4.6 (panel D6). The $MSqD_{int}$ also exhibit stronger variations at the summer and equinoctial months and the afternoon variations are slightly greater than the pre-noon and both variations generally appeared weak with much fluctuation in winter months. The $MSqD_{int}$ are also not exception to these "W shape" seen only in May and July at the latitudes of MND, ROC, MLB and MCQ during the dip minimum solar activity indication that the north-south component of the induced current appeared disturbed during the winter months.

Figures 4.4 to 4.6 (panels Z4 to Z6) illustrates the internal field variations of the Z component $MSqZ_{int}$ from dip minimum to moderate solar activity years. It is obvious that the current resulting to $MSqZ_{int}$ variations exhibit opposite sign north and south of the magnetic dip equator. In the southern hemisphere, night-time positive $MSqZ_{int}$ variations between 16:00 and 06:00 LT hrs and daytime negative variations between 07:00 and 15:00 LT hrs are features seen across the latitudes mostly during summer and equinoctial months. Exceptions to these variations are LKW and MND on the magnetic equator. In these stations (LKW and MND) the amplitudes of $MSqZ_{int}$ fluctuate particularly during the winter months. Besides these variations, $MSqZ_{int}$ reached its maximum amplitude ~-14 nT around 11:00 LT in MLB, see Figure 4.4 (panel Z4). In the northern region, $MSqZ_{int}$ exhibit night-time negative amplitudes seen between 16:00 and 06:00 LT and daytime positive amplitudes between 07:00 and 15:00 LT in most cases in contrast to what was observed in the southern hemisphere. Exception of DLT and PHU during the winter months (November-February). In these latitudes DLT and PHU in the northern

hemisphere exhibit night-time and daytime positive and negative $MSqH_{int}$ amplitudes similar to the southern hemisphere current pattern. Beside these variations, $MSqZ_{int}$ amplitudes reached their maximum ~18 and 18 nT around 11:00 each at BMT during low and moderate solar activity, see Figures 4.5 (panel H5) and 4.6 (panel H6).

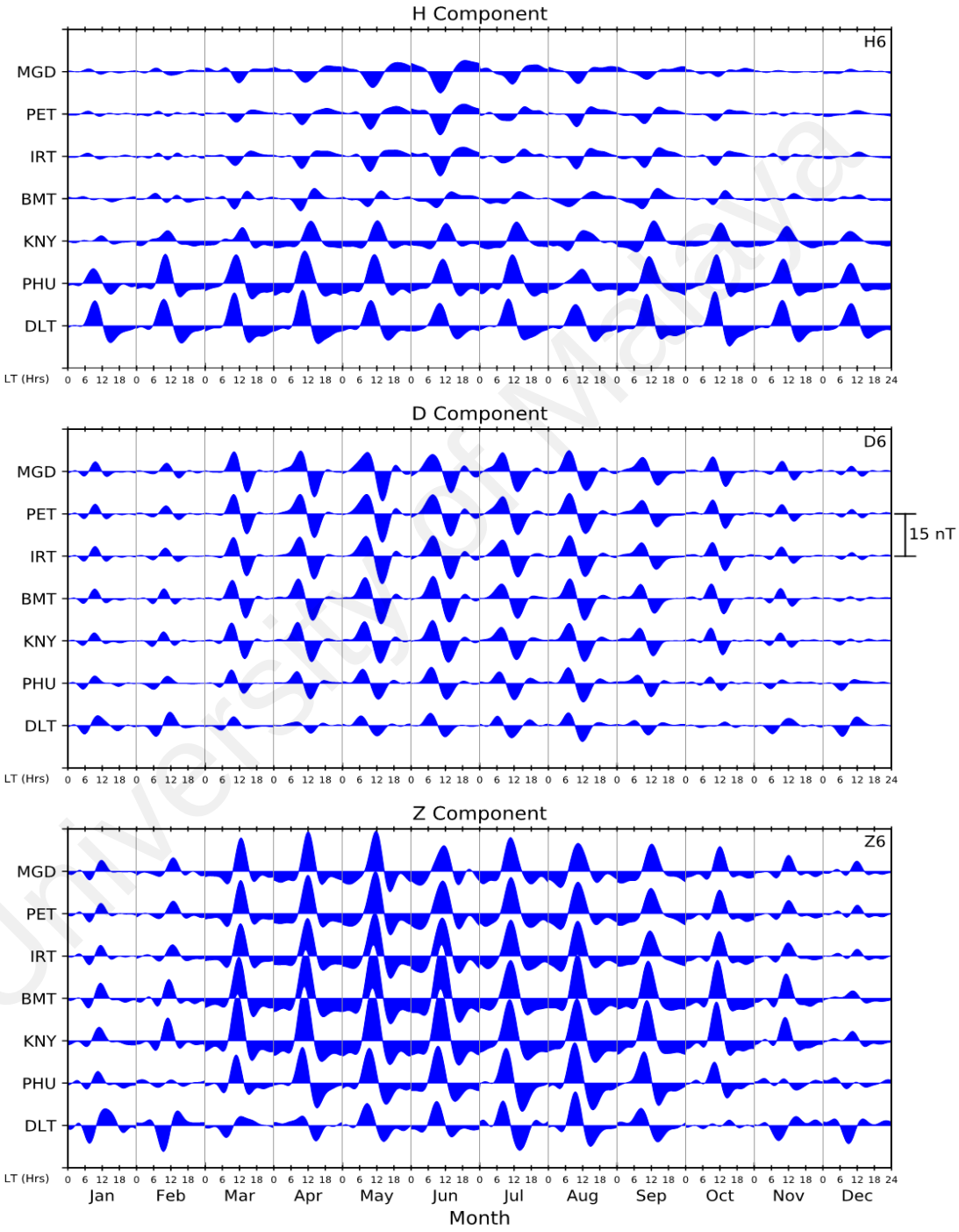

Figure 4.6: Month-by-month internal field variations of the three orthogonal components (H, D, and Z) reconstructed from the internal spherical harmonic coefficients at some selected magnetic observatories in 2012.

Figures 4.7 to 4.9 show the sum (external plus internal) of the quiet field reconstructed from SHA for each of the components (H, D and Z) during the dip minimum to moderate solar activity years. It is apparently seen from Figure 4.7 (panel J) that the sum of the horizontal quiet field $MSqH_{Tot}$ show semi-annual variation pattern with night-time negative amplitudes between 16:00 and 07:00 LT hrs in most cases and a daytime positive amplitudes between 08:00 and 15:00 LT hrs. These features persist from the latitudes of LKW to KPG in the southern hemisphere see Figure 4.7 (panel J). Similar variations are observed at the latitudes of DLT and PHU in the northern hemisphere during low and moderate solar activity years 2017 and 2012, see Figures 4.8 (panel Q) and 4.9 (panel M). The daytime $MSqH_{Tot}$ peak amplitudes reached about 35 nT in May at LKW during the dip minimum solar activity as shown in Figure 4.7 (panel J). With increase in solar activity the $MSqH_{Tot}$ amplitudes increases to about 53 and 65 nT each in March 2017 and 2012. Those peak amplitudes are all observed around 11:00 LT hrs and show the influence of increasing solar activity. During these periods, the maximum negative $MSqH_{Tot}$ amplitude ∼-30 nT was observed in February at MCQ in southern hemisphere during the dip minimum solar activity year 2008 as shown in Figure 4.7 (panel J). During low and moderate solar activity year 2017, the daytime maximum negative $MSqH_{Tot}$ amplitudes reached ∼-20 and -30 nT seen at MGD each in June, see Figures 4.8 (panel M) and 4.9 (panel Q). Just like the $MSqH_{ext}$ amplitudes the daytime $MSqH_{Tot}$ amplitudes in both hemispheres decreases with increasing latitudes and the negative amplitudes appear weak at mid-latitude but seem to increase with increasing latitudes. Generally, the $MSqH_{Tot}$ amplitudes appear stronger in summer and equinoctial months and weaker in winter months.

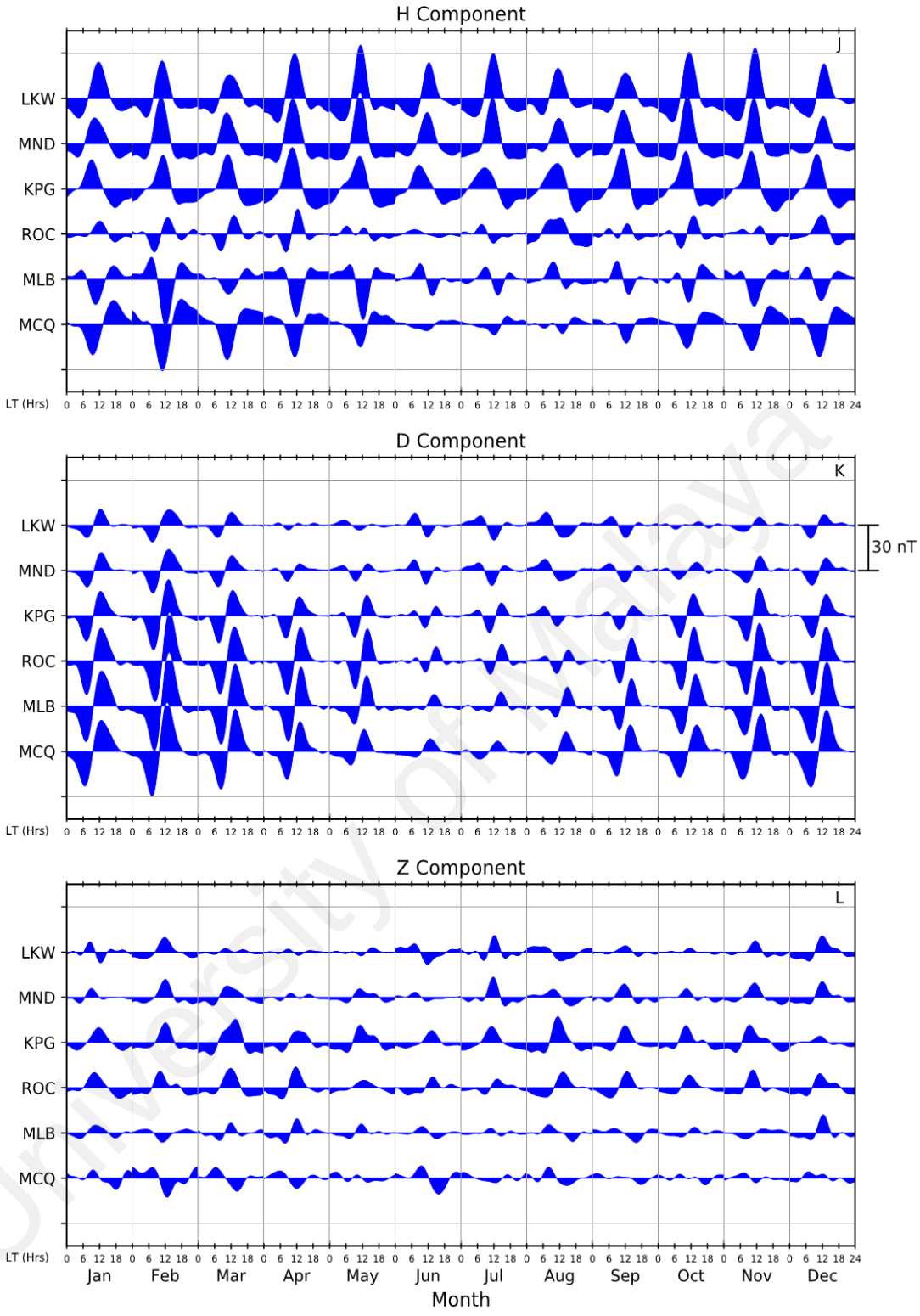

Figure 4.7: Sum of the quiet monthly field variations reconstructed from the spherical harmonic coefficients at some selected magnetic observatories in 2008.

The sum (external plus internal) of the quiet eastward D component $MSqD_{Tot}$ variations in the southern hemisphere during the dip minimum solar activity are illustrated in Figure 4.7 (panel K). The features shows a well-defined northward and southward directed current flow generating negative and positive $MSqD_{Tot}$ amplitudes during the pre-noon and afternoon hours. These variations pattern are consistent with the D-component located southward of the magnetic dip equator. The maximum pre-noon and afternoon $MSqD_{Tot}$ amplitudes reached ~-30 nT and 33 nT around 07:00 LT and 13:00 LT hrs at MCQ and MLB each in February during the dip minimum solar activity year 2008, see Figure 4.7 (panel K). In the northern hemisphere, $MSqD_{Tot}$ amplitudes show southward and northward flow of current during the pre-noon and afternoon hours generating positive and negative amplitudes at these periods. The pre-noon peak amplitudes reach about 27 nT and 30 nT in May and June each at BMT around 10:00 and 07:00 LT during low and moderate solar activity as depicted in Figures 4.8 (panel R) and 4.9 (panel N). Their afternoon negative $MSqD_{Tot}$ amplitudes reached ~-29 nT and -28 nT around 13:00 LT in July and May during low and moderate solar activity. Throughout the years, the variations of $MSqD_{Tot}$ amplitudes have not really shown much changes in magnitudes with increasing solar activity but generally appeared stronger in summer and equinoctial months and weaker in winter months.

Figure 4.7 (panel L) show the sum of the field variations of the Z-component $MSqZ_{Tot}$ during the dip minimum solar activity year 2008 in the southern hemisphere. The $MSqZ_{Tot}$ amplitudes appeared variable across all the latitudes exception of KPG and ROC. The variable pattern suggests the magnetic fields record may likely be affected by the geological location of the magnetic observatories or the Z-field component may be contaminated by the induced sub-surface currents. However, night-time negative

$MSqZ_{Tot}$ amplitudes are eminent between 17:00 and 07:00 LT at KPG and ROC and the daytime positive amplitudes are seen between 08:00 and 16:00 LT.

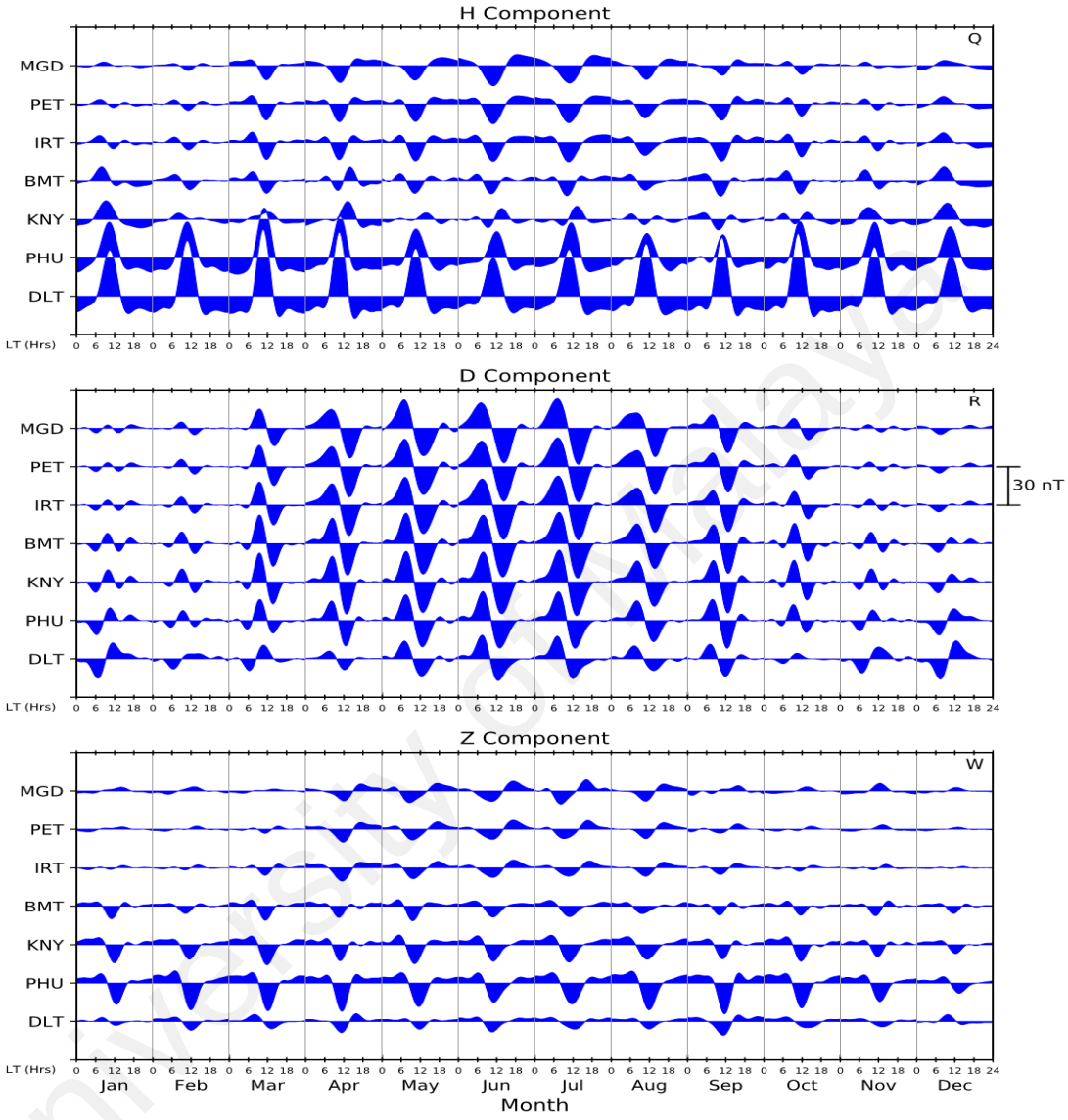

Figure 4.8: Sum of the quiet monthly field variations reconstructed from the spherical harmonic coefficients at some selected magnetic observatories in 2017.

The daytime maximum $MSqZ_{Tot}$ amplitude ~23 nT occurred around 11:00 LT in August at KPG see Figure 4.7 (panel L). At the northern hemisphere the $MSqZ_{Tot}$ appeared less variable with night-time positive variation between 16:00 and 08:00 LT in most cases and daytime negative variations between 09:00 and 15:00 LT during low solar activity, Figure 4.8 (panel W). Similar variations are observed during moderate solar activity as illustrated

in Figure 4.9 (panel P). During these periods, the highest daytime negative $MSqZ_{Tot}$ amplitudes ~-28 and -35 nT occurred around 11:00 LT at PHU each in September 2017 and 2012. The $MSqZ_{Tot}$ generally increases with increasing solar activity.

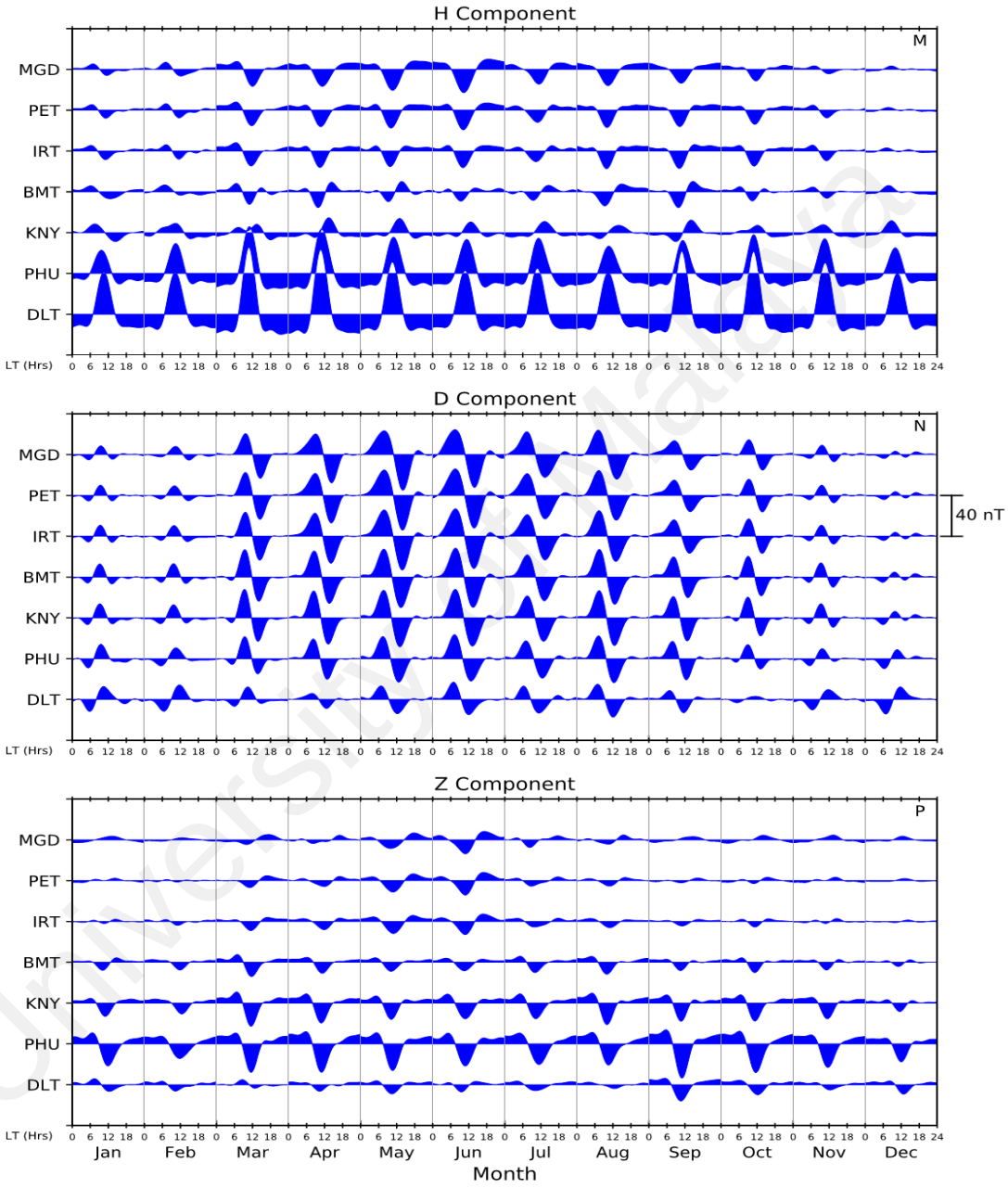

Figure 4.9: Sum of the quiet monthly field variations reconstructed from the spherical harmonic coefficients at some selected magnetic observatories in 2012.

It is worthy to note that in the southern hemisphere, the daytime Sq current is usually negative and any enhancement in the current will definitely corresponds to decrease in the current system (i.e. the current becomes more negative). Because minima in the equivalent Sq current function at the southern hemisphere are related to enhanced currents, the description of this southern minima would be taken as maxima throughout the remainder of this text. The month-by-month equivalent current system computed from the external and internal parts of the geomagnetic field records for the solar quiet years 2008, 2012 and 2017 are illustrated in Figures 4.10 to 4.15. The Sq current contour of each month are plotted in local time against the geomagnetic latitude of the stations and the current between adjacent contours is about 10^4A.

The month-by-month external equivalent currents illustrated in Figure 4.10 shows that they are characterized by a single daytime current vortex near mid-latitude that appears stronger in summer months (November-February) and weaker in winter months (May-August) during the dip minimum solar activity year 2008.

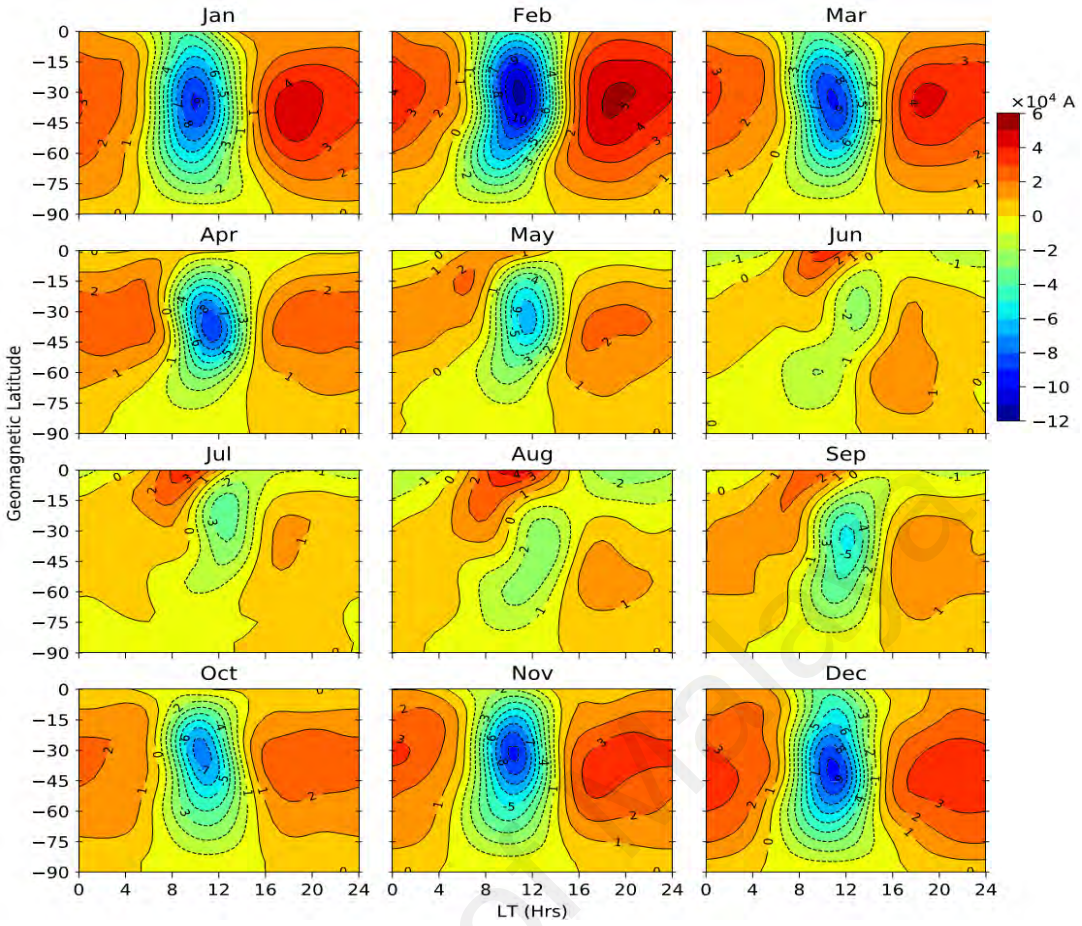

Figure 4.10: Month-by-month external equivalent current system determined from the external spherical harmonic coefficients in southern hemisphere in the year 2008.

Similar behavior is observed in the northern hemisphere, the external equivalent current vortex appears stronger in summer months (May-August) and weaker in winter months (November-February) as indicated in Figures 4.11 and 4.12 respectively. The maximum intensity of the Sq current in the southern hemisphere reached ~-10.5 × 10^4A in summer (February) and its minimum intensity is ~-2.0 × 10^4A in winter (June) during the dip minimum solar activity year 2008 see Figure 4.10. As solar activity increases, the intensity of the external equivalent current reached about 11.7 × 10^4A and its minimum ~-1.0 × 10^4A occurred in July and January as shown in Figure 4.11.

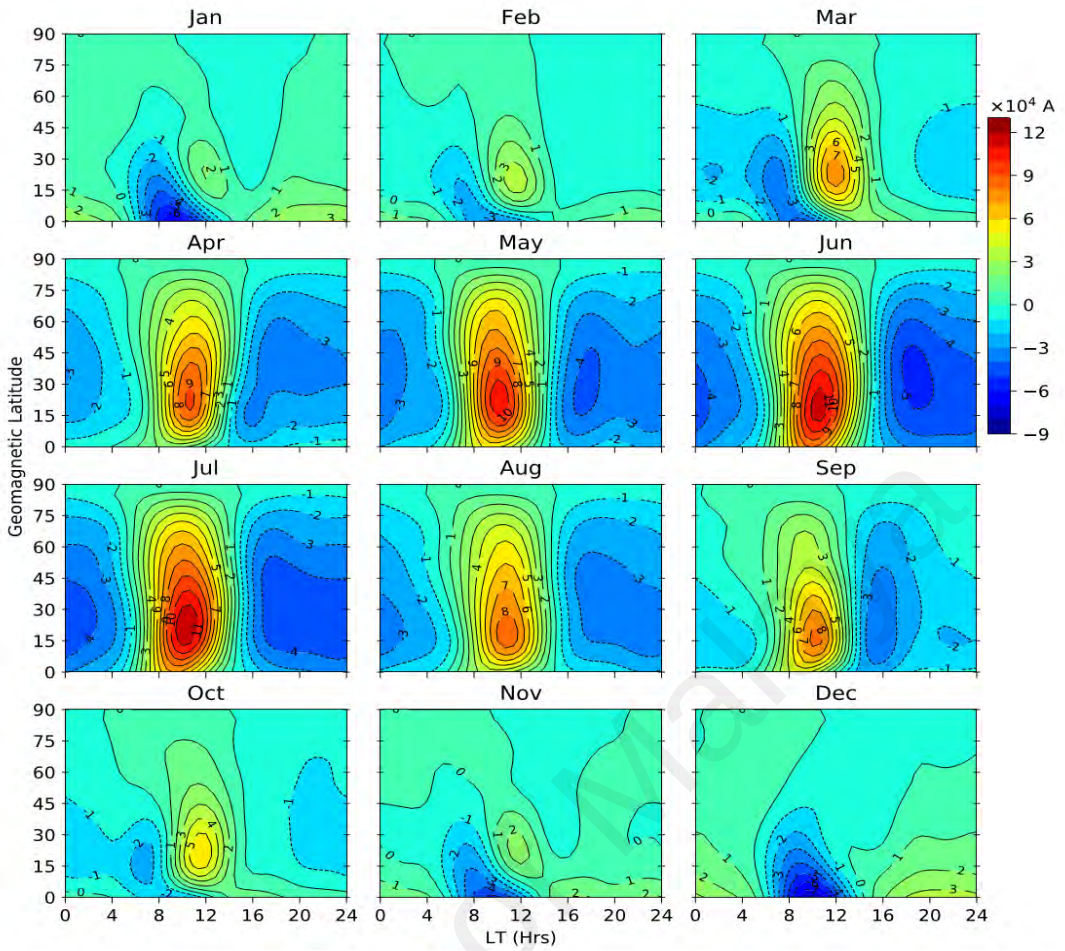

Figure 4.11: Month-by-month external equivalent current system determined from the external spherical harmonic coefficients in northern hemisphere in the year 2017.

These magnitudes were further observed to increase to about 15.5×10^4A in June with minimum intensity of about 1.0×10^4A in December during moderate solar activity year 2012 as shown in Figure 4.12. The magnitudes of these external equivalent currents implies that they increase with increasing solar activity. During these times when the external current was minimum in the southern hemisphere during the dip minimum solar activity, the daytime external current appeared very weak in winter months (May-August) with its vortex at the lowest latitude ~25° in July and disappeared in August as shown in Figure 4.10. In the northern hemisphere, during low solar activity the daytime external Sq current vortex appears weak in winter months and disappeared only in December as indicated in Figure 4.11. During moderate solar activity, the external current vortex only

appeared weak and drops to its lowest latitude ~15° in January and December with no disappearances as illustrated in Figure 4.12.

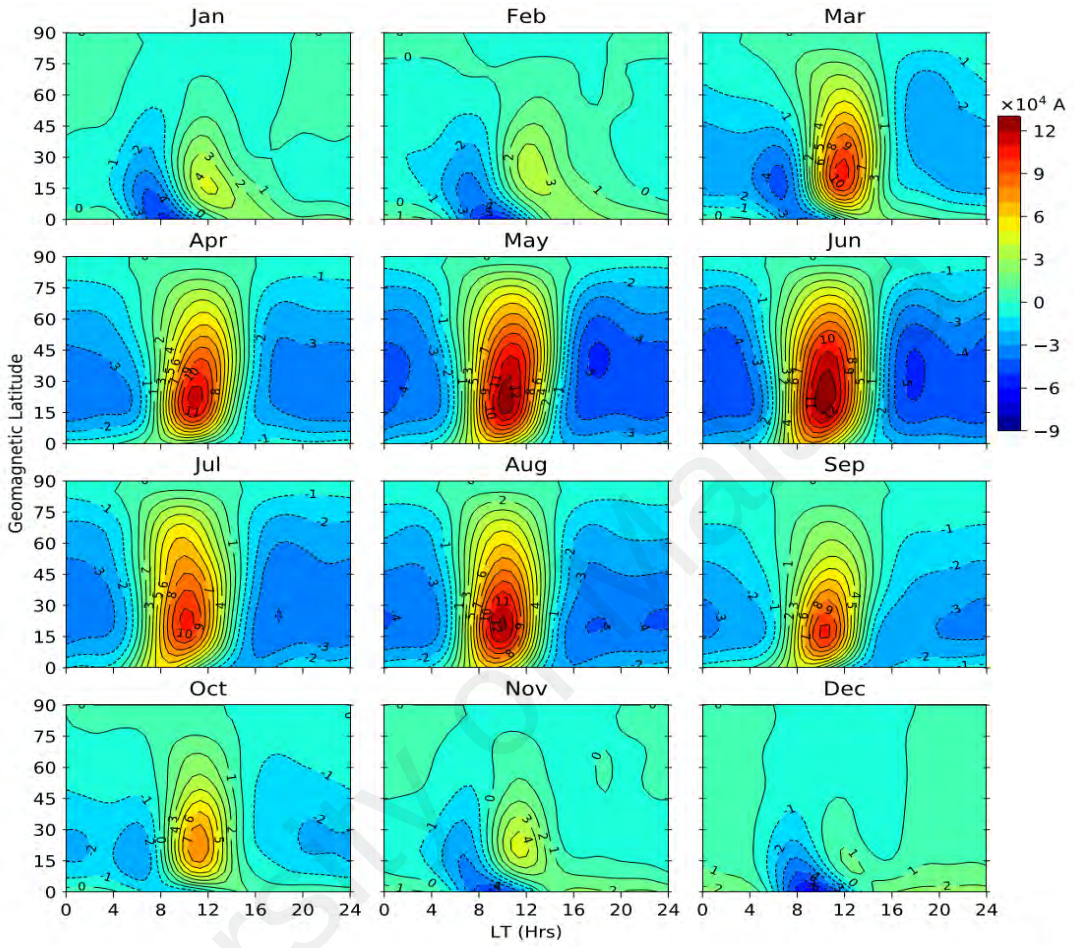

Figure 4.12: Month-by-month external equivalent current system determined from the external spherical harmonic coefficients in northern hemisphere in the year 2012.

The latitudinal position of the Sq current focus in both hemispheres exhibit seasonal dependence. In the southern hemisphere, the latitudinal positions of the external current focus fluctuate between ~-30° and -35° in summer months (November-February) and drop to its minimum in July during dip minimum solar activity, while in winter months with April and October included (April-October), the external focus fluctuate at lower latitudes ~-25° and -32° see Figure 4.10. These southern hemisphere latitudinal range of

the external focus positions indicates slightly poleward appearance in summer than in winter months.

In the northern hemisphere, the external focus is seen in the range between ∼22° and 24° in summer months with April included (April-August) while in January-March-October-November, the external focus lie in the range between ∼25° and 28° as depicted in Figure 4.11. When the solar activity was moderate, the latitudinal position of the external focus range between ∼22° and 24° in summer months inclusive of April (April-August) and ranged between ∼25° and 28° in February-March-October-November, then decreases significantly to about ∼15° in January and December as shown in Figure 4.12. These results seems to show that in the northern hemisphere, the latitudinal position of the external current vortex appeared at lower latitudes in summer than in winter months. Exception to this are January and December which are sub-division of winter months during moderate solar activity. In these months (January and December) the latitudinal position of the external current focus are at lower latitudes. Besides these latitudinal range, careful observation of the external current focus show that they generally drop to their minimum latitude ∼15° and ∼18° in September during low and moderate solar activity, see Figures 4.11 and 4.12. The result thus indicates that when the external current focus drops equatorward in September, it remained relatively poleward at ∼25° in March.

The internal equivalent current system presented in Figures 4.13 to 4.15 reflect most of the general features of the external Sq current but are only about 0.80, 0.56 and 0.50 times as large in 2008, 2017 and 2012. The internal Sq current also appear stronger (weaker) in summer (winter) months in both hemispheres. In the southern hemisphere, the maximum summertime intensity of the internal equivalent current reached $\sim -9.0 \times 10^4$A in February and its minimum intensity $\sim 1.0 \times 10^4$A in winter (June) 2008 as

depicted in Figure 4.13. As solar activity increases slightly, the maximum intensity reached about -6.5 × 10^4A in summer (July) and it minimum amplitude ~ −1.0 × 10^4A occurred in winter (February) 2017 as shown in Figure 4.14. During moderate solar activity year 2012, the internal current reached its maximum amplitude ~-7.5 × 10^4A in summer (June or May) and the minimum amplitude ~-1.0 × 10^4A appeared in winter (December), see Figure 4.15.

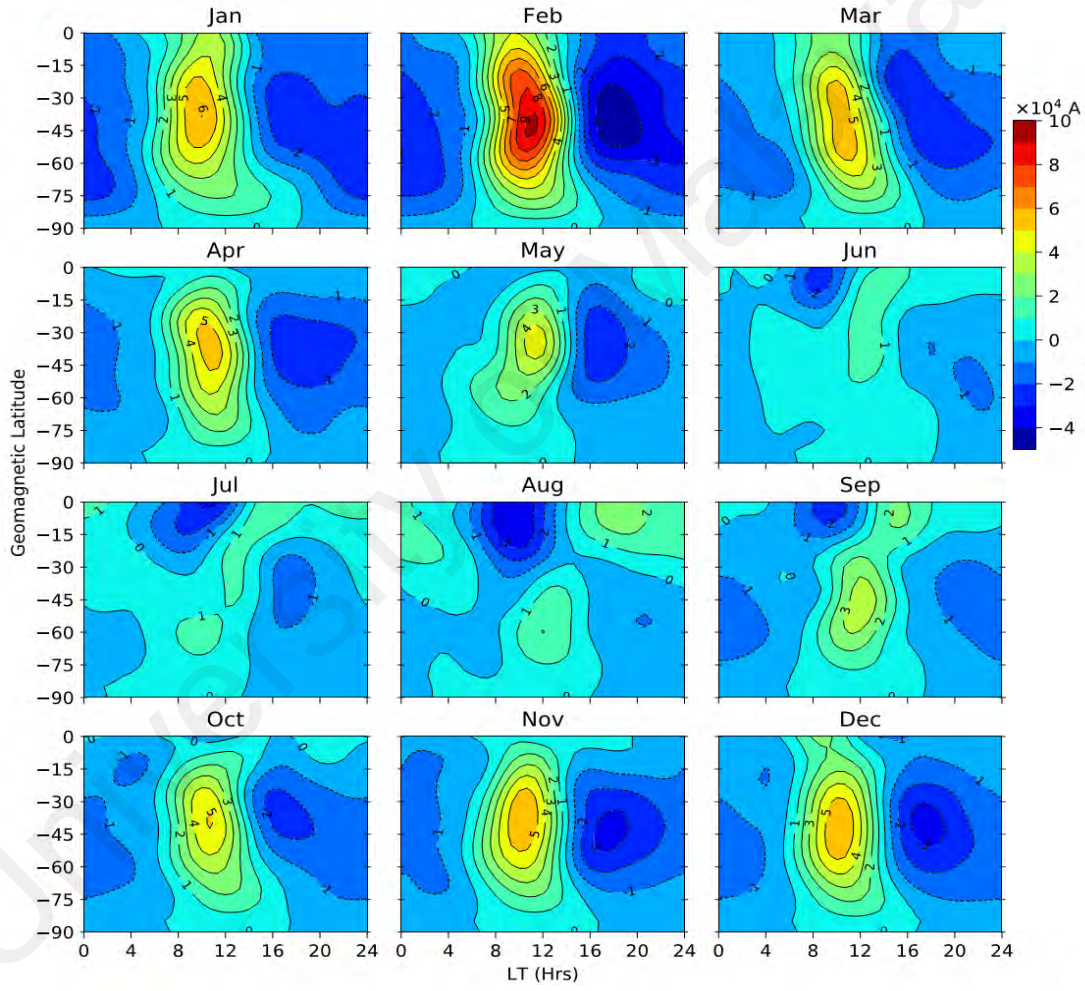

Figure 4.13: Month-by-month internal equivalent current system determined from the internal spherical harmonic coefficients in southern hemisphere in the year 2008.

Just like the external currents, the internal equivalent current vortices are not exception to these disappearances seen in winter months (June, July and August) during the dip minimum solar activity as depicted in Figure 4.14. Similar disappearance of internal

current vortex occur in winter months (November-December) during low solar activity, see Figure 4.14. During the moderate solar activity, the internal current vortex only disappeared in December as shown in Figure 4.15.

Apart from the disappearances of internal current vortices in winter months, they also exhibit latitudinal variations apparently seen across all the months. In the southern hemisphere, during the dip minimum solar activity, the internal current focus lie between ~-32° and -37° in summer months (November-February) and fluctuate between ~-33° and -40° in winter with April and October included (April-October), see Figure 4.13.

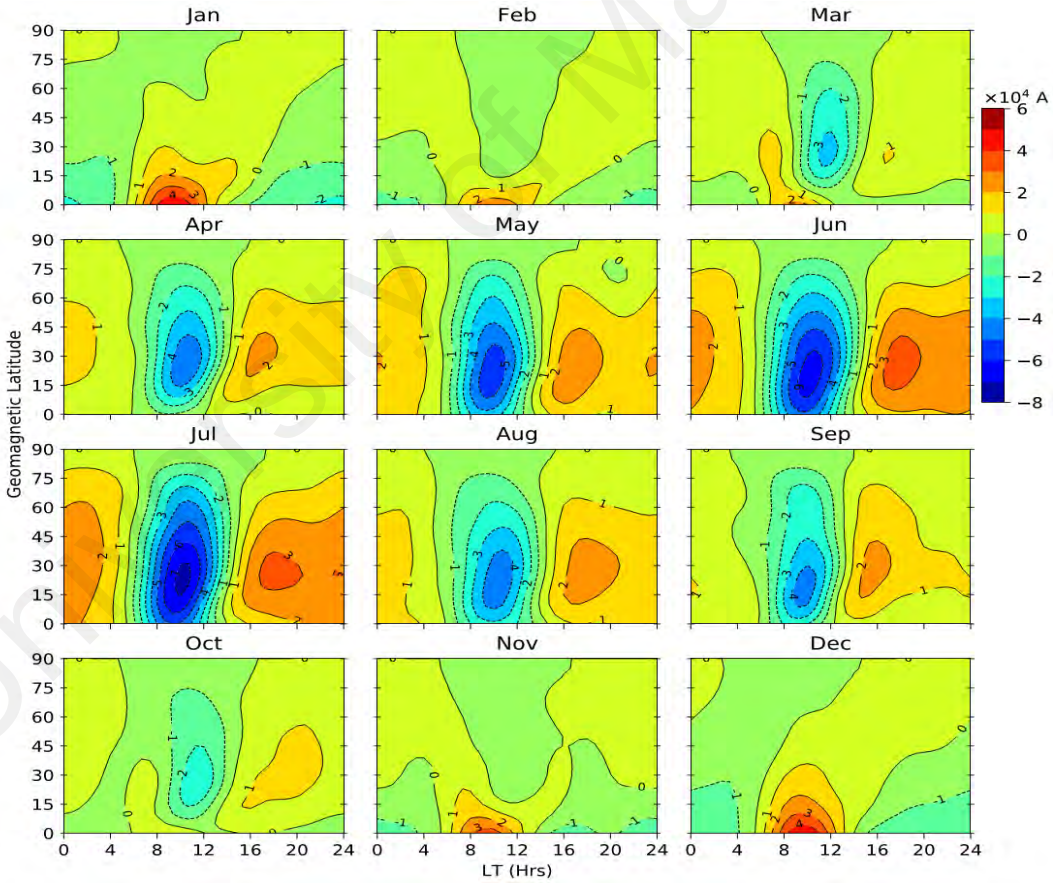

Figure 4.14: Month-by-month internal equivalent current system determined from the internal spherical harmonic coefficients in northern hemisphere in the year 2017.

The result thus indicates that in the southern hemisphere, the latitudinal range of the internal currents focus appeared slightly poleward in winter than in summer months and opposite was the case for the external current. During low solar activity, the internal current focus ranged between ~17° and 25° in summer months with April included (April-August), see Figure 4.14. In February-October-November which are sub-division of northern winter months, the internal current focus lie between 27° and 29°. When solar activity was moderate, the internal current focus fluctuate between ~25° and 30° in summer months inclusive of April (April-August) and ranged between ~31° and 35° in October-November-January-February which are sub-division of winter months see Figure 4.15.

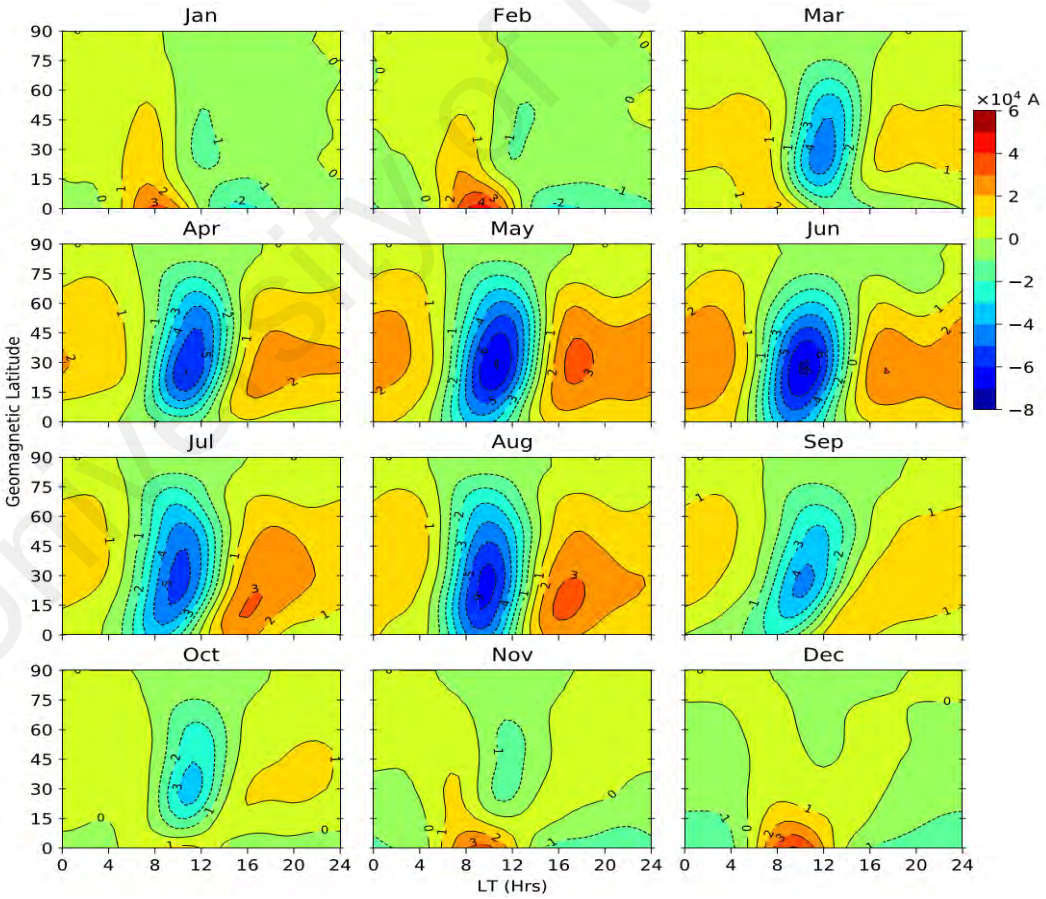

Figure 4.15: Month-by-month internal equivalent current system determined from the internal spherical harmonic coefficients in northern hemisphere in the year 2012.

These results in the northern hemisphere clearly reveals that the latitudinal position of the internal current focus is located at higher (more poleward) latitude in winter than in summer months. Unlike the external current, the latitudinal range of the internal current vortices appeared more variable in summer than in winter months. Another feature observed is that the internal current focus drop to its minimum latitude ~15° in September and remained relatively poleward ~25° in March during low solar activity, see Figure 4.14. Such features is not obvious on the internal current during moderate solar activity. Besides the substantial decrease in the latitudinal position of the external current focus in January and December during moderate solar activity, the results established that the latitudinal range of both external and internal current vortices mostly appeared at lower latitudes in summer than in winter months in the northern hemisphere. Throughout the years, the internal current focus seems to be relatively more poleward than their corresponding external focus.

Figures 4.16 to 4.18 shows the mantle electrical conductivity-depth profile of Asia sub-region during the dip minimum to moderate solar activity years. The dotted points are the computed conductivity values.

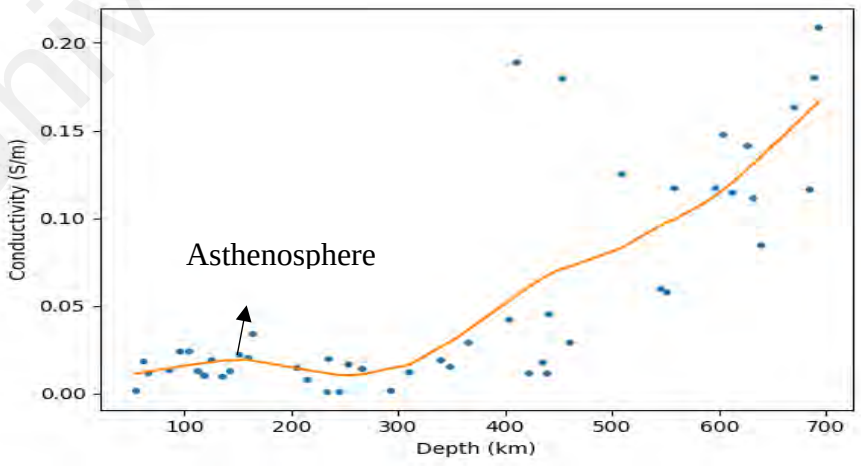

Figure 4.16: Electrical conductivity-depth profile of the upper mantle and transition zone from quiet-time magnetic field record of the year 2008 in Asia sub-region.

The locally weighted regression fitting to the conductivity values is given by the solid line computed using the locally weighted scatterplot smoothing (LOWESS) best fit technique earlier described by (Cleveland, 1979). A small group of conductivity values mostly at depth range between ~200 and 400 km are observed in Figures 4.16, 4.17 and 4.18. These conductivity values are not certain whether they are actually real or outliers or there may be times when the varying source of Sq field is inducing a response from a small scale, high conductivity anomaly at those locations. It also possible that the quiet days selected for the study may contribute to some extent the observed group of conductivity values.

Apart from these small groups of conductivity values, generally the scattered points on these figures are much concentrated within the first few kilometers down to a depth of about 450 km and beyond which, the density of the scattered point tends to decrease to a depth of about 680, 770 and 750 km in 2008, 2012 and 2017 respectively. These scattered points resulted from series of factors among them includes; error incurred from the field measurements, error from spherical harmonic analysis (SHA) fitting, various sources of current such as field-aligned currents (FACs), equatorial electrojet current (EEJ). The selected quiet days may also contribute some error. It is worthy to note that the original data has some noise and the effect of lateral inhomogeneity which both constitute to some extent error that that is very difficult to evaluate accurately, hence what could be termed an error is in the measurement of the regression fitting for the scattered conductivity values.

Despite the scatter in the conductivity values, the LOWESS fitting showed the general features of the conductivity variations from the sub-crustal surface level down to the lower mantle depth. The LOWESS conductivity profile seems to appear sharp and faster

down to the lower mantle depth during moderate solar activity year 2012 (Figure 4.17) and sluggishly increase during dip minimum and low solar activity years 2008 and 2017 (see Figures 4.16 and 4.17) . It is obvious from these figures that the conductivity profile increases with depth from the sub-crustal surface having an initial magnitude of ~0.01, 0.01 and 0.02 S/m at depths of about 40, 30, 40 km in 2008, 2012 and 2017. The profile gradually rose to about 0.02, 0.035 and 0.025 S/m at depths of 100, 120 and 130 km seen in 2008, 2012 and 2017. These profiles suddenly rose to about 0.025, 0.05 and 0.04 S/m at depths of about 180, 280 and 300 km in 2008, 2012 and 2017 respectively. During the dip minimum solar activity, the conductivity profile decreases to about 0.01 S/m at depth range of about 240-280 km as depicted in Figure 4.16. Generally at each depth range, the conductivity profile during the moderate solar activity exhibit higher magnitude (see Figure 4.17) and the lower magnitude mostly occur during the dip minimum solar activity, Figure 4.16.

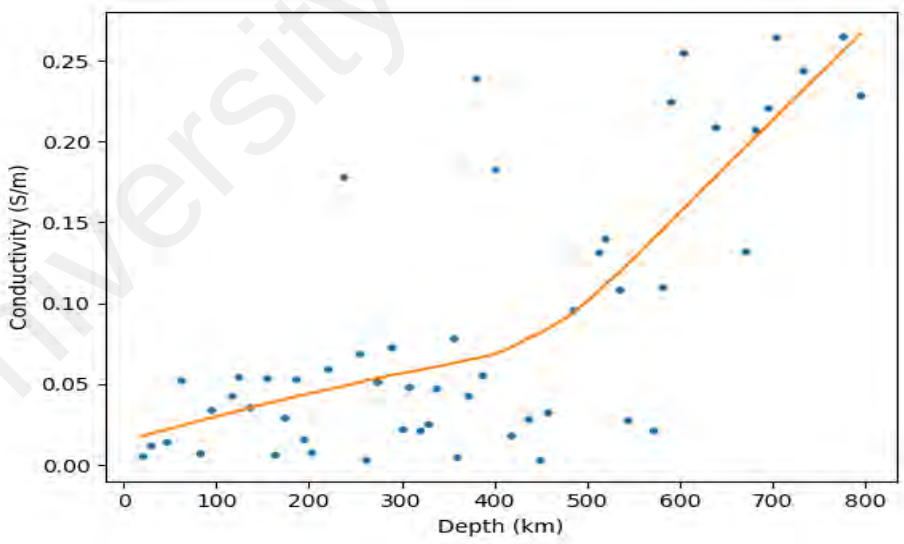

Figure 4.17: Electrical conductivity-depth profile of the upper mantle and transition zone from quiet-time magnetic field record of the year 2012 in Asia sub-region.

Subsequently, a sharp increase in the conductivity profile was observed at depth near 310 km during dip minimum solar activity year 2008, Figure 4.16, with similar effect at about 350 km during low solar activity year 2017 Figure 4.18 and this effect was not observed until at depth near 420 km during moderate solar activity year 2012 as shown in Figure 4.17. The conductivity profile corresponding to these depths are 0.03, 0.06 and 0.05 S/m. These profiles steepen to about 0.07, 0.09 and 0.08 S/m near 450, 480 and 600 km depths in 2008, 2012 and 2017 respectively. Shortly after these features, a slight decrease in conductivity profile of about 0.07 S/m occurred at depth range of about 570-590 km closely followed by a sharp steep increase to about 0.1 S/m near 600 km during low solar activity year 2017, see Figure 4.18.

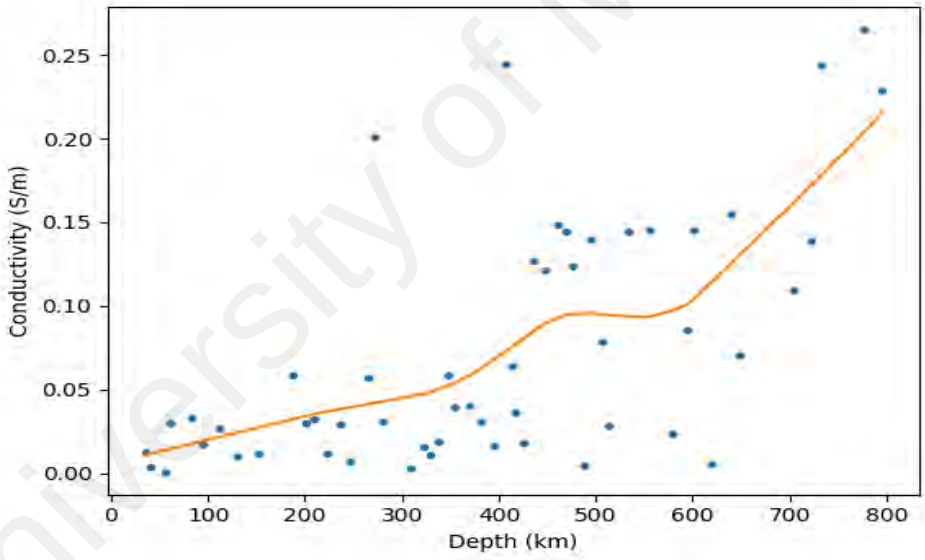

Figure 4.18: Electrical conductivity-depth profile of the upper mantle and transition zone from quiet-time magnetic field record of the year 2017 in Asia sub-region

This increase becomes steeper through the mantle to about 0.2 S/m near 770 km as the maximum depth it could reach without leveling off during low solar activity, see Figure 4.18. During moderate solar activity year 2012, a sharp rapid increase was observed below the depth of about 500 km and reached about 0.175 S/m at depth near 650 km. The profile continues to rise faster to about 0.30 S/m at depth near 800 km with no indication

of leveling off. The increase in conductivity profile is more rapid during the moderate solar activity as shown in Figure 4.17 and slowest during the dip minimum solar activity as depicted in Figure 4.16. An evidence of discontinuity was clearly observed at depths of about 380-460 km, 390-480 km and 570-640 km in 2008, 2012 and 2017.

CHAPTER 5: DISCUSSIONS OF RESULTS

The solar daily variations of the external and internal field on quiet days at mid-low latitude stations are important features of the mid-low latitude ionosphere. These night-time negative $MSqH_{ext}$ amplitudes observed at the latitudes of LKW, MND and KPG in the southern hemisphere with similar variations at DLT, PHU and KNY in the northern hemisphere indicate a well-defined westward flow of current in the E-region of the ionosphere mostly between 17:00 and 07:00 LT hrs. These variations are consistent with the main expectation of the night-time Sq current distributions earlier established (e.g., Fejer, 1981; Stening & Winch, 1987; Takeda & Araki, 1985). These authors observed that the ionospheric currents and electric field reverse their directions and flow westward at night-time hours. The night-time positive $MSqH_{ext}$ amplitudes at the latitudes of the MLB and MCQ in the southern hemisphere during dip minimum solar activity year 2008 with similar variations at BMT up to the latitude of MGD in the northern hemisphere during low and moderate solar activity years 2017 and 2012 are indications of well-defined eastward flow of current system which will be extensively discussed later.

The irregular $MSqH_{int}$ variations during the year of dip minimum solar activity may likely be affected by local anomalies. During low and moderate solar activity, the variations of $MSqH_{int}$ assumed regular occurring pattern that indicates the east-west component of the night-time induced current flow westward at DLT up to the latitude of KNY and beyond which it flowed eastward. In general, the night-time (daytime) variations of both $MSqH_{ext}$ and $MSqH_{int}$ shows the presence of westward (eastward) currents at the equatorial and low latitude regions and changeover to eastward (westward) currents somewhere at mid-latitude region. The daytime eastward current generally decreases with increasing latitudes while the westward current seems to increase with increasing latitudes.

The salient feature to note from the result presented in Figure 4.1 (panel H1) is that the reduced $MSqH_{ext}$ magnitudes and phase shift at KPG and the changeover to negative amplitude at the latitude of ROC with similar reduced $MSqH_{ext}$ magnitudes at PHU and switched over to negative amplitudes at KNY as depicted in Figures 4.2 (panel H2) and 4.3 (panel H3) suggest likely presence of the external current focus nearer the latitude of ROC and KNY in the southern and northern hemispheres respectively. This could be one of the reason for the observed night-time positive and negative $MSqH_{ext}$ amplitudes at stations above and below ROC in the southern hemisphere and KNY in the northern hemisphere. Similarly, the daytime positive and negative $MSqH_{ext}$ amplitudes equatorward and poleward of ROC in the southern hemisphere and KNY in the northern hemisphere are due to the presence of the external current focus. Another interesting result is that during the dip minimum solar activity year 2008, the daytime positive $MSqH_{ext}$ amplitudes at the latitudes of ROC in April, August, October and December indicates that the southern external current focus in these months are located southward (poleward) of ROC while in other months it remained relatively northward (equatorward). Similar features are observed at the latitudes of KNY in the northern hemisphere during low solar activity year 2017 at the months of January, April, November and December with similar effect in May 2012. These features in the northern hemisphere suggest that the external current focus lie northward (poleward) of KNY at the aforementioned months and remained southward (equatorward) in other months. This further established that under normal ionospheric conditions, the daytime latitudes equatorward (poleward) of the Sq current focus are bounded by eastward (westward) flow of currents. Takeda (1990) discussed that the eastward current at the latitudes between the current vortex and the magnetic dip equator are created by eastward electric field (EEF) and the westward currents at latitudes higher than the current vortex are caused by induced field. This present result further established that Sq current focus exhibit latitudinal variations as

earlier observed (e.g., Tarpley 1973; Stening, 2005; Stening et al., 2007; Vichare et al., 2017).

The marked reduction in $MSqH_{int}$ amplitudes at the latitude of ROC and changeover from eastward to westward field at MLB as depicted in Figure 4.4 (panel H4) shows the presence of southern internal current focus near the latitude of MLB. Similar reduced $MSqH_{int}$ amplitudes that occurred at KNY and changeover to westward field at BMT as illustrated in Figures 4.5 (panel H5) and 4.6 (panel H6) suggest likely position of northern internal current focus nearer to BMT. These results shows that the internal Sq foci are relatively more poleward than their corresponding external. This difference in latitudinal position between the external and internal current foci may likely be caused by the local conductive region of the upper mantle on the induced currents (Campbell & Schiffmacher, 1985)

Apart from these variations, the daytime $MSqH_{ext}$ and $MSqH_{int}$ amplitudes that reached their peak mostly between 10:00 and 13:00 LT hrs are evidences of stronger Sq current due to intense ionospheric conductivity caused by stronger dynamo action around these periods. The variations in their time of peak may likely be due to variability of the prevailing wind system. Anderson & Roble (1981); Martyn (1947) and Okeke & Hamano (2000) earlier suggested that the tendency of the solar quiet SqH fields to reach peak amplitudes earlier or at a latter local time (LT) depends on the relative strength of the neutral wind present. Both $MSqH_{ext}$ and $MSqH_{int}$ amplitudes show semidiurnal variations at the equatorial latitudes and decreases to annual variations with increasing latitudes. The daytime positive $MSqH_{ext}$ and $MSqH_{int}$ amplitudes show the effect of solar activity, they increases with increasing solar activity and were generally observed to decrease with increasing latitudes. The increase in solar activity cause corresponding increase of solar

fluxes and consequent increase of ionization in the ionosphere resulting to greater conductivity of the dynamo region that produce the higher intensity of both $MSqH_{ext}$ and $MSqH_{int}$ amplitudes during the moderate solar activity of this study. The daytime negative $MSqH_{ext}$ and $MSqH_{int}$ amplitudes poleward of the Sq focus have not really conformed to any pattern but are consistently lower than their corresponding positive amplitudes equatorward of the focus. Month-to-month amplitudes variations of the external and internal fields shows that $MSqH_{ext}$ magnitudes are about twice larger than the $MSqH_{int}$ amplitudes. Their greater magnitudes reflect direct effect of ionospheric conductivity.

Generally the $MSqH_{ext}$ showed a conspicuous variability both in phase and intensity from month-to-month indication of variations in the overhead Sq current system and this induced corresponding variations in $MSqH_{int}$ amplitudes. Various mechanisms have been suggested for such variations. Early studies on the day-to-day variability of both phase and amplitudes of Sq current system attributed it to changes in either conductivity or the dynamo driving force (Okeke & Hamano, 2000; Schlapp, 1968). Mazaudier (1993) explained explicitly that the day-to-day variations of the regular external current is due to large but regular variations in the tidal winds that is mostly present in the magnetic field records. Thakur & Sontake (1981) explained that changes in ionospheric conductivity directly affect the SqH amplitudes and the observed phase variations is likely attributed to changes in atmospheric tidal wind pattern. The LKW and DLT that lies close to the magnetic dip equator have exceptionally large $MSqH_{ext}$ amplitudes due to the presence of equatorial electrojet current caused by the orthogonality of electric and magnetic fields at these latitudes.

Since the $MSqH_{int}$ variations are induced by the external source currents, they reflect most of the features associated with the external field exception of Figure 4.4 (panel H4). In this Figure, the $MSqH_{int}$ show variable pattern which may likely be affected by geological condition of the magnetic observatories used in the study. The $MSqH_{int}$ amplitudes equatorward of the Sq focus exhibit phase variations from one latitude to the other more than those poleward of the focus. Month-to-month correspondence of the $MSqH_{int}$ and $MSqH_{ext}$ amplitudes show they exhibit slight phase variations that is believed to arise from electromagnetic induction effect.

The negative and positive $MSqD_{ext}$ amplitudes in the southern hemisphere during the pre-noon and afternoon hours in summer and equinoctial months (September-April) suggest a well-defined northward and southward flow of current during these periods. These variations are consistent with the D-component southward of the magnetic dip equator. Similar but oppositely directed $MSqD_{ext}$ variations occurred in the northern hemisphere during the pre-noon and afternoon sectors in summer and equinoctial months (April-September). These $MSqD_{ext}$ variations which indicates southward and northward flow of currents are also consistent with northerly stations (Mazaudier & Venkateswaran, 1985). Patil et al. (1985) and Stening & Winch (2013) have also observed similar variations in India and Australian region. These variations during the pre-noon and afternoon hours are due to meridional currents flowing around these periods.

Apart from these normal $MSqD_{ext}$ variations in the northern hemisphere, the additional negative $MSqD_{ext}$ amplitudes between 05:00 and 07:00 LT hrs at the months of March and October across the years decreases with increasing latitudes indication that they may be related to field-aligned currents (FACs) while the smaller positive $MSqD_{ext}$ amplitudes that appeared between 16:00 and 18:00 LT in April, May and September during low solar

activity as shown in Figure 4.2 (panel D2) may be associated to the eastward current. Stening (1989) studied the variations of current intensity with local time for various latitudes. He introduced the (2, 3) tidal mode to be able to produce the obvious changes on the ΔD variations on some abnormal quiet days during the winter months. He observed secondary peak around 16:00 LT hrs in ΔD which he attributed to resultant effect of currents of the (2, 3) mode resembling the north-south current flow pattern of the "inversion" from the southward to the northern hemisphere. This could probably account for the small positive variations between 16:00 and 18:00 LT hrs in the present study. The $MSqD_{ext}$ variations generally increase as solar activity increases with afternoon magnitudes mostly greater than the pre-noon. Their greater magnitudes are consequences of enhanced conductivity of the dynamo region cause by intense solar heating around these periods. Owing to increased insolation, the conductivity in the dynamo region is greatly enhanced in the summer hemisphere generating $MSqD_{ext}$ variations that are consistently stronger (weaker) in summer (winter) months throughout the years and this reflect differences in ionospheric conductivity between the summer and winter hemisphere.

In the southern hemisphere during the summer and equinoctial months (September-April), $MSqD_{int}$ show negative and positive amplitudes during the pre-noon and afternoon hours indication that the north-south component of the induced current flow northward and southward around these periods in consistent with stations southerly to the magnetic equator. Similar but oppositely directed currents flow occur in the northern hemisphere and this generates the observed positive and negative $MSqD_{int}$ amplitudes during the pre-noon and afternoon hours as depicted in Figures 4.5 (panel D5) and 4.6 (panel D6). These observed $MSqD_{int}$ variations are consistent with a typical north-south induced current system for stations northerly of magnetic equator. The enhanced $MSqD_{int}$ amplitudes in

the summer and equinoctial months is no surprise since they are induced by the $MSqD_{ext}$ variations that appeared maximum around these periods. Throughout the years, the $MSqD_{ext}$ amplitudes are about twice larger than the $MSqD_{int}$ magnitudes. Their greater magnitudes are consequences of direct effect of ionospheric conductivity.

During the winter months, two forms of $MSqD_{ext}$ variations pattern are commonly seen: those with "M shape" and "W shape" variations. In the southern hemisphere, during the winter months, the "M shape" variations pattern that appeared at the latitudes of MND and KPG indicates pre-noon and afternoon southward currents on either side of a relatively large northward current near noon generating smaller positive $MSqD_{ext}$ amplitudes on either side of a relatively large negative amplitudes that was observed in Figure 4.1 (panel D1). The additional smaller pre-noon (06:00-07:00 LT) positive $MSqD_{ext}$ amplitudes indicating southward flow of current may likely be associated to morning eastward field. This variation pattern is contrary to the expectation of the D component southward of the magnetic equator and suggest possible disturbances in the external current system. Similar variations have been earlier observed over the Australian region (Stening et al., 2005). Those $MSqD_{ext}$ amplitudes with "W shape" in June and July at the latitudes of ROC and MLB indicate relatively large southward current with smaller northward currents on either sides. This produced the relatively large positive $MSqD_{ext}$ amplitudes near noon having smaller pre-noon and afternoon negative amplitudes as depicted in Figure 4.1 (panel D1). Such variations are also not consistent with the typical eastward D component southward of the magnetic dip equator in which the north-south component of the ionospheric current flow northward and southward during the pre-noon and afternoon hours. The additional afternoon (16:00-18:00 LT) negative $MSqD_{ext}$ amplitudes that indicates northward flow of current in these months may likely be attributed to field-aligned current (FACs).

These $MSqD_{ext}$ amplitudes with "W shape" that appeared in few months during the dip minimum solar activity year 2008, increases in winter months (November-February) during low and moderate solar activity years seen across all the latitudes exception of DLT. This implies that as solar activity increases the abnormal $MSqD_{ext}$ variations in winter months become more prevalent. These variations pattern indicate distortions in the north-south component of the current system during the winter months having two smaller pre-noon and afternoon northward currents each on either side of a relatively large southward current near noon. The $MSqD_{int}$ variations are not exception to these "W shape" indication that even the north-south component of the induced current flow southward having smaller northward currents on either sides. Various mechanisms have been suggested to explain the apparent distortion of the Sq current system and its variability particularly during the winter months. Arora et al. (1980) attributed the apparent distortions of Sq current system in winter months to combined effect of ionospheric dynamo and electric fields that is transmitted from the summer to winter hemisphere. The variations of $MSqD_{ext}$ amplitudes at the latitudes of LKW and DLT closer to the magnetic dip equator appeared weak. These weaker amplitudes may be explained as a result of the stations location at the equatorial latitudes. At these latitudes, the daytime ionospheric currents (equatorial electrojet current) flow mostly in the eastward direction (Chapman, 1951).

The noticeable absence of prominent northward and southward flow of currents expected during the pre-noon and afternoon hours at the latitudes of LKW in winter months (May-August) with similar absence of southward and northward flow of currents vortex expected at the latitude of DLT suggest likely intrusion of the stronger summertime current vortex of the opposite hemisphere to the winter hemisphere at low latitude locations appearing most frequently during the pre-noon hours in the southern hemisphere

and in the afternoon hours in the northern hemisphere as observed in the present study. Takeda (1990) observed possible intrusion of the strong summer current vortex into the winter hemisphere through the field-aligned currents (FACs) generated by the asymmetry in the ionospheric dynamo. It is possible that the opposite $MSqD_{ext}$ variations at LKW and DLT during the winter months are caused by the summertime intrusion of the Sq current vortex through the field-aligned currents (FACs).

The night-time and daytime negative and positively enhanced $MSqZ_{ext}$ amplitudes observed in Figure 4.1 (panel Z1) are consistent with the geometrical configuration of stations located southward of magnetic dip equator as earlier established (Chapman, 1919). The $MSqZ_{ext}$ variations reached their daytime peak amplitudes at different times, indication of variable pattern of the driving source currents with severe effect at low latitudes. In the southern hemisphere the daytime positive $MSqZ_{ext}$ amplitudes appeared stronger during the summer and equinoctial months (September-April) with exceptional enhancement at the latitudes of KPG and ROC closer to the Sq focus and became weaker at the winter months (May-August).

At the northern hemisphere, the night-time and daytime positive and negative $MSqZ_{ext}$ variations illustrated in Figures 4.2 (panel Z2) and 4.3 (panel Z3) are typical signatures of Z-component northward of the magnetic dip equator as earlier described by (Chapman, 1919). Exception to these fields' variations is DLT with daytime positive $MSqZ_{ext}$ amplitudes at the northern winter months when negative amplitudes are expected during low solar activity year 2017. This variation pattern are contrary to the expectation of a typical northerly $MSqZ_{ext}$ variations and may likely be a resultant effect of the strong summertime intrusion of the opposite hemisphere current vortex into the winter hemisphere. The sharp decrease of $MSqZ_{ext}$ amplitudes at LKW and DLT in the southern

and northern hemisphere are consistent with the Chapman's theory that the field variations at the magnetic dip equator are flat (zero). These stations (LKW and DLT) since are not exactly at the magnetic dip equator suffered reduced magnitudes.

Besides these abnormal variations, the $MSqZ_{ext}$ field variations which are primarily of ionospheric current system, reflect features of the Sq current system that generally appear stronger at the summer and equinoctial months (March-October), and weaker at the winter months (November-February). The $MSqZ_{ext}$ amplitudes appeared exceptionally large at the latitudes of PHU and KNY closer to the Sq current focus clearly permitting an inference that the reduction in $MSqH_{ext}$ amplitudes at the latitudes of PHU and KNY closer to the Sq focus cause incredible enhancement on the form of $MSqZ_{ext}$ magnitudes. The $MSqZ_{int}$ amplitudes show remarkable changes which are more variable in the southern region during the dip minimum solar activity year 2008 as given in Figure 4.4 (panel Z4). They also appeared stronger during the summer and equinoctial months and decreases in winter in consistent with the level of ionization. Throughout the years, the $MSqZ_{ext}$ amplitudes are consistently higher than the $MSqZ_{int}$ and both variations increase with increasing solar activity.

The sum (external plus internal) field variations of the horizontal component $MSqH_{Tot}$ presented in Figures 4.7, 4.8 and 4.9 (panels J, Q and M) show semi-annual variations pattern at the equatorial latitudes and decreases with respect to annual variations as the latitudes increases. These variations are similar to the North American region earlier observed, (Campbell & Schiffmacher, 1985). The significant reduction in the strength and phase shift of $MSqH_{Tot}$ amplitudes at the latitudes of KPG and PHU and the change over from daytime eastward to westward field at ROC and KNY in the southern and northern hemisphere suggest likely position of the sum of the total focal latitudes between

KPG and ROC in the southern hemisphere and between PHU and KNY in the northern hemisphere. The positive and negative $MSqH_{Tot}$ amplitudes at the latitudes equatorward and poleward of the northern hemisphere Sq focus confirmed the earlier observation by (Shiraki, 1973) that stations southward and northward of the Sq focus exhibit daytime positive and negative amplitudes. This implies that latitudes equatorward of the Sq focus are bounded by eastward current (in most cases) that decreases with increasing latitudes generating the positively enhanced $MSqH_{Tot}$ that also decreases with latitudes while the negative variations poleward of the Sq focus that indicates dominant westward currents seems to increase with increasing latitudes. The drastic reduction of $MSqH_{Tot}$ amplitudes at mid-latitude region is due to the presence of Sq focus. The daytime positively enhanced $MSqH_{Tot}$ amplitudes across all the months at the latitude of ROC during the dip minimum solar activity year 2008 suggest southward (poleward) appearance of the Sq current focus to the latitude of ROC. Exception to these positive $MSqH_{Tot}$ amplitudes are May, June, July and September with negative amplitudes that indicates northward (equatorward) appearance of Sq focus. Similar daytime positive $MSqH_{Tot}$ amplitudes are also obvious across all the months at the latitude of KNY in the northern hemisphere during low and moderate solar activity indicating northward (poleward) appearance of Sq focus. Exception of February, May, August, September and October with negative amplitudes. The Sq focus in these months lie southward (equatorward) of KNY. These results established that the Sq focus exhibit latitudinal variability even during quiet days.

Generally, the $MSqH_{Tot}$ amplitudes increases with increasing solar activity and vary both in phase and magnitudes as the latitudes increases. The increase is due to linear proportional relationship between ionospheric conductance and solar flux. Yacob & Prabhavalkar (1965) and Yacob & Rao (1966) studied the daily variations of SqH from 1905 and 1960 and concluded that the increase of daily SqH magnitudes with solar

activity is due to the effect of solar activity on the ionization intensity. Rastogi (1993) explained that the changes in the amplitude and phase of the Sq field is due to combined effect of ionospheric conductivity and electric field. Modelling the Sq current at different solar epoch (Takeda et al., 1986) found that changes in ionospheric conductivity causes corresponding change in the intensity of the Sq current between solar minimum and maximum. It is believed that increase in solar activity enhances the ionospheric conductivity resulting in greater magnitudes of $MSqH_{Tot}$ observed during the moderate solar activity year of this study.

The monthly features of the $MSqD_{Tot}$ showed normal variation type with a well-defined northward and southward flow of currents during the pre-noon and afternoon hours. These features are specially observed at the equinoctial and summer months (September-April) and correspond well with the effect of an ideal Sq current southerly of the magnetic dip equator. Similar but oppositely directed currents generating eastward and westward fields during the pre-noon and afternoon periods are eminent in the northern hemisphere. These variations as earlier discussed are due to meridional current flowing around these periods. It is obvious that the "M shape" observed in the external field appears in $MSqD_{Tot}$ variations seen in June and July at the latitudes of MND, KPG and ROC in the southern hemisphere, while the "W shape" dominates in the winter months (November-February) in the northern hemisphere.

In the southern hemisphere, the additional morning positive $MSqD_{Tot}$ amplitudes that appeared in the winter months (June and July) may be associated to eastward field as earlier discussed. At the northern hemisphere the additional negative $MSqD_{Tot}$ amplitudes that appeared between 05:00 and 07:00 LT hrs in winter months may be due to field-aligned currents (FACs) as also earlier discussed. The $MSqD_{Tot}$ amplitudes generally

increases with increasing solar activity and appeared stronger and weaker in summer and winter months. From the relationship between the Sq amplitudes with electric field and ionospheric conductivity study (Takeda et al., 2003) explained that the difference in neutral winds results to variation of Sq amplitudes since neutral winds blowing from subsolar points are much stronger in summer than in winter and hence Pedersen current driven by such wind enhances the $MSqD_{Tot}$ variations in summer as obvious in the present study. Another mechanism is the field-aligned currents (FACs) flowing from summer to winter in the morning sector and back to summer at noon and dusk as theoretically predicted by (Fukushima, 1979) and observationally confirmed, (e.g., Abidin et al., 2018; Park et al., 2011; Yamashita & Iyemori, 2002). The field-aligned currents (FACs) may also contributes to the increase of $MSqD_{Tot}$ amplitudes in summer and decrease it in winter (Takeda, 1982; Thu et al., 2011). The early occurrences of the pre-noon and afternoon $MSqD_{Tot}$ amplitudes in summer months and later occurrences in winter months across the years reflect the effect of field-aligned currents (FACs) (Abidin et al., 2018a).

It is obvious that $MSqZ_{Tot}$ amplitudes appeared variable across all the latitudes exception of KPG and ROC as indicated in Figure 4.7 (panel L). These variable pattern suggests the magnetic field records may be affected by the geological location of the observatories since the vertical component largely depends on the regional and local anomalies. However, the daytime positively enhanced $MSqZ_{Tot}$ amplitudes across the latitudes are in agreement with the Chapman's theory of stations on the southern hemisphere, exception of LKW and MCQ with daytime negative amplitudes during the winter months. These variations are contrary to the expectation of vertical component southward of the magnetic equator. This indicates that the daytime negative $MSqZ_{Tot}$ amplitudes at the latitude of LKW may likely result from the northern intrusion of the strong summertime Sq current vortex into the southern region and completely invades the

effect of the southern Sq current vortex as earlier discussed, while these negative amplitudes at MCQ may be due to resultant effect of the auroral electrojet since the station is closer to the high latitude region where auroral activity and magnetospheric processes are dominant (Vichare et al., 2012). The phase variations of $MSqZ_{Tot}$ amplitude from one latitude to the other may be due to electromagnetic induction effect. The increase in $MSqZ_{Tot}$ amplitudes with increasing solar activity is no surprise since ionospheric source current that induces the $MSqZ_{Tot}$ increases with solar activity; it is expected to cause corresponding effect on the other components of the geomagnetic field of which the vertical Z-component is no exception.

The month-by-month equivalent current system computed from the external and internal parts of the geomagnetic field records for the solar quiet years 2008, 2012 and 2017 are illustrated in Figures 4.10 to 4.15. In each month, the equivalent current contour is plotted in local time against the geomagnetic latitudes of the stations and the current between adjacent contours is about 10^4 A. The figures represent the surface fields but in a current pattern that is generated in the E-region of the ionosphere through a dynamo process. Such representation provides useful information on the conductivity of the ionosphere and thermal tidal motions that produce the Sq fields in the ionosphere. Figures 4.10 to 4.12 shows the month-by-month external equivalent current that could be responsible for the observed monthly external MSq fields. The currents show simple vortices that are centered near mid-latitude region in both hemispheres. It is apparent from these figures that the intensity of the external current changes from month-to-month. Kirchhoff & Carpenter (1976) observed that the variability of the intensity of Sq current system is associated to variation in ionospheric conductivity modulated by solar ultra-violet radiation and ionospheric conditions. The ionospheric electric and geomagnetic fields study (Takeda & Yamada, 1987) revealed that semidiurnal winds make significant

contribution to the strength of the total Sq current during low solar activity. Park et al. (2011) observed that the intensity and structure of the Sq current system are primarily controlled by ionospheric conductivity and prevailing tidal winds system in the E-region of the ionosphere. All these studies point to the fact that there are obvious changes in both phase and intensity of the Sq current system similar to what is observed in the present study.

In the southern hemisphere, the external equivalent current that appears stronger during the summer months (November-February) and weaker in winter months (May-August) as illustrated in Figure 4.10 is consistent with the earlier findings of (Cambell & Schiffmacher, 1988). These authors observed maximum and minimum intensity of external equivalent current in summer and winter in South America, Africa and Australian region. Similar variations occurred in the northern hemisphere, the external equivalent current appears stronger in summer months (May-August) and weaker in winter months (November-February) as shown in Figures 4.11 and 4.12. Their greater magnitudes in summer months is due to enhanced dynamo process in the E-region of the ionosphere modulated by solar radiations that are stronger in summer months. This accounts for the maximum intensity of the Sq current system observed in the southern summer months (February) and northern summer hemisphere months (June and July) in the present study. Matsushita & Maeda (1965) examined the Sq current vortex using global IGY geomagnetic stations distributed around the globe which they grouped into three zones-zone 1 (Europe-Africa), zone 2 (Asia-Australia) and zone 3 (North-South America). They observed that the intensity of external current is greater in equinox and smaller in solstices in contrast to what is observed in the present study. This discrepancy may likely arise from the longitudinal variations of the Earth's main magnetic field (Stening, 1971). Study on the longitudinal inequality of the Sq current system by (Bhardwaj & Rao, 2016)

revealed that the longitudinal differences in seasonal and Sq current system may either be related to variations in ionospheric conductivity or tidal winds or combination of both. Another possible mechanism that may likely cause discrepancy between the continental sectors is the presence of tidal wind system that drives the ionospheric wind dynamo. Tidal winds are often described with respect to geological coordinates while ionospheric currents are arranged with respect to magnetic coordinates (Bhardwaj & Rao, 2016). The offset between the geographic and geomagnetic equator may also introduce longitudinal variations in the Sq current system.

Besides these variations, the external equivalent current vortex linearly increased from $\sim$-10.5 $\times$ 10^4A during the dip minimum solar activity year 2008 to about 11.7 $\times$ 10^4 and 15.5 $\times$ 10^4A during low and moderate solar activity years 2017 and 2012. The variations in the intensity of the external Sq currents from dip minimum to moderate solar activity of this study is associated to changes in solar flux and this modulate the electron density in the ionosphere resulting to significant changes of the dynamo currents of moderate solar activity year to be larger than those of minimum solar activity years of this present study. The changes in the dynamo current with increasing solar activity is obvious from the intensities of the external Sq current from the dip minimum to moderate solar activity presented in this study. Modeling the Sq current system at different solar epoch (Takeda et al., 1986) found that changes in ionospheric conductivity causes corresponding changes in the intensity of the Sq current.

The internal equivalent current system presented in Figures 4.13 to 4.15 reflect most of the general features of the external equivalent current system but are only about 0.80, 0.56 and 0.50 times as large in 2008, 2017 and 2012. They also appeared stronger in summer and weaker in winter months in both hemispheres in consistent with the South

America, Australia and African sectors by (Campbell & Schiffmacher, 1988) that observed higher and lower intensity of the internal equivalent currents in summer and winter months.

Apart from their magnitudes, the external and internal current vortices mostly disappears particularly during the winter months. The disappearances of both external and internal current vortices of this study are mostly preceded by their lowest latitudinal positions. In the southern hemisphere, the disappearance of external current focus in winter (August) and its internal focus in June to August during the dip minimum solar activity with similar disappearance of external current focus in December and its internal vortex in December-February during low solar activity in the northern hemisphere are consistent with earlier works of (Campbell et al., 1993), they observed disappearance of external current vortices in winter months in India-Siberia region. These results are in sharp contrast to North American region earlier estimated (Campbell, 1983). The author did not observed any disappearance of both external and internal Sq current focus during solar quiet year 1965. This discrepancy may likely be attributed to variations in the intensity of the Sq current and prevailing wind system between the continental regions.

During moderate solar activity, the external equivalent current vortex only appeared weak and dropped to its lowest latitude ~15° in winter months (January and December) as illustrated in Figure 4.12 with no noticeable disappearance. The disappearances of both external and internal current vortices particularly in winter months marked major changes in ionospheric conductivity and prevailing wind system between the summer and winter hemispheres. Statistically, the internal equivalent current vortices were generally observed to disappear more than the external and the disappearance of both external and internal current vortices decreases with increasing solar activity. This indicate that the

disappearance of Sq current vortex to a large extent has some measure of dependence on solar activity. This could be the reason for the frequent disappearance of the internal current focus during the winter months since the current is induced by weaker external current due to reduced ionization in these months. Recently (Bhardwaj & Rao, 2016) investigated the longitudinal inequalities of Sq current system using quiet data sets of 1976 and 1977. Their principal component analysis (PCA) of the Sq(D) variations indicate the presence of two distinct pattern: one corresponding to daily Sq variations and the other to a certain extent is associated to a component which has a different waveform both in the northern and southern hemispheres. The second component shows the presence of strong inter-hemispheric currents with strong seasonal variability than the first component. It is concluded that the magnetic effects associated with these currents tend to dominate the weaker winter Sq dynamo effects accounting for the disappearance of Sq current vortex in both hemispheres during the winter months.

In addition to the disappearances, the external and internal current vortices exhibit latitudinal variations throughout the months. In the southern hemisphere, the latitudinal range of the external Sq current vortex that appeared slightly poleward in summer months (November-February) than in winter months during the dip minimum solar activity are similar to the earlier works of (Matsushita & Maeda, 1965). Those authors examined the Sq current vortices from the IGY geomagnetic data distributed around the world. They observed that for all the three zones in the southern hemisphere, the latitudinal position of the external current vortex appeared higher (more poleward) in summer than in winter similar to the southern hemisphere of the present study. The difference in the latitudinal position of the external current vortex in summer and winter hemispheres may possibly be attributed to the variability of the wind system between both hemispheres (Takeda, 1990). The poleward appearance of the external current vortices in summer months and

the subsequent decrease to lower latitude in winter months is a clear indication of variability of solar activity and prevailing wind system. The corresponding internal current vortices that appeared more poleward in winter months (April-October) is in contrast to what was observed on the external current. The latitudinal difference between the external and internal current focus position may be caused by the local conductive region of the upper mantle on the induced currents (Campbell & Schiffmacher, 1985). In the southern hemisphere, the latitudinal range of both external and internal current foci that appeared more variable in winter than in summer months are believed to arise from the differences in the prevailing wind systems between the hemispheres.

In the northern hemisphere, the latitudinal position of both external and internal current vortices that mostly appears at lower latitudes in summer than winter months is good agreement with the earlier works of (Chapman & Bartels, 1940; Hasegawa, 1960) that used solar quiet data and observed lower latitudinal position of the Sq current focus in summer than in winter. Similar result has been earlier reported in the India-Russian region (Patil et al., 1985;) and Indian region (Shiraki, 1974). This present result is not consistent with the North America and West Pacific region earlier estimated (Matsushita, 1960; Shiraki, 1972). Their results showed that the latitude of the Sq current focus in summer months are relatively higher than those in winter. Again this difference may likely be associated to variability of the wind pattern between the continental sectors and hence established that Sq current vortex exhibit longitudinal variability. Takeda (1990) asserted that the difference in latitudinal position of the Sq current vortices in summer and winter hemisphere may probably be explained by the difference in the wind system between the hemispheres. The movement of both external and internal current focus of this study seems to point to the roles of the ionospheric conductivity and tidal winds with the former more active in the intensity of the Sq current system and the later more

dominant in the relative position of the Sq current focus. Stening et al. (2005) used array of data from the Australian and Japanese region and observed meridional movement of the Sq current vortex from one quiet day to the other. Tarpley (1973) and Shiraki (1974) examined the likely mechanism responsible for the movement of Sq current focus and attributed it mainly to variability in the winds driving the ionospheric dynamo rather than variations in ionospheric conductivity or magnetospheric effects. On average, the internal current focus appeared more poleward than the external current focus in all the years. Exception of summer months during low solar activity year 2017 in which the external current focus latitude is slightly higher than the internal focus. As earlier mentioned, the subtle differences in the latitudinal position of the external and internal current vortices of this study reflect the resultant effect of the local upper mantle conductivity on the induced currents in the Earth.

The sharp drop of both external and internal current focus in September and its relative poleward appearance in March indicates that the Sq current system in March and September which are sub-division of March equinox and September equinox seasons exhibit some differences in their vortices that are more prevalent during low solar activity of the northern hemisphere as evidently seen from the present result. Tarpley (1973) and Thakur & Alex (1977) carefully examined the day-to-day variability of the Sq focus position and its seasonal dependence. They observed that for the northern region the Sq focus moves equatorward in September and remained poleward in March similar to what is observed in the present study.

Apart from their latitudinal position, the Sq current vortices presented in Figures 4.10 to 4.15 were generally observed to occur at different time scale. In the southern region, the external current vortex lie between 10:00 and 11:30 LT in summer months including

October (October-February) and shifted to between 11:00 and 13:00 LT in winter months with March, April and September included (March-September). This implies that the external Sq current vortex occurs at earlier and later local time in summer and winter months. Cambell & Schiffmacher (1988) carried out a monumental study on the quiet ionospheric current system of the southern hemisphere that includes South America, Africa and Australian region. In their study they observed earlier and later occurrence of external current vortices in summer and winter months similar to the result of the present study. In the northern hemisphere, the external current vortex lie between 10:00 and 10:30 LT hrs during the summer months with April and September included (April-September) and fluctuate between 11:30 and 12:00 LT hrs in winter months with March and October included (October-March) during low solar activity year 2017, as shown in Figure 4.11. During moderate solar activity year 2012, the external vortex fluctuate between 10:00 and 10:30 LT hrs similar to what was observed during low solar activity but lie between 11:00 and 13:00 LT hrs in winter months (October-March). In an earlier study (Matsushita & Maeda, 1965; Stening & Winch, 2013; Yamazaki et al., 2011) observed earlier occurrence of Sq current vortex in summer than in winter months in the northern region of their respective study similar to what is observed in the present study.

During the winter months in both hemispheres, the Sq current system generally appears weak due to low level of ionization. The large intrusion of the stronger summertime current of the opposite hemisphere into the winter hemisphere seems to push the weaker wintertime currents to later hour as obvious in the present study. The movement of the Sq current vortex has been explained in terms of the magnetic effect of the field-aligned currents (FACs) flowing from the current vortex center in winter to the summer hemisphere at noon as predicted by theoretical works of (Fukushima, 1979) and observationally confirmed (e.g., Abidin et al., 2018a; Park et al., 2011; Yamashita &

Iyemori, 2002). Fukushima (1979) suggested that the FACs flowing from the winter to the summer hemisphere in the region of the current vortex generate an eastward geomagnetic field variation near the local noon at the ground surface. The generated eastward directed field advances the current vortex of the summer months and delays the vortex in the winter hemisphere. This could be the main reason for the Sq current vortices appearing at later hour of the day in winter months across the years in the present study.

Figure 4.16 to 4.18 that showed the electrical conductivity-depth profile of Asia sub-region during the dip minimum, low and moderate solar activity allow the upper mantle to be viewed as a stack of inhomogeneous spherical layers in contrast to the general model obtained under certain assumption of a spherically symmetric Earth (Banks, 1972; Hobbs, 1887; Parkinson, 1974). These authors used symmetric distribution model that allows the upper mantle to be seen as a single homogeneous spherical layer. It is obvious from these figures that a downward increase in conductivity bound these regions in consistent with the earlier findings in Australia, India and other parts of the world (Abidin et al., 2018b; Arora et al., 1995; Campbell et al., 1998; Campbell & Schiffmacher, 1988; Obiora et al., 2015). The downward increase is no surprise since for a given Earth's interior the temperature increases with depth (Tozer, 1970), it is expected of the electrical conductivity-depth profile to increase accordingly. The downward increase in conductivity profile seems to appear sharp and faster during the moderate solar activity year 2012 and slower during the dip minimum and low solar activity years 2008 and 2017. The increase in conductivity from ~0.01-0.020, 0.01-0.035 and 0.02-0.025 S/m at depths range of about ~40-100, 30-120 km and 40-130 km in 2008, 2012 and 2017 indicate the existence of weak conductivity zones. These findings are consistent with the Malaysian region (Abidin et al., 2018b). Laboratory experiment by (Yoshino et al., 2006) estimated the electrical conductivity of hydrous olivine to about 10^{-2}S/m at depth of about 100 km

similar to what is observed in the present study. Campbell & Schiffmacher (1988) earlier estimated electrical conductivity profile beneath seven sub-continental regions of the world. Their profile beneath Africa, Central and East Asian region closely agrees with the present profile at a depth range between about 50 and 130 km but their North and South American sectors are in sharp contrast with the present profiles. They observed an incredible increase in conductivity profile at this depth range. This difference may largely be attributed to lateral inhomogeneity among the continental regions. The electrical conductivity within the first few kilometers of the crust largely depends on the amount of interstitial water that is present (Abidin et al., 2018b). This weak conductivity profile within the first few kilometers may likely be due to dehydration of the crust through metamorphic processes in a stable shield areas as earlier discussed by (Hyndman & Hyndman, 1968).

The slight increase in conductivity profile at depths between 100-180 km, during the dip minimum solar activity year 2008, with steep increase at depths between 130-300 km and 130-280 km during moderate and low solar activity years 2012 and 2017 corresponds to asthenosphere region identified with high electrical conductivity, global seismic low velocity as earlier identified on seismic records (Dziewonski & Anderson, 1981; Karato, 1990; Kennett & Engdahl, 1991; Shankland et al., 1981). These peculiar features of the asthenosphere have been largely attributed to the presence of small amount of partial melt (Clark & Ringwood, 1964; Thybo, 2006). This result is in sharp contrast with the North American sector earlier reported by (Campbell & Schiffmacher, 1988). These authors observed low electrical conductivity profile at these depth range. This difference in electrical conductivity behavior of the asthenosphere may be attributed to the variations in the amount of partial melts between the continental regions. Various suggestions have been put forward to explain the high electrical conductivity of the asthenosphere. For

example, petrological studies has earlier shown that melts are thermodynamically stable in the asthenosphere due to traced volatile components such as H_2O and CO_2. These traced elements also contributes to the enhanced electrical conductivity of the asthenosphere (Shankland & Ander, 1983). Evidences have emerged that partial melt exist in the global seismic low velocity zone (asthenosphere) and this also enhances the electrical conductivity of the zone as widely reported by research workers (e.g., Shankland et al., 1981). Laboratory experiment (Hirth & Kohlstedt, 1996; Karato & Jung, 1998) confirmed its existence and also attributed the enhanced electrical conductivity to partial melt and olivine hydration. The salient feature to note is that at each depth range, the conductivity profile during the moderate solar activity year 2012 is higher than the profile during dip minimum to low solar activity year 2008 and 2017. This difference could be due to increasing effect of solar activity and ionospheric conductivity or lateral variations or combination of both.

The electrical conductivity of the upper mantle which depend mainly upon the rock type, chemical composition, saturation phase and prevailing temperature differ among regions (Abidin et al., 2018b; Glover & Vine, 1994; Obiora et al., 2014; Okeke & Obiora, 2016). Laboratory-based experiment by (Xu et al., 2000) showed that changes in electrical conductivity strictly follow changes in mantle mineral compositions. The sharp steep increase in conductivity profiles at depths near 310, 350 and 410 km in 2008, 2017 and 2012 marked the transition zone and reflect phase changes of the mineralogical composition of the upper mantle. Xu et al. (2000) observed that the dominant upper mantle rock type is the peridotite composed of four (4) main minerals; Olivine $(Mg,Fe)_2 Si_2 O_4$, orthopyroxene $(Mg,Fe)_2 Si_2 O_6$, clinopyroxene $Ca(Mg,Fe) Si_2 O_6$ and with some aluminous phase (such as plagioclase, spinel or garnet). These authors demonstrated that phase changes in upper mantle depths between 300 and 410 km corresponds to depth at

which orthopyroxene the second most abundant mineral of the mantle transform to clinopyroxene. The changes in conductivity profiles observed at depths of 310, 350 and 410 km in the present study may likely reflect such transformation of the mantle mineral composition. At each depth range, the magnitude of the conductivity depth profile appeared larger during moderate solar activity year 2012 than any of the year considered in the study.

The steep rise in conductivity profile at depth range between 310-500 km, 350-500 km and 410-600 km in 2008, 2012 and 2017 of this study corresponds to the main mantle transition zone identified with high electrical conductivity (Utada et al., 2003). The major constituent of the mantle transition zone are the hydrous Wadsleyite and hydrous Ringwoodite that contain voluminous amount of water content in their respective phases (Inoue et al., 1995; Kohlstedt et al., 1996). The mantle transition zone has been identified as the most likely important water reservoir on Earth due to its ability to accommodate water content of more than 2 wt% (Ohtani & Sakai, 2008). Over the years, geophysical observations such as electrical conductivity are known to be sensitive to water content (Wang et al., 2006). The enhanced conductivity profiles in the mantle transition zone of this study may likely be influence by the presence of water content within the region. The olivine which is the main constituent of the mantle rock is unstable at high temperature and pressure conditions and causes the mantle mineralogy to change with depth (Katsura & Ito, 1989). The discontinuity profile observed at ~380-460 km, 390–480 km depth during dip minimum and moderate solar activity years 2008 and 2012 is likely associated to the transformation of α-phase of olivine to β at high temperature and pressure (Katsura & Ito, 1989) while the dissociation of γ is ascribed to the seismic discontinuity at 570–640 km during low solar activity year 2017 (Ito & Takahashi, 1989). The γ-phase split into perovskite and magnessiowustite at the transition zone and even beyond

(Chandrasekhar, 2011). Generally, at greater depths, the transformation of olivine into β and γ phases is mainly responsible for the major discontinuous changes in the electrical conductivity profiles (Chandrasekhar, 2011).

In general, the increase in conductivity at depth range between 350-800 km in all the profiles of the present study agrees well with the global models that showed increase in electrical conductivity at depth interval of 400-800 km and this depict phase transition of the mantle materials as discussed by previous workers (e.g., Arora et al., 1995; Campbell et al., 1998; Adams, 1991).

CHAPTER 6: CONCLUSIONS AND SUMMARY

Herein, the magnetic field records below 70 °N and 70 °S in Asia sub-region are fully engaged to delineate the features of both external and internal solar quiet fields with their associated currents and the separated field contributions are further used to probe the mantle electrical conductivity profile beneath this region. These field variations are believed to be generated in the ionosphere and current induced into the conductive Earth and hence reflect true features of the Sq current system that changes slowly with local time (LT) of the day. The study has effectively shown that the external, internal and sum of the quiet horizontal field ($MSqH_{ext}$, $MSqH_{int}$ and $MSqH_{Tot}$) equatorward of the Sq focus are bounded by daytime eastward current generating positive amplitudes that increases with increasing solar activity and decrease as the latitudes increases while those poleward of the Sq focus are dominated by westward current responsible for the negative amplitudes that seems to increase with increasing latitudes but show no linear increase with solar activity.

It has been shown that $MSqD_{ext}$ exhibit stronger (weaker) amplitudes in summer (winter) months throughout the years reflecting differences in ionospheric conductivity between the summer and winter hemispheres while $MSqZ_{ext}$ amplitudes appear exceptionally large at the latitudes of PHU and KNY closer to the southern and northern focus clearly permitting an inference that the reduction in the source of $MSqH_{ext}$ amplitudes at the latitudes of PHU and KNY closer to the Sq focus cause incredible enhancement on the form of $MSqZ_{ext}$ variations. The study has also demonstrated that the external $MSqH_{ext}$, $MSqD_{ext}$ and $MSqZ_{ext}$ amplitudes are about twice larger than their corresponding internal $MSqH_{int}$, $MSqD_{int}$ and $MSqZ_{int}$ magnitudes in any of the year and both exhibit slight phase variations that are believed to arise from electromagnetic induction effect. The LKW and DLT that lies close to the magnetic dip equator have

exceptionally large $MSqH_{ext}$ amplitudes due to influence of equatorial electrojet (EEJ) current.

The study has also shown that external Sq current vortices linearly increased with midday summer amplitudes reaching ~-10.5 $\times 10^4$ A during the dip minimum solar activity year 2008 to about 11.7 $\times 10^4$ and 15.5 $\times 10^4$ A during low and moderate solar activity years 2017 and 2012. The internal Sq current vortices are only about 0.8, 0.56 and 0.50 times as large in 2008, 2017 and 2012. The noticeable absence of prominent northward and southward currents flow at the latitude of LKW with similar absence of southward and northward currents vortex at DLT in the winter months suggest likely intrusion of strong summertime current vortex of the opposite hemisphere to the winter hemisphere at low latitude locations appearing most frequently during the pre-noon hours in the southern hemisphere and afternoon hours in the northern hemisphere. The study shows that internal Sq current vortices generally disappear more frequently than the external and the disappearance of both external and internal current vortices decreases with increasing solar activity. This indicates that the disappearance of Sq current vortex has some measure of dependence on solar activity and prevailing wind system. Generally, the internal current focus appeared more poleward than the external focus in all the years' exception of summer months during low solar activity year 2017 and the subtle differences between them reflect resultant effect of the local upper mantle conductivity on the induced currents in the Earth.

The research has demonstrated that the regression line fitted to the estimated conductivity values show a downward increase in electrical conductivity beneath this region with a sharp steep increase at depth of about 310, 350 and 410 km in 2008, 2012 and 2017. The profiles have not shown significant variations in their depth of penetrations

despite major differences in their annual sunspot numbers, but the higher magnitude, sharp and rapid increase in conductivity profile in 2012 and the lower and slow increase in conductivity profile in 2008 at any particular depth level could be the resultant effect of difference in solar activity or lateral heterogeneity in the electrical conductivity of the mantle or combination of both.

6.1 Future works

In future there is need to perform a quality check on the data as to eliminate possible spikes that may likely be present on the data and to also estimate the electrical conductivity profile of the Earth's mantle using solar disturbed (SD) variations in order to advance our understanding on the subject matter during times of irregular variations.

REFERENCES

Abidin, Z. Z., Jusoh, M., Abbas, M., Bolaji, O., & Yoshikawa, A. (2018a). Features of the inter-hemispheric field-aligned current system over Malaysia ionosphere. *Journal of Atmospheric and Solar-Terrestrial Physics*. https://doi.org/ 10.1016 /j.jastp.2018.01.012.

Abidin, Z. Z., Jusoh, M. H., Abbas, M., & Yoshikawa, A. (2018b). Application of solar quiet (Sq) current in determining mantle conductivity-depth structure in Malaysia. *Journal of Atmospheric and Solar-Terrestrial Physics*. https://doi.org/10.1016 /j.jastp.2018.01.019.

Adam, A. (1980). Relation of mantle conductivity to physical conditions in the asthenosphere. *Geophysical Surveys, 4*(1-2), 43-55.

Alabi, A., Camfield, P., & Gough, D. (1975). The North American central plains conductivity anomaly. *Geophysical Journal International, 43*(3), 815-833.

Amory-Mazaudier, C. (2009). Electric current systems in the earth's environment. *Niger Journal of Space Research, 8*, 178-255.

Amory-Mazaudier, C., Bolaji, O., & Doumbia, V. (2017). On the historical origins of the CEJ, DP2, and Ddyn current systems and their roles in the predictions of ionospheric responses to geomagnetic storms at equatorial latitudes. *Journal of Geophysical Research: Space Physics, 122*(7), 7827-7833.

Anderson, D., & Roble, R. (1981). Neutral wind effects on the Equatorial F-region ionosphere. *Journal of Atmospheric and Terrestrial Physics, 43*(8), 835-843.

Anderson, D. L. (1979). The upper mantle transition region: Eclogite? *Geophysical Research Letters, 6*(6), 433-436.

Anderson, O. L. (1967). Equation for thermal expansivity in planetary interiors. *Journal of Geophysical Research, 72*(14), 3661-3668.

Appleton, E. V., & Barnett, M. (1925). On some direct evidence for downward atmospheric reflection of electric rays. *Proceeding of the Royal Society London. 109*(752), 621-641.

Arora, B. R. (1980). Latitudinal variations of geomagnetic solar and lunar tides in the Indian region. *Proceeding Indian Academy Science, 89*, 333-346.

Arora, B. R., Campbell, W. H., & Schiffmacher, E. R. (1995). Upper mantle electrical conductivity in the Himalayan region. *Journal of Geomagnetism and Geoelectricity, 47*(7), 653-665.

Baba, K., Utada, H., Goto, T.-n., Kasaya, T., Shimizu, H., & Tada, N. (2010). Electrical conductivity imaging of the Philippine Sea upper mantle using seafloor magnetotelluric data. *Physics of the Earth and Planetary Interiors, 183*(1-2), 44-62.

Banks, R. (1972). The overall conductivity distribution of the Earth. *Journal of Geomagnetism and Geoelectricity, 24*(3), 337-351.

Basavaiah, N. (2012). Geomagnetism: Solid earth and upper atmosphere perspectives. New Delhi, India; Springer.

Bhardwaj, S., & Rao, P. S. (2016). Longitudinal inequalities in Sq current system along 200-2100 E meridian. *Journal Indian Geophysics, 20*(5), 462-471.

Booker, J. R., Favetto, A., & Pomposiello, M. C. (2004). Low electrical resistivity associated with plunging of the Nazca flat slab beneath Argentina. *Nature, 429*(6990), 399-403.

Brett, L. (1988). Methods of spherical harmonic analysis. *Quarterly Journal of the Royal Astronomical Society, 29*, 129-155.

Brown, G., & Williams, W. (1969). Some properties of the day-to-day variability of Sq (H). *Planetary and Space Science, 17*(3), 455-470.

Cambell, W. H., & Schiffmacher, E. R. (1988). Quiet ionospheric currents of the southern hemisphere derived from geomagnetic records. *Journal of Geophysical Research: Space Physics, 93*(A2), 933-944.

Campbell, W. H. (1983). A description of the external and internal quiet daily variation currents at North American locations for a quiet-Sun year. *Geophysical Journal International, 73*(1), 51-64.

Campbell, W. H. (1987). The upper mantle conductivity analysis method using observatory records of the geomagnetic field. *Pure and Applied Geophysics, 125*(2-3), 427-457.

Campbell, W. H. (1989). The regular geomagnetic-field variations during quiet solar conditions. *Geomagnetism, 3*, 385-460.

Campbell, W. H. (1990). Differences in geomagnetic Sq field representations due to variations in spherical harmonic analysis techniques. *Journal of Geophysical Research: Space Physics, 95*(A12), 20923-20936.

Campbell, W. H. (2003). Introduction to geomagnetic fields (2nd ed.), London, England: *Cambridge University Press, United Kingdom.*

Campbell, W. H., & Anderssen, R. S. (1983). Conductivity of the subcontinental upper mantle: an analysis using quiet-day geomagnetic records of North America. *Journal of Geomagnetism and Geoelectricity, 35*(10), 367-382.

Campbell, W. H., Arora, B. R., & Schiffmacher, E. R. (1993). External Sqcurrents in the India-Siberia region. *Journal of Geophysical Research: Space Physics, 98*(A3), 3741-3752.

Campbell, W. H., Barton, C. E., & Welsh, W. (1998). Quiet-day ionospheric currents and their application to upper mantle conductivity in Australia. *Earth, Planets and Space, 50*(4), 347-360.

Campbell, W. H., & Schiffmacher, E. R. (1985). Quiet ionospheric currents of the northern hemisphere derived from geomagnetic field records. *Journal of Geophysical Research: Space Physics, 90*(A7), 6475-6486.

Campbell, W. H., & Schiffmacher, E. R. (1986). A comparison of upper mantle subcontinental electrical conductivity for North America, Europe, and Asia. *Journal of Geophysics - Zeitschrift fur Geophysik, 59*(1), 56-61.

Campbell, W. H., & Schiffmacher, E. R. (1987). Quiet ionospheric currents and earth conductivity profile computed from quiet-time geomagnetic field changes in the region of Australia. *Australian Journal of Physics, 40*(1), 73-88.

Campbell, W. H., & Schiffmacher, E. R. (1988). Upper mantle electrical conductivity for seven subcontinental regions of the Earth. *Journal of Geomagnetism and Geoelectricity, 40*(11), 1387-1406.

Carbonell, M., Oliver, R., & Ballester, J. (1993). On the asymmetry of solar activity. *Astronomy and Astrophysics, 274*, 497-504.

Chandrasekhar, E. (2011). Regional Electromagnetic Induction Studies Using Long Period Geomagnetic Variations. In E. Petrovský, E. Herrero-Bervera, T. Harinarayana, & D. Ivers. (Eds.), *The Earth's Magnetic Interior* (pp. 31-42). New York, London: Springer Dordrecht.

Chapman, S. (1919). I. The solar and lunar diurnal variations of terrestrial magnetism. *Philosophical Transaction of the Royal Socety London. 218*(561-569), 1-118.

Chapman, S. (1951). The equatorial electrojet as detected from the abnormal electric current distribution above Huancayo, Peru, and elsewhere. *Archiv Fuer Meteorologie, Geophysik und Bioklimatologie, Serie A, 4*(1), 368-390.

Chapman, S., & Bartels, J. (1940). Geomagnetism. (1st ed.), New York, England: Oxford University Press.

Chapman, S., & Price, A. (1930). The electric and magnetic state of the interior of the earth, as inferred from terrestrial magnetic variations. *Philosophical Transaction of the Royal Society London, 229*(670-680), 427-460.

Chapman, S., & Whitehead, T. (1923). On the observations of Earth potential-gradients at Ebro. *Journal of Geophysical Research, 28*(4), 125-128.

Clark, S. P., & Ringwood, A. (1964). Density distribution and constitution of the mantle. *Reviews of Geophysics, 2*(1), 35-88.

Cleveland, W. S. (1979). Robust locally weighted regression and smoothing scatterplots. *Journal of the American Statistical Association, 74*(368), 829-836.

Daniel, N., & Francisca, N. (2013). Crustal and upper mantle electrical conductivity structure in north central Nigeria. *International Journal of Physical Sciences, 8*(42), 1975-1982.

Deuss, A., & Woodhouse, J. (2001). Seismic observations of splitting of the mid-transition zone discontinuity in Earth's mantle. *Science, 294*(5541), 354-357.

Drury, M., & Hyndman, R. (1979). The electrical resistivity of oceanic basalts. *Journal of Geophysical Research: Solid Earth, 84*(B9), 4537-4545.

Dziewonski, A. M., & Anderson, D. L. (1981). Preliminary reference Earth model. *Physics of the Earth and Planetary Interiors, 25*(4), 297-356.

Evans, R. L., Hirth, G., Baba, K., Forsyth, D., Chave, A., & Mackie, R. (2005). Geophysical evidence from the MELT area for compositional controls on oceanic plates. *Nature, 437*, 249-252.

Fairfield, D. H. (1963). Ionosphere current patterns in high latitudes. *Journal of Geophysical Research, 68*(12), 3589-3602.

Fejer, B. G. (1981). The equatorial ionospheric electric fields. A review. *Journal of Atmospheric and Terrestrial Physics, 43*(5-6), 377-386.

Fukushima, N. (1979). Electric potential difference between conjugate points in middle latitudes caused by asymmetric dynamo in the ionosphere. *Journal of Geomagnetism and Geoelectricity, 31*(3), 401-409.

Garland, G. (1975). Correlation between electrical conductivity and other geophysical parameters. *Physics of the Earth and Planetary Interiors, 10*(3), 220-230.

Gauss, C. F. (1841). *Allgemeine Theories des Erdmagnetismus, in Resultate aus den Beobachtungen des magnetis chem Vereins in Yahr*. (E. Sabine & R. Taylor). Germany: Scientific Memoir Selection Transaction of Foreign Academy of science Learned Societies Foreign Journals. (Original work published 1838).

Glover, P. W., & Vine, F. (1994). Electrical conductivity of the continental crust. *Geophysical Research Letters, 21*(22), 2357-2360.

Goncz, J. H., & Cleary, J. R. (1976). Variations in the structure of the upper mantle beneath Australia, from Rayleigh wave observations. *Geophysical Journal International, 44*(2), 507-516.

Graves, R. W., & Helmberger, D. V. (1988). Upper mantle cross section from Tonga to Newfoundland. *Journal of Geophysical Research: Solid Earth, 93*(B5), 4701-4711.

Gunnarsdóttir, E. L. (2012). *The Earth's Magnetic Field.* (Unpublished Ph.D Thesis). University of Iceland, Iceland.

Hasegawa, M. (1960). On the position of the focus of the geomagnetic Sq current system. *Journal of Geophysical Research, 65*(5), 1437-1447.

Hirth, G., & Kohlstedt, D. L. (1996). Water in the oceanic upper mantle: implications for rheology, melt extraction and the evolution of the lithosphere. *Earth and Planetary Science Letters, 144*(1-2), 93-108.

Hobbs, B. A., (1887). Conductivity profiles from global data. *Pure and Applied Geophysics*, *125*(2-3), 393-407.

Hyndman, R., & Hyndman, D. (1968). Water saturation and high electrical conductivity in the lower continental crust. *Earth and Planetary Science Letters*, *4*(6), 427-432.

Ichiki, M., Uyeshima, M., Utada, H., Guoze, Z., Ji, T., & Mingzhi, M. (2001). Upper mantle conductivity structure of the back-arc region beneath northeastern China. *Geophysical Research Letters*, *28*(19), 3773-3776.

Inoue, T., Yurimoto, H., & Kudoh, Y. (1995). Hydrous modified spinel, Mg_1. 75SiH0. 5O4: a new water reservoir in the mantle transition region. *Geophysical Research Letters*, *22*(2), 117-120.

Ito, E., & Katsura, T. (1989). A temperature profile of the mantle transition zone. *Geophysical Research Letters*, *16*(5), 425-428.

Ito, E., & Takahashi, E. (1989). Postspinel transformations in the system Mg_2SiO_4-Fe_2SiO_4 and some geophysical implications. *Journal of Geophysical Research: Solid Earth*, *94*(B8), 10637-10646.

Jiracek, G. R., Ander, M. E., & Holcombe, H. T. (1979). Magnetotelluric soundings of crustal conductive zones in major continental rifts. In *Rio Grande Rift: Tectonics and Magmatism* (pp. 209-222). Washington, DC.

Jones, A. G. (1983). On the equivalence of the "Niblett" and "Bostick" transformations in the magnetotelluric method. *Journal of. Geophysics*, *53*(1), 72-73.

Kaila, K., Tewari, H., Chowdhury, K. R., Rao, V., Sridhar, A., & Mall, D. (1987). Crustal structure of the northern part of the Proterozoic Cuddapah basin of India from deep seismic soundings and gravity data. *Tectonophysics*, *140*(1), 1-12.

Karato, S.-I. (1990). The role of hydrogen in the electrical conductivity of the upper mantle. *Nature*, *347*(6290), 272-273.

Karato, S.-i., & Jung, H. (1998). Water, partial melting and the origin of the seismic low velocity and high attenuation zone in the upper mantle. *Earth and Planetary Science Letters*, *157*(3-4), 193-207.

Karato, S. i. (1992). On the Lehmann discontinuity. *Geophysical Research Letters*, *19*(22), 2255-2258.

Katsura, T., & Ito, E. (1989). The system Mg_2Si_{O4}-Fe_2SiO_4 at high pressures and temperatures: Precise determination of stabilities of olivine, modified spinel, and spinel. *Journal of Geophysical Research: Solid Earth*, *94*(B11), 15663-15670.

Kawasaki, K., Matsushita, S., & Cain, J. (1989). Least squares and integral methods for the spherical harmonic analysis of the Sq-field. *Pure and Applied Geophysics*, *131*(3), 357-370.

Kelbert, A., Schultz, A., & Egbert, G. (2009). Global electromagnetic induction constraints on transition-zone water content variations. *Nature, 460*(7258), 1003-1006.

Kennett, B., & Engdahl, E. (1991). Traveltimes for global earthquake location and phase identification. *Geophysical Journal International, 105*(2), 429-465.

Kirchhoff, V. W., & Carpenter, L. A. (1976). The day-to-day variability in ionospheric electric fields and currents. *Journal of Geophysical Research, 81*(16), 2737-2742.

Kohlstedt, D., Keppler, H., & Rubie, D. (1996). Solubility of water in the α, β and γ phases of $(Mg, Fe)_2 SiO_4$. *Contributions to Mineralogy and Petrology, 123*(4), 345-357.

Kolomyceva, G. (1972). On electrical conductivity distribution in the Earth's mantle from data of the secular variations of the geomagnetic field. *Geomagnetism Aeronomy, 12*(6), 1082-1085.

Kuvshinov, A., & Olsen, N. (2006). A global model of mantle conductivity derived from 5 years of CHAMP, Ørsted, and SAC-C magnetic data. *Geophysical Research Letters, 33*(18), 1-5.

Lahiri, B., & Price, A. (1939). Electromagnetic induction in non-uniform conductors, and the determination of the conductivity of the earth from terrestrial magnetic variations. *Philophical Transaction of Royal Society of London, 237*(784), 509-540.

Lanza, R., & Meloni, A. (2006). *The Earth's magnetism*. Würzburg, Germany: Springer.

Le Sager, P., & Huang, T. (2002). Longitudinal dependence of the daily geomagnetic variation during quiet time. *Journal of Geophysical Research: Space Physics, 107*(A11), 1-8.

Leven, J., Jackson, I., & Ringwood, A. (1981). Upper mantle seismic anisotropy and lithospheric decoupling. *Nature, 289*, 234-239.

Lilley, F., Woods, D., & Sloane, M. (1981a). Electrical conductivity from Australian magnetometer arrays using spatial gradient data. *Physics of the Earth and Planetary Interiors, 25*(3), 202-209.

Lilley, F., Woods, D., & Sloane, M. (1981b). Electrical conductivity profiles and implications for the absence or presence of partial melting beneath central and southeast Australia. *Physics of the Earth and Planetary Interiors, 25*(4), 419-428.

Livingston, W., & Penn, M. (2009). Are sunspots different during this solar minimum? *Eos, Transactions American Geophysical Union, 90*(30), 257-258.

Lizarralde, D., Chave, A., Hirth, G., & Schultz, A. (1995). Northeastern Pacific mantle conductivity profile from long-period magnetotelluric sounding using Hawaii-to-California submarine cable data. *Journal of Geophysical Research: Solid Earth, 100*(B9), 17837-17854.

Love, J. J., & Gannon, J. L. (2009). Revised Dst and the epicycles of magnetic disturbance: 1958-2007. *Annales Geophysicae Atmospheres, Hydrospheres and Space Sciences,* 27, 3101-3131.

Malin, S., & Gupta, J. (1977). The Sq current system during the International Geophysical Year. *Geophysical Journal International, 49*(2), 515-529.

Malin, S. R. C. (1973). Worldwide distribution of geomagnetic tides. *Philsophical Transaction of the Royal Society of London. 274*(1243), 551-594.

Martyn, D. F. (1947). Atmospheric tides in the ionosphere-I. Solar tides in the F2 region. *Proceedings of the Royal Society of London, 189*(1017), 241-260.

Marquis, G., & Hyndman, R. D. (1992). Geophysical support for aqueous fluids in the deep crust: seismic and electrical relationships. *Geophysical Journal International, 110*(1), 91-105.

Mayaud, P. N. (1980). *Derivation, meaning, and use of geomagnetic Indices*. Washington, D. C: American Geophysical Union.

Matsushita, S. (1960). Seasonal and day-to-day changes of the central position of the Sq overhead current system. *Journal of Geophysical Research, 65*(11), 3835-3839.

Matsushita, S. (1967). *III-1 - Solar Quiet and Lunar Daily variation fields.* In S. Matsushita & W. H. Campbell (Eds.), International Geophysics (Vol. 11, pp. 301-424): Academic Press.

Matsushita, S., & Maeda, H. (1965). On the geomagnetic solar quiet daily variation field during the IGY. *Journal of Geophysical Research, 70*(11), 2535-2558.

Matsushita, S., & Xu, W. Y. (1982). Equivalent ionospheric current systems representing solar daily variations of the polar geomagnetic field. *Journal of Geophysical Research: Space Physics, 87*(A10), 8241-8254.

Mayaud, P. N. (1965). Analyse morphologique de la variabilite jour-a-jour de la variation journaliere "reguliere" SR du champ magnetique terrestre, II.-Le systeme de courants CM (Regions non-polaires). *Annale Geophysicae, 21*, 514-544.

Mazaudier, C. (1993). On the relationship between ionospheric phenomena and the day-to-day variability of the earth magnetic field regular variation" S_R" Advances made during the two last decades with the incoherent scatter sounder network results. *Trends Geophysics Research, 2*, 397-421.

Mazaudier, C., & Venkateswaran, S. (1985). Strange currents over Saint-Santin. *Journal of Geophysical Research: Space Physics, 90*(A10), 9727-9735.

McDonald, K. L. (1957). Penetration of the geomagnetic secular field through a mantle with variable conductivity. *Journal of Geophysical Research, 62*(1), 117-141.

Mechie, J., Egorkin, A., Fuchs, K., Ryberg, T., Solodilov, L., & Wenzel, F. (1993). P-wave mantle velocity structure beneath northern Eurasia from long-range recordings along the profile Quartz. *Physics of the Earth and Planetary Interiors, 79*(1-2), 269-286.

Meghani, N. (2016). The structure of the earth. Retrieved January 15, 2018 from https://www.e-education.psu.edu/marcellus/node/870.

Mitra, A. P. (1968). A review of D-region processes in non-polar latitudes. *Journal of Atmospheric and Terrestrial Physics, 30*(6), 1065-1114.

Miyahara, S., & Ooishi, M. (1997). Variation of Sq induced by atmospheric tides simulated by a middle atmosphere general circulation model. *Journal of Geomagnetism and Geoelectricity, 49*(1), 77-87.

Nataf, H. C., Nakanishi, I., & Anderson, D. L. (1984). Anisotropy and shear-velocity heterogeneities in the upper mantle. *Geophysical Research Letters, 11*(2), 109-112.

Nishida, A. (1968). Geomagnetic DP_2 fluctuations and associated magnetospheric phenomena. *Journal of Geophysical Research, 73*(5), 1795-1803.

Obiora, D. N., Okeke, F. N., & Yumoto, K. (2015). Electrical conductivity of mantle in the North Central region of Nigeria. *Journal of African Earth Sciences, 101*, 274-281.

Obiora, D. N., Okeke, F. N., Yumoto, K., & Agha, S. O. (2014). Mantle electrical conductivity profile of Niger delta region. *Journal of Earth System Science, 123*(4), 827-835.

Ohtani, E., & Sakai, T. (2008). Recent advances in the study of mantle phase transitions. *Physics of the Earth and Planetary Interiors, 170*(3-4), 240-247.

Okeke, F. (1995). *Day-to-day variability in the geomagnetic variations in the equatorial zone.* (Unpublished Ph. D Thesis). University of Nigeria, Nsukka, Nigeria.

Okeke, F., & Hamano, Y. (2000). Daily variations of geomagnetic H, D and Z-field at equatorial latitudes. *Earth, Planets and Space, 52*(4), 237-243.

Okeke, F. N., & Obiora, D. N. (2016). Application of solar quiet day (Sq) current in determining mantle electrical-depth conductivity structure–A review. *Journal of African Earth Sciences, 114*, 54-62.

Olhoeft, G. R. (1981). Electrical properties of granite with implications for the lower crust. *Journal of Geophysical Research: Solid Earth, 86*(B2), 931-936.

Olsen, N. (1998). Estimation of C-responses (3 h to 720 h) and the electrical conductivity of the mantle beneath Europe. *Geophysics Journal International, 133*, 298-308.

Omura, K. (1991). Change of electrical conductivity of olivine associated with the olivine-spinel transition. *Physics of the Earth and Planetary Interiors, 65*(3-5), 292-307.

Park, J., Luhr, H., & Min, K. (2011). Climatology of the inter-hemispheric field-aligned current system in the equatorial ionosphere as observed by CHAMP. *Annales Geophysicae 29*, 573-582.

Parkinson, W. (1974). The reliability of conductivity derived from diurnal variations. *Journal of Geomagnetism and Geoelectricity, 26*(2), 281-284.

Patil, A., Arora, B.R., & Rastogi, R.G. (1985). Seasonal variations in the intensity of Sq current system and its focus latitude over the Indian region. *Indian Journal of Radio and Space Physics, 14*, 131–135.

Patil, A., Rao, D., & Rastogi, R. (1990). Equatorial electrojet strengths in the Indian and American sectors. *Journal of Geomagnetism and Geoelectricity, 42*(7), 801-811.

Pecova, J., Pec, K., & Praus, O. (1980). Remarks on spatial distribution of long period variations in the geomagnetic field over European area. *Journal of Geomagnetism and Geoelectricity, 32*, SI171-SI185.

Pedatella, N. M., Forbes, J. M., & Richmond, A. D. (2011). Seasonal and longitudinal variations of the solar quiet (Sq) current system during solar minimum determined by CHAMP satellite magnetic field observations. *Journal of Geophysical Research: Space Physics, 116*(A4), 1-13.

Price, A. T. (1970). The electrical conductivity of the Earth. *Quarterly Journal of the Royal Astronomical Society, 11*, 23-42.

Poirier, J. P. (2000). *Introduction to the Physics of the Earth's Interior*. (2nd ed.). England: Cambridge University Press.

Price, A. T., & Wilkins, G. A. (1963). New methods for the analysis of geomagnetic fields and their application to the Sq field of 1932-3. *Philosophical Transaction of the Royal Society of London, 256*(1066), 31-98.

Rastogi, R. G. (1989). The equatorial electrojet: magnetic and ionospheric effects. *Geomagnetism, 3*, 461-525.

Rastogi, R. (1992). Geomagnetic disturbance effects on equatorial electrojet current. *Journal of Geomagnetism and Geoelectricity, 44*(5), 317-324.

Rastogi, R. (1993). Geomagnetic field variations at low latitudes and ionospheric electric fields. *Journal of Atmospheric and Terrestrial Physics, 55*(10), 1375-1381.

Rastogi, R. G., Chandra, H., & Chakravarty, S. C. (1971). The disappearance of equatorial E s and the reversal of electrojet current. *Proceedings of the Indian Academy of Sciences-Section, 74*, 62-67.

Revenaugh, J., & Jordan, T. H. (1991). Mantle layering from ScS reverberations: 1. Waveform inversion of zeroth-order reverberations. *Journal of Geophysical Research: Solid Earth, 96*(B12), 19749-19762.

Richmond, A. (1979). Large-amplitude gravity wave energy production and dissipation in the thermosphere. *Journal of Geophysical Research: Space Physics, 84*(A5), 1880-1890.

Richmond, A. D., Matsushita, S., & Tarpley, J. D. (1976). On the production mechanism of electric currents and fields in the ionosphere. *Journal of Geophysical Research, 81*(4), 547-555.

Rikitake, T. (1950). Electromagnetic induction within the earth and its relation to the electrical state of the earth's interior. *Bulletin Earthquake Research Institute, 28*, 45-100.

Rikitake, T. (1966). *Electromagnetism and the Earth's Interior*. (pp. 221-226). Elsevier, Amsterdam: Elsevier.

Roberts, R. (1984). The long-period electromagnetic response of the Earth. *Geophysical Journal International, 78*(2), 547-572.

Roberts, R. (1986). The deep electrical structure of the Earth. *Geophysical Journal International, 85*(3), 583-600.

Rotanova, N. M., Abramova, D. Y., & Semenov, V. Y. (1993). On the radial geoelectrical structure of the mid-mantle from magnetovariational sounding using MAGSAT data. *Journal of Geomagnetism and Geoelectricity, 45*(11-12), 1415-1423.

Runcorn, S. (1955). The electrical conductivity of the earth's mantle. *Eos, Transactions American Geophysical Union, 36*(2), 191-198.

Sakyo-ku, K. C. (2017). World data center for geomagnetism, Kyoto. Retrieved December 31, 2017 from http://wdc.kugi.kyoto-u.ac.jp/.

Schlapp, D. (1968). World-wide morphology of day-to-day variability of Sq. *Journal of Atmospheric and Terrestrial Physics, 30*(10), 1761-1776.

Schmucker, U. (1970). Anomalies of geomagnetic variations in the southwestern United States. *Bulletin of the Scripps Institution Oceanography, 13*, 1-165.

Schmucker, U. (1987). Substitute conductors for electromagnetic response estimates. *Pure and Applied Geophysics, 125*(2-3), 341-367.

Schock, R. N., Duba, A. G., & Shankland, T. J. (1989). Electrical conduction in olivine. *Journal of Geophysical Research: Solid Earth, 94*(B5), 5829-5839.

Schultz, A., Kurtz, R., Chave, A., & Jones, A. (1993). Conductivity discontinuities in the upper mantle beneath a stable craton. *Geophysical Research Letters, 20*(24), 2941-2944.

Schultz, A., & Larsen, J. (1987). On the electrical conductivity of the mid-mantle-I. Calculation of equivalent scalar magnetotelluric response functions. *Geophysical Journal International, 88*(3), 733-761.

Schultz, A., & Larsen, J. (1990). On the electrical conductivity of the mid-mantle: II. Delineation of heterogeneity by application of extremal inverse solutions. *Geophysical Journal International, 101*(3), 565-580.

Schultz, A., & Pritchard, G. (1999). Three-Dimensional Inversion for Large-Scale Structure in a Spherical Domain'. *Three Dimensional Electromagnetics, SEG Geophysical Developments Series, 7*, 451-476.

Schuster, A. (1889). IV. The diurnal variation of terrestrial magnetism. *Proceedings of the Royal Society of London, 45*(273-279), 481-486.

Schuster, A. (1907). The diurnal variation of terrestrial magnetism. *Proceeding of the Royal Society of London, 80*(535), 80-82.

Semenov, V. Y. (1989). Evaluation of mantle conductivity beneath northern hemisphere continents. *Izvestiya Earth Physics, 25*, 221-226.

Semenov, V. Y., & Jozwiak, W. (1999). Model of the geoelectrical structure of the mid- and lower mantle in the Europe–Asia region. *Geophysical Journal International, 138*(2), 549-552.

Shankland, T., O'Connell, R., & Waff, H. (1981). Geophysical constraints on partial melt in the upper mantle. *Reviews of Geophysics, 19*(3), 394-406.

Shankland, T., & Waff, H. (1977). Partial melting and electrical conductivity anomalies in the upper mantle. *Journal of Geophysical Research, 82*(33), 5409-5417.

Shankland, T. J., & Ander, M. E. (1983). Electrical conductivity, temperatures, and fluids in the lower crust. *Journal of Geophysical Research: Solid Earth, 88*(B11), 9475-9484.

Shiraki, M. (1972). Geomagnetic solar daily variations at the middle latitude and the day-to-day variability of equivalent overhead current system. *Memoir of the Kakioka Magnetic Observation, 15*, 19-30.

Shiraki, M. (1973). Variation of focus latitude and intensity of overhead current system of Sq with the solar activity. *Memoirs of the Kakioka Magnetic Observatory, 15*, 107-126.

Shiraki, M. (1974). Variations of focus latitude and intensity of equivalent current system of geomagnetic solar daily variation with a period from about ten to thirty days. *Memoirs of the Kakioka magnetic Observation, 16*, 29-43.

Solanki, S., & Rüedi, I. (2003). Spatial and temporal fluctuations in sunspots derived from MDI data. *Astronomy & Astrophysics, 411*(2), 249-256.

Stanley, W., Boehl, J., Bostick, F., & Smith, H. (1977). Geothermal significance of magnetotelluric sounding in the Eastern Snake River Plain-Yellowstone Region. *Journal of Geophysical Research, 82*(17), 2501-2514.

Stening, R. J. (2008). The shape of the Sq current system. *Annales Geophysicae: Atmospheres, Hydrospheres and Space Sciences, 26*, 1767-1775.

Stening, R., & Reztsova, T. (2007). Variation of Sq focus latitudes in the Australian/Pacific region during a quiet sun year. *Journal of Atmospheric and Solar-Terrestrial Physics, 69*(6), 734-740.

Stening, R., Reztsova, T., & Minh, L. H. (2005). Day-to-day changes in the latitudes of the foci of the Sq current system and their relation to equatorial electrojet strength. *Journal of Geophysical Research: Space Physics, 110*(A10), 1-6.

Stening, R. J. (1971). Longitude and Seasonal Variations of theSqCurrent System. *Radio Science, 6*(2), 133-137.

Stening, R. J. (1989). A calculation of ionospheric currents due to semidiurnal antisymmetric tides. *Journal of Geophysical Research: Space Physics, 94*(A2), 1525-1531.

Stening, R. J., & Winch, D. E. (1987). Night-time geomagnetic variations at low latitudes. *Planetary and space science, 35*(12), 1523-1539.

Stening, R. J., & Winch, D. E. (2013). The ionospheric Sq current system obtained by spherical harmonic analysis. *Journal of Geophysical Research: Space Physics, 118*(3), 1288-1297.

Sternberg, B. K., & Clay, C. (1977). Flambeau Anomaly: A High-Conductivity Anomaly in the Southern Extension of the Canadian Shield. *The Earth's Crust, 20,* 501-530.

Stesky, R., & Brace, W. (1973). Electrical conductivity of serpentinized rocks to 6 kilobars. *Journal of Geophysical Research, 78*(32), 7614-7621.

Stewart, B. (1882). *Terrestrial magnetism*. (Vol. 16. pp 159-184). New York, CS: Encyclopedia Brittanica, *16*, 159-184.

Subbotin, S., Naumchik, G., & Rakhimova, I. S. (1965). Structure of the earth's crust and upper mantle. *Tectonophysics, 2*(2-3), 111-150.

Suzuki, A. (1978). Geomagnetic Sq field at successive universal times. *Journal of Atmospheric and Terrestrial Physics, 40*(4), 449-463.

Suzuki, A. (1979). UT and day-to-day variations in equivalent current systems for world geomagnetic variations. *Journal of Geomagnetism and Geoelectricity, 31*(1), 21-46.

Svalgaard, L. (2016). Reconstruction of solar extreme ultraviolet flux 1740–2015. *Solar Physics, 291*(9-10), 2981-3010.

Svalgaard, L., & Cliver, E. W. (2007). Calibrating the sunspot number using "the magnetic needle". *Cawses Newsletter*, *4*(1), 6-8.

Takeda, M. (1982). Three dimensional ionospheric currents and field aligned currents generated by asymmetrical dynamo action in the ionosphere. *Journal of Atmospheric and Terrestrial Physics, 44*(2), 187-193.

Takeda, M. (1984). Day-to-day variation of equivalent Sq current system during March 11-26, 1970. *Journal of Geomagnetism and Geoelectricity, 36*(5), 215-228.

Takeda, M. (1990). Geomagnetic field variation and the equivalent current system generated by an ionospheric dynamo at the solstice. *Journal of Atmospheric and Terrestrial Physics, 52*(1), 59-67.

Takeda, M. (1999). Time variation of global geomagnetic Sq field in 1964 and 1980. *Journal of Atmospheric and Solar-Terrestrial Physics, 61*(10), 765-774.

Takeda, M. (2002a). The correlation between the variation in ionospheric conductivity and that of the geomagnetic Sq field. *Journal of Atmospheric and Solar-Terrestrial Physics, 64*(15), 1617-1621.

Takeda, M. (2002b). Features of global geomagnetic Sq field from 1980 to 1990. *Journal of Geophysical Research: Space Physics, 107*(A9), 1-8.

Takeda, M., & Araki, T. (1984). Time variation of instantaneous equivalent Sq current system. *Journal of Atmospheric and Terrestrial Physics, 46*(10), 911-915.

Takeda, M., & Araki, T. (1985). Electric conductivity of the ionosphere and nocturnal currents. *Journal of Atmospheric and Terrestrial Physics, 47*(6), 601-609.

Takeda, M., Iyemori, T., & Saito, A. (2003). Relationship between electric field and currents in the ionosphere and the geomagnetic Sq field. *Journal of Geophysical Research: Space Physics, 108*(A5), 1-4.

Takeda, M., & Yamada, Y. (1987). Simulation of ionospheric electric fields and geomagnetic field variation by the ionospheric dynamo for different solar activity. *Annales Geophysicae*, 5, 429-433.

Takeda, M., Yamada, Y., & Araki, T. (1986). Simulation of ionospheric currents and geomagnetic field variations of Sq for different solar activity. *Journal of Atmospheric and Terrestrial Physics, 48*(3), 277-287.

Tarpley, J. (1973). Seasonal movement of the Sq current foci and related effects in the equatorial electrojet. *Journal of Atmospheric and Terrestrial Physics, 35*(6), 1063-1071.

Thakur, N., & Sontakke, K. (1981). On abnormal quiet day Sq (Z) ranges in the Indian region. *Journal of Atmospheric and Terrestrial Physics, 43*(10), 1107-1111.

Thu, H. P. T., Amory-Mazaudier, C., & Le Huy, M. (2011). Sq field characteristics at Phu Thuy, Vietnam, during solar cycle 23: Comparisons with Sq field in other longitude sectors. *Annales Geophysicae, 108*, 1-17.

Thybo, H. (2006). The heterogeneous upper mantle low velocity zone. *Tectonophysics, 416*(1-4), 53-79.

Tozer, D. (1970). Temperature, conductivity, composition and heat flow. *Journal of Geomagnetism and Geoelectricity, 22*(1-2), 35-51.

Utada, H., Koyama, T., Shimizu, H., & Chave, A. (2003). A semi-global reference model for electrical conductivity in the mid-mantle beneath the north Pacific region. *Geophysical Research Letters, 30*(4), 1-4.

Vestine, E. (1960). The survey of the geomagnetic field in space. *Earth Observing system Transactions American Geophysical Union, 41*(1), 4-21.

Vichare, G., Rawat, R., Hanchinal, A., Sinha, A., Dhar, A., & Pathan, B. (2012). Seasonal evolution of Sq current system at sub-auroral latitude. *Earth, Planets and Space, 64*(11), 1023-1031.

Vichare, G., Rawat, R., Jadhav, M., & Sinha, A. K. (2017). Seasonal variation of the Sq focus position during 2006–2010. *Advances in Space Research, 59*(2), 542-556.

Vidale, J. E., & Benz, H. M. (1992). Upper-mantle seismic discontinuities and the thermal structure of subduction zones. *Nature, 356*, 678-683.

Wang, D., Mookherjee, M., Xu, Y., & Karato, S. (2006). The effect of water on the electrical conductivity of olivine. *Nature, 443*(7114), 977-980.

Winch, D. (1981). Spherical harmonic analysis of geomagnetic tides, 1964-1965. *Philosophical Transaction of the Royal Society of London, 303*(1473), 1-104.

Wood, B. (1995). The effect of H_2O on the 410-kilometer seismic discontinuity. *Science, 268*(5207), 74-76.

Woods, D., & Lilley, F. (1979). Geomagnetic induction in central Australia. *Journal of Geomagnetism and Geoelectricity, 31*(4), 449-458.

Xu, Y., Poe, B. T., Shankland, T. J., & Rubie, D. C. (1998). Electrical conductivity of olivine, wadsleyite, and ringwoodite under upper-mantle conditions. *Science, 280*(5368), 1415-1418.

Xu, Y., Shankland, T. J., & Poe, B. T. (2000). Laboratory-based electrical conductivity in the Earth's mantle. *Journal of Geophysical Research: Solid Earth, 105*(B12), 27865-27875.

Yacob, A., & Prabhavalkar, A. (1965). Solar control of the amplitude and phase of the yearly mean Sq (H) at Alibag for the period 1905 to 1960. *Journal of Atmospheric and Terrestrial Physics, 27*(1), 73-80.

Yacob, A., & Rao, D. R. (1966). Solar cycle and annual variations of Sq (H) at Alibag. *Journal of Atmospheric and Terrestrial Physics, 28*(4), 351-360.

Yamashita, S., & Iyemori, T. (2002). Seasonal and local time dependences of the interhemispheric field-aligned currents deduced from the Ørsted satellite and the ground geomagnetic observations. *Journal of Geophysical Research: Space Physics, 107*(A11), 1-11.

Yamazaki, Y., & Maute, A. (2017). Sq and EEJ—A review on the daily variation of the geomagnetic field caused by ionospheric dynamo currents. *Space Science Reviews, 206*(1-4), 299-405.

Yamazaki, Y., Yumoto, K., Uozumi, T., Abe, S., Cardinal, M., McNamara, D., Marshall, R., Shevtsov, B., & Solovyev, S. (2010). Reexamination of the Sq-EEJ relationship based on extended magnetometer networks in the East Asian region. *Journal of Geophysical Research: Space Physics, 115*(A9), 1-8.

Yamazaki, Y., Yumoto, K., Uozumi, T., & Cardinal, M. (2011). Intensity variations of the equivalent Sq current system along the 210 magnetic meridian. *Journal of Geophysical Research: Space Physics, 116*(A10), 1-8.

Yamazaki, Y., Yumoto, K., Uozumi, T., Yoshikawa, A., & Cardinal, M. G. (2009). Equivalent current systems for the annual and semiannualSqvariations observed along the 210°MM CPMN stations. *Journal of Geophysical Research: Space Physics, 114*(A12), 1-9.

Yoshino, T., & Katsura, T. (2009). Effect of iron content on electrical conductivity of ringwoodite, with implications for electrical structure in the transition zone. *Physics of the Earth and Planetary Interiors, 174*(1-4), 3-9.

Yoshino, T., & Katsura, T. (2013). Electrical conductivity of mantle minerals: role of water in conductivity anomalies. *Annual Review of Earth and Planetary Sciences, 41*, 605-628.

Yoshino, T., Matsuzaki, T., Yamashita, S., & Katsura, T. (2006). Hydrous olivine unable to account for conductivity anomaly at the top of the asthenosphere. *Nature, 443*(7114), 973-976.

Zharkov, S., & Zharkova, V. (2006). Statistical analysis of the sunspot area and magnetic flux variations in 1996–2005 extracted from the Solar Feature Catalogue. *Advances in Space Research, 38*(5), 868-875.

LIST OF PUBLICATIONS AND PAPERS PRESENTED

LIST OF PUBLICATIONS:

1. Abidin, Z. Z., Jusoh, M. H., **Abbas, M.,** & Yoshikawa, A. (2018). Application of solar quiet (Sq) current in determining mantle conductivity-depth structure in Malaysia. *Journal of Atmospheric and Solar-Terrestrial Physics*. https://doi.org/10.1016 /j.jastp.2018.01.019.

2. Abidin, Z. Z., Jusoh, M. H., **Abbas, M.,** Bolaji, O. S., & Yoshikawa, A. (2018). Features of the inter-hemispheric field-aligned current system over Malaysia ionosphere. *Journal of Atmospheric and Solar-Terrestrial Physics*. https://doi.org/ 10.1016 /j.jastp.2018.01.012.

PAPERS PRESENTED

1. **Abbas M.**, Jusoh, M. H., & Abidin, Z. Z. (2018). *Solar quiet (Sq) and conductivity-depth structure of Asia sub-region using solar quiet (Sq) field variations.* Paper presented at the International Conference on Space Weather and Satellite Application, 7-9th August 2018, Shah Alam, Malaysia.

2. **Abbas M.**, Jusoh, M. H., & Abidin, Z. Z. (2017). *The upper mantle electrical conductivity-depth structure of Malaysia.* Paper presented at the 2nd National School on Space and Earth Electromagnetim, 8-11th August 2017, Johor, Malaysia.

3. **Abbas M.**, Jusoh, M. H., & Abidin, Z. Z. (2016). *Climatology of the inter-hemispheric field-aligned currents over Malaysia ionosphere***.** Paper presented at the National Physics Conference, 21-22nd December 2016, Kuala Lumpur, Malaysia.